



UNIVERSITÀ DI PISA

Dipartimento di Fisica "Enrico Fermi"

Corso di Laurea Magistrale in Fisica teorica

Wormhole solutions in Einstein-Weyl
gravity

Candidato

Alessandro Zuccotti
Matricola 497524

Relatore interno

Damiano Anselmi

Relatore esterno

Alfio Maurizio Bonanno

Anno Accademico 2019/20

Abstract

In this work we are going to study wormhole solutions in Einstein-Weyl gravity. Such solutions emerge when looking for a static spherically symmetric metric in the vacuum, in the more general context of classical quadratic gravity. Classical quadratic gravity is the theory of gravitation that comes out when including quadratic terms in the curvature in the Einstein-Hilbert action of general relativity. The study of such theory is motivated by the presence of quadratic corrections in almost all attempts to find a consistent description of quantum gravity. Indeed, it is well known that general relativity can be consistent as a quantum field theory only as a low-energy effective theory. We are not going to discuss the quantum aspects of the quadratic action: instead, we consider what happens to the classical description of the space-time when quadratic corrections are taken into account. In order to do that, we restrict to the simplest non-trivial case, that is a static spherically symmetric space-time in the vacuum. Given these restrictions in general relativity, we have the well known Schwarzschild solution, i.e. black hole solution. In classical quadratic gravity the Schwarzschild solution is still present, but we can also find many different classes of solutions: the aim of this thesis is to classify the various solutions families, as well as to characterize a specific family that covers a large part of the solution space, i.e. wormhole solutions. We solve the geodesic equation in such solutions which shows the reason why we call them traversable wormholes. We report all the solution families found in previous works while adding a new subfamily of the generic wormhole solutions.

When studying different classes of solutions we are assisted by a Lichnerowicz-type theorem which removes the contributions of the R^2 term from the equations of motion under some assumptions, in particular when an horizon is present. When such contribution is absent, the quadratic theory reduces to Einstein-Weyl gravity.

By numerically solving the equations of motion in the Einstein-Weyl theory, we classify the various solution families in a phase diagram of the theory. By using the shooting method for the boundary value problem between spatial infinity and the radius of the wormholes, we find the geometric properties of the wormhole solutions, and in particular we characterize the behavior of these solutions in function of their position on the phase diagram. Then we use the results to explore both the interior $r < r_0$ of the wormholes and the new "copy" of $r > r_0$ that emerges in such solutions. We report a qualitative analysis of the behavior of the metric in this new $r > r_0$ region, discovering that it has a finite proper volume for $r \rightarrow \infty$ for almost all solutions, due to a strongly non-flat behavior of the metric. We conclude with a physical discussion about the case of a massive observer that falls into these solutions.

Contents

1	Introduction	5
1.1	Conventions and notation	10
2	Classical quadratic gravity	11
2.1	Equations of motion	11
2.2	Static spherically symmetric case	13
2.3	Reducing to Einstein-Weyl gravity	17
2.4	Linearised theory and asymptotically flat solutions	19
2.5	Vacuum solutions	20
2.5.1	Second order corrections	22
2.6	Linearised solutions coupled with a point source and the complete linearised vacuum	22
2.7	Small radius and strong curvature regime	24
2.7.1	Frobenius method	24
2.8	Solutions around the origin	26
2.8.1	The $(0,0)_0$ family	27
2.8.2	The $(1,-1)_0$ family	27
2.8.3	The $(2,2)_0$ family	28
2.8.4	Generalized Frobenius solutions	29
2.9	Solutions around $r_0 \neq 0$	30
2.9.1	Black hole solutions	31
2.9.2	The $(1,0)_{r_0}$ family: wormhole solutions	32
2.9.3	Non-Frobenius solutions	36
2.9.4	The $(\frac{3}{2}, \frac{1}{2})_{r_0,1/2}$ family	36
2.9.5	The $(1,0)_{r_0,1/2}$ family: generic wormholes	37
2.9.6	A new subfamily of the $(1,0)_{r_0,1/2}$	38
2.9.7	Other possible solution families	40
3	Numerical methods	41
3.1	Numerical solutions of ordinary differential equations	41
3.2	Numerical roots of multivariable functions	43
3.3	Shooting method	43
4	Numerical results and physical discussion	46
4.1	Ghost unit and physical scale	46
4.2	Solution space	47
4.3	Solutions without singularity	49
4.4	Solutions with singularity	53

5 Black hole solutions	54
5.1 Shooting method for black hole solutions	54
5.2 General features of black hole solutions	57
5.3 Precision of the method and errors estimation	61
6 Wormhole solutions	64
6.1 Shooting method for wormhole solutions	64
6.2 General features of wormhole solutions	65
6.3 Solutions with $b_{1/2} = 0$	71
6.4 Interior of wormholes	74
6.5 Coupling with matter	79
6.6 The new region $\rho < 0$	81
6.7 Physical discussion	87
6.7.1 Solutions with $b_{1/2} \leq 0$	91
7 Conclusions	95
8 Ringraziamenti	101

1 Introduction

General relativity, after few years of its release, proved to be one of the most successful existing theories. It reproduces the Newton's gravitation in the weak field limit, but it also predicts a large number of phenomena that cannot be correctly described by the previous gravitational theories. Examples of such phenomena include gravitational time dilation, gravitational lensing, the gravitational redshift of light, and static space-time with singularity, i.e. black holes. The prediction of many of these phenomena agrees with optimal precision with the experimental data. General relativity changed the meaning of space-time that becomes an actual dynamical object. Modern cosmology is based on the Einstein equations of general relativity and it turned out to be a good description of the universe at large scale.

On the other hand, Standard Model obtained a great success as a theory describing particle physics at the microscopical scale, where quantum effects are dominant. Based on quantum field theory, it gives the description of three of the four known fundamental forces: the electromagnetic, weak, and strong interactions. It had a huge success in providing experimental predictions. In such description, the three fundamental interactions emerge as gauge theory.

In both general relativity and gauge theories, the physical laws are required to be invariant under some local symmetry. Indeed general relativity requires a covariant formulation under general coordinate transformations. In such context, the space-time distance $ds^2 = -dt^2 + dx^2$ is generalized as

$$ds^2 = g_{\mu\nu}(x)dx^\mu dx^\nu \quad (1.1)$$

that is measured in terms of the metric tensor $g_{\mu\nu}$. The derivatives ∂_μ must be replaced with the covariant derivatives: if a_μ is a covariant vector

$$\partial_\mu a_\nu \rightarrow \nabla_\mu a_\nu = \partial_\mu a_\nu - \Gamma_{\mu\nu}^\rho a_\rho \quad (1.2)$$

where the Levi-Civita connection $\Gamma_{\mu\nu}^\rho(g) = \frac{1}{2}g^{\rho\alpha}(-\partial_\alpha g_{\mu\nu} + \partial_\mu g_{\alpha\nu} + \partial_\nu g_{\alpha\mu})$ is involved. From the connection $\Gamma_{\mu\nu}^\rho$, it can be derived the Riemann tensor

$$R^\rho_{\sigma\mu\nu} = \partial_\mu \Gamma_{\nu\sigma}^\rho - \partial_\nu \Gamma_{\mu\sigma}^\rho + \Gamma_{\mu\alpha}^\rho \Gamma_{\nu\sigma}^\alpha - \Gamma_{\nu\alpha}^\rho \Gamma_{\mu\sigma}^\alpha \quad (1.3)$$

which encodes a geometrical property of the space-time that does not depend on the specific coordinate system: the curvature. In general relativity the presence of a gravitational field is manifested through the curvature of the space-time.

Quantum electrodynamics, as example of gauge theory, requires a covariant formulation under local transformation of the group $U(1)$. In such context the standard derivatives must be replaced with the covariant derivatives

$$\partial_\mu \rightarrow D_\mu = \partial_\mu - ieA_\mu \quad (1.4)$$

where the four-potential A_μ appears. From A_μ it can be derived the electromagnetic tensor

$$F_{\mu\nu} = \partial_\mu A_\nu - \partial_\nu A_\mu \quad (1.5)$$

which encodes the effective electromagnetic force in his components, as well as the Riemann tensor and its traces (the Ricci tensor $R_{\mu\nu}$ and the Ricci scalar R) encode the gravitational field in general relativity. The action of both the theories must be invariant under the respective local symmetries. In general relativity we have the Einstein-Hilbert action plus the matter action¹

$$S = S_{EH} + S_M = \frac{1}{16\pi G} \int d^4x \sqrt{-g} R + S_M \quad (1.6)$$

which is invariant under coordinate transformations. In QED we have

$$S_{QED} = \int d^4x \left[-\frac{1}{4} F_{\mu\nu} F^{\mu\nu} + \bar{\psi}(i\gamma^\mu D_\mu - m)\psi \right] \quad (1.7)$$

which is gauge invariant, with $D_\mu = \partial_\mu - ieA_\mu$. The classical aspect of both theories can be studied by varying the action with respect to the dynamical field of the theory:

- in general relativity, by varying the action with respect to the inverse of the metric $g^{\mu\nu}$, we obtain as equations of motion the Einstein equations

$$R_{\mu\nu} - \frac{1}{2} R g_{\mu\nu} = 8\pi G T_{\mu\nu} \quad (1.8)$$

- in QED, by varying the action with respect to the four-potential A_μ , we obtain as equations of motion

$$\partial_\nu F^{\nu\mu} = -e\bar{\psi}\gamma^\mu\psi \quad (1.9)$$

that with the Lorenz gauge $\partial_\mu A^\mu = 0$ becomes

$$-\square A_\mu = eJ_\mu \quad (1.10)$$

which is the wave equation for the four-potential in presence of a source, and which summarizes the Maxwell equations in the Lorenz gauge.

Despite these similarities, general relativity is not a gauge theory. This because, in contrast with QED², where the dynamical field is the four-potential A_μ that appears in the covariant derivatives, in general relativity we take as dynamical field the metric $g_{\mu\nu}$ instead of the connection $\Gamma_{\mu\nu}^\rho$. This becomes relevant when we want to consider the quantum aspect of the theory. Indeed, if gauge theories turned out

¹We assume that the cosmological constant can be included in the matter sector.

²or with the other gauge theories of the Standard Model.

suitable to be quantized, it is well known that general relativity can be a consistent quantum field theory only as low-energy effective theory. This relies on its non-renormalizability.

Renormalization is a procedure designed to cancel the divergences that appear in a quantum field theory. In a general quantum field theory the calculation of the Feynman diagrams at one or more loop generically brings divergences in the theory. These divergences can be canceled by introducing new counterterms in the Lagrangian of the theory. However, every counterterm introduced brings a coupling constant. If the theory contains N coupling constants, at least N experiments are necessary to fix them. A quantum field theory is renormalizable if divergences can be canceled with a finite number of counterterms. If not, an infinite number of experiments would be necessary to fix all the coupling constants of the theory, and such theory would not be predictive. Unfortunately this is the case of general relativity. When trying to quantize the metric $g_{\mu\nu}$, starting from the Einstein-Hilbert action, infinite counterterms are required to cancel all divergences. The necessary counterterms to cancel one-loop divergences are of the form

$$\sim R^2 \quad \text{and} \quad \sim R_{\mu\nu}R^{\mu\nu}$$

as shown in [6] by 't Hooft and Veltman. In [3], Goroff and Sagnotti have found that the two-loops divergences, instead, require cubic terms in the curvature tensor. However, if the Einstein-Hilbert action is not renormalizable, one-loop counterterms motivate the study of the action

$$S_{G^2} = \int d^4x \sqrt{-g} [\gamma R + (\alpha + \frac{2}{3}\beta)R^2 - 2\alpha R_{\mu\nu}R^{\mu\nu}] \quad (1.11)$$

This is the action of quadratic gravity, since it contains the two simplest quadratic terms in the curvature. $R_{\mu\nu\rho\sigma}R^{\mu\nu\rho\sigma}$ is excluded since it is related to the other two terms by the Gauss-Bonnet theorem. Such theorem allows us to rewrite the action as

$$S_{G^2} = \int d^4x \sqrt{-g} [\gamma R + \beta R^2 - \alpha C_{\mu\nu\rho\sigma}C^{\mu\nu\rho\sigma}] \quad (1.12)$$

since the two forms differ by a total derivative. In (1.12) the Weyl tensor $C_{\mu\nu\rho\sigma}$ appears, instead of the Ricci tensor $R_{\mu\nu}$, and the choice of the parameterization of the coupling constants α and β is explicit. The action of quadratic gravity results to be renormalizable but the theory results to be non-unitary. Indeed, if we expand the metric as

$$g_{\mu\nu} = \eta_{\mu\nu} + h_{\mu\nu}(x)$$

where $\eta_{\mu\nu} = \text{diag}(-1, 1, 1, 1)$ is the Minkowski flat metric, the propagator of the field $h_{\mu\nu}$ can be written as

$$D_{\mu\nu\rho\sigma}(k) = \frac{1}{(2\pi)^4 i} \left(\frac{2P_{\mu\nu\rho\sigma}^{(2)}(k) - 4P_{\mu\nu\rho\sigma}^{(0-s)}(k)}{k^2} - \frac{2P_{\mu\nu\rho\sigma}^{(2)}(k)}{k^2 + m_2^2} + \frac{4P_{\mu\nu\rho\sigma}^{(0-s)}(k)}{k^2 + m_0^2} \right) + \text{gauge fixing terms} \quad (1.13)$$

where $P_{\mu\nu\rho\sigma}^{(2)}(k)$ and $P_{\mu\nu\rho\sigma}^{(0-s)}(k)$ are the projectors for a symmetric rank-two tensor, and where we have defined $m_0^2 = \frac{\gamma}{6\beta}$ and $m_2^2 = \frac{\gamma}{2\alpha}$. Then the dynamical content of such theory includes: the usual mass-less spin-two graviton, a massive scalar field, and a massive spin-two ghost. The negative residue in the massive spin-two sector, i.e. the ghost, is a serious problem since it makes the theory having negative norm state, and the vacuum unstable. This is an effect of quadratic terms in the Lagrangian, i.e. of the higher derivatives involved. Such effect has been known since many years in the context of classical theories with higher derivatives, namely Ostrogradsky's instabilities. However, many authors proposed a way to deal with the ghost problem, that could lead to a consistent predictive theory of quantum gravity. A way to possibly save the theory of higher derivative gravity was presented by Hawking and Hertog in [4], where a toy model of a scalar field was used as an analogy for higher-derivative gravity, and a prescription for calculating amplitudes was presented.

Salvio and Strumia suggested in [10] of building a usable theory with mixed states with both positive and negative norm, even if a probabilistic interpretation of the theory is yet to be found.

In [1], Anselmi introduced fakeons, degrees of freedom that do not belong to the physical spectrum but that propagate inside the Feynman diagrams. Such fake degrees of freedom can be used to make higher-derivative theories unitary.

In the asymptotic safety scenario, if general relativity is not renormalizable in the standard perturbative sense, it could be renormalizable in a non-perturbative way, as formulated by Weinberg in [13]: from the study of the renormalization group flow it seems that gravity has a non-Gaussian fixed point in the UV limit, with a three-dimensional critical surface. In other words, in the high energy limit the theory could be determined only by three coupling constants, and the corrections to the Einstein-Hilbert action are expected to be quadratic.

All these reasons make the action (1.12) of great interest, for the purpose of finding a consistent quantum theory of gravity. We are going to work with the action (1.12) but we will not focus on the quantum aspect of this theory. Instead we consider what happens to the classical description of the space-time when quadratic corrections are taken into account. In order to do that, we restrict to the simplest non-trivial case, that is a static spherically symmetric space-time in the vacuum. When looking

for vacuum spherically symmetric solutions in general relativity, we must solve the Einstein equation

$$R_{\mu\nu} - \frac{1}{2}Rg_{\mu\nu} = 0 \quad (1.14)$$

with a metric of the form

$$ds^2 = g_{\mu\nu}dx^\mu dx^\nu = -B(r,t)dt^2 + \frac{1}{f(r,t)}dr^2 + r^2d\theta + r^2\sin^2\theta d\phi^2 \quad (1.15)$$

It follows that the solution must be also static and that it is equal to

$$B(r) = f(r) = 1 - \frac{2GM}{r} \quad (1.16)$$

i.e. the Schwarzschild solution. The Schwarzschild solution gives an exact description of particular macroscopical objects, the black holes. Such objects present a singularity of the coordinate system at $r = r_0 = 2MG$ (the horizon), and a true space-time singularity at the origin $r = 0$ that cannot be canceled with any coordinate change. Even in the black hole case, problems arise when quantum effects are taken into account. It is known that, due to such effects, black holes should emit a weak radiation, the Hawking radiation. Even if very weak, such emission could make a black hole to totally evaporate, and it follows the information paradox. This is an additional hint to take into consideration the quadratic action (1.12). Indeed, from such action, some more general equations of motion emerge. They are still solved by the Schwarzschild solution, but many other solution families appear in this theory, which avoid the information paradox (most of them without horizon). The aim of this thesis is to classify the solution families of classical quadratic gravity, focusing on characterizing a particular family: the wormhole solutions. Large part of the work considers the restriction of the action (1.12) with $\beta = 0$, that is the Einstein-Weyl theory. In [8] they considered static solutions (not requiring spherical symmetry) and proved that the Ricci scalar must vanish under certain conditions, in particular when imposing asymptotic flatness in presence of an horizon.

This thesis primarily follows the works of Stelle, Lu, Pope, and Perkins [12], [7]. First we derive the equations of motion from the action (1.12). Then we restrict to the static spherically symmetric solutions, and consider the case when the Ricci scalar vanishes. We show the solutions of the linearised theory, as well as the solutions in series expansion around a certain radius. We solve the radial geodesic equation for the main objects of this work, the wormhole solutions, showing why they are interpreted as traversable wormholes. After restricting to the Einstein-Weyl theory, we present our numerical results in a phase diagram of the theory. Such results are obtained with standard numerical integration, by connecting the large radius regime where we impose asymptotic flatness, to the small radius one. We describe the black hole and wormhole solutions by using a shooting method between spatial

infinity and the "singular" radius of the solution, characterizing it with great precision around this radius. Then we use these results to explore the solutions in regions of the space-time that would be prohibited for the standard numerical integration. We conclude by giving a complete view of the wormhole solutions, showing what happens to an observer that falls into such solutions.

1.1 Conventions and notation

We work in unit of $c = 1$, $\hbar = 1$. We use the "mostly plus" convention for the metric, so its signature is

$$(-, +, +, +)$$

The connection, the Riemann tensor, the Ricci tensor, the Ricci scalar and the Weyl tensor are

$$\Gamma_{\mu\nu}^\rho(g) = \frac{1}{2}g^{\rho\alpha}(-\partial_\alpha g_{\mu\nu} + \partial_\mu g_{\alpha\nu} + \partial_\nu g_{\alpha\mu}) \quad (1.17)$$

$$R_{\sigma\mu\nu}^\rho(\Gamma) = \partial_\mu\Gamma_{\nu\sigma}^\rho - \partial_\nu\Gamma_{\mu\sigma}^\rho + \Gamma_{\mu\alpha}^\rho\Gamma_{\nu\sigma}^\alpha - \Gamma_{\nu\alpha}^\rho\Gamma_{\mu\sigma}^\alpha$$

$$R_{\mu\nu} = R_{\mu\rho\nu}^\rho$$

$$R = g_{\mu\nu}R^{\mu\nu}$$

$$W_{\mu\nu\rho\sigma} = R_{\mu\nu\rho\sigma} - \frac{1}{2}(R_{\mu\sigma}g_{\nu\rho} + R_{\nu\rho}g_{\mu\sigma} - R_{\mu\rho}g_{\nu\sigma} - R_{\nu\sigma}g_{\mu\rho}) + \frac{1}{6}(g_{\mu\rho}g_{\nu\sigma} - g_{\mu\sigma}g_{\nu\rho})$$

The covariant derivatives are indicated with ∇_μ , except in section 2.3 where we use D_a to indicate the covariant derivative for the spatial part of the metric h_{ab} . We consider

$$\gamma = \frac{1}{16\pi G} = \frac{M_p^2}{16\pi}$$

in order to have a correspondence with general relativity.

When doing numerical work we set $\gamma = 1$, but when recalling the Schwarzschild solution we still write $r_S = 2GM$ instead of $r_S = \frac{M}{8\pi}$.

We often use the abbreviations e.o.m. for equations of motion, and o.d.e. for ordinary differential equations. We often refer to the new region $r > r_0$, that emerges in wormhole solutions, as the new "copy" of $r > r_0$, even if the metric can be different in the two patches $r > r_0$.

2 Classical quadratic gravity

In this section we will give a description of classical quadratic gravity, focusing on static spherically symmetric solutions in the vacuum.

Unlike general relativity, there is not a uniqueness theorem about the static spherically symmetric solutions, neither one ensuring that generic spherically symmetric solutions are static. In general relativity, Birkhoff's theorem states that any spherically symmetric solution of the vacuum field equations must be static and asymptotically flat. When coupling with a matter distribution, the Birkhoff's theorem also implies that such solution depends only on the mass. Indeed by solving the Einstein equation, a unique solution can be found, that is the Schwarzschild solution. On the contrary, in classical quadratic gravity we will find several solution families, and in their general form they are not asymptotically flat. An exact form of these solutions is lacking, but we will see how to classify them with respect to their behavior in specific radius regimes.

Furthermore, we will focus on the action containing just the Ricci term and the Weyl squared term and the respective static spherically symmetric solutions, i.e. the Einstein-Weyl theory. We will also present a useful theorem found in [8] that motivates our interest in the Einstein-Weyl restriction.

2.1 Equations of motion

Here we give a brief overview of how to derive the equations of motion of classical quadratic gravity. The e.o.m. are obtained by performing the variation of the Lagrangian with respect to $g^{\mu\nu}$. We adopt the usual second order formalism, assuming the connection depending on the metric and equal to the Levi-Civita connection (1.17).

The action of classical quadratic gravity can be written in the two equivalent forms

$$S_{G^2} = \int d^4x \sqrt{-g} [\gamma R + \beta R^2 - \alpha C_{\mu\nu\rho\sigma} C^{\mu\nu\rho\sigma}] \quad (2.1)$$

$$S_{G^2} = \int d^4x \sqrt{-g} [\gamma R + (\alpha + \frac{2}{3}\beta)R^2 - 2\alpha R_{\mu\nu} R^{\mu\nu}] \quad (2.2)$$

These two forms are correlated by the Gauss-Bonnet term. We use here the (2.2) in order to have just the variation of the Ricci tensor and the scalar curvature.

By varying the first term in the action (2.2) we obtain the usual Einstein tensor

$$\delta S_1 = \gamma \int d^4x \sqrt{-g} (R_{\mu\nu} - \frac{1}{2}Rg_{\mu\nu}) \delta g^{\mu\nu} \quad (2.3)$$

The second term of the action (2.2) gives

$$\begin{aligned}\delta S_2 = & (\beta + \frac{2}{3}\alpha) \int d^4x \sqrt{-g} \left(-\frac{1}{2}R^2 g_{\mu\nu} \delta g^{\mu\nu} + 2RR_{\mu\nu} \delta g^{\mu\nu} + \right. \\ & \left. + 2Rg^{\mu\nu}(\nabla_\alpha \delta \Gamma_{\mu\nu}^\alpha - \nabla_\mu \delta \Gamma_{\alpha\nu}^\alpha) \right)\end{aligned}\quad (2.4)$$

where we used the Palatini identity $\delta R_{\mu\nu} = \nabla_\alpha \delta \Gamma_{\mu\nu}^\alpha - \nabla_\mu \delta \Gamma_{\alpha\nu}^\alpha$.

By moving the covariant derivatives from the connections to the factor $2\sqrt{-g}Rg^{\mu\nu}$ in the last terms, it is easy to see that this variation becomes

$$\delta S_2 = (\beta + \frac{2}{3}\alpha) \int d^4x (2R_{\mu\nu}R - \frac{1}{2}R^2 g_{\mu\nu} + 2g_{\mu\nu}\square R - 2\nabla_\mu \nabla_\nu R) \delta g^{\mu\nu} \quad (2.5)$$

The variation of the third term of (2.2) gives

$$\begin{aligned}\delta S_3 = & -2\alpha \int d^4x \sqrt{-g} \left(-\frac{1}{2}R_{\alpha\beta}R^{\alpha\beta} g_{\mu\nu} \delta g^{\mu\nu} + 2R_{\mu\alpha}R_\nu^\alpha \delta g^{\mu\nu} + \right. \\ & \left. + 2R^{\mu\nu}(\nabla_\alpha \delta \Gamma_{\mu\nu}^\alpha - \nabla_\mu \delta \Gamma_{\alpha\nu}^\alpha) \right)\end{aligned}\quad (2.6)$$

We can manipulate the last term of the (2.6) by moving the covariant derivatives and by using the second Bianchi identity for the Ricci tensor, that becomes

$$\begin{aligned}2R^{\mu\nu}(\nabla_\alpha \delta \Gamma_{\mu\nu}^\alpha - \nabla_\mu \delta \Gamma_{\alpha\nu}^\alpha) = & \\ = & \sqrt{-g}(-2\nabla_\alpha R^{\mu\nu} \delta(-\frac{1}{2}g^{\alpha\beta}\partial_\beta g_{\mu\nu} + g^{\alpha\beta}\partial_\mu g_{\beta\nu}) + \nabla^\nu R \delta(\frac{1}{2}g^{\alpha\beta}\partial_\nu g_{\alpha\beta})) + (\text{tot. deriv.})\end{aligned}\quad (2.7)$$

By moving all the derivatives, adding and subtracting some terms in the form $\Gamma(\nabla Ric)\delta g^{\mu\nu}$, we finally get

$$\begin{aligned}\delta S_3 = & -2\alpha \int d^4x \sqrt{-g} \left(-\frac{1}{2}R_{\alpha\beta}R^{\alpha\beta} g_{\mu\nu} + 2R_{\mu\alpha}R_\nu^\alpha + \frac{1}{2}\square R g_{\mu\nu} + \right. \\ & \left. + \square R_{\mu\nu} - 2\nabla_\alpha \nabla_\mu R_\nu^\alpha \right) \delta g_{\mu\nu}\end{aligned}\quad (2.8)$$

The full e.o.m. are

$$\begin{aligned}\frac{1}{2}T_{\mu\nu} = H_{\mu\nu} = & \frac{1}{\sqrt{-g}} \frac{\delta S_{G^2}}{\delta g^{\mu\nu}} = \gamma(R_{\mu\nu} - \frac{1}{2}Rg_{\mu\nu}) + \\ & + \beta(2R_{\mu\nu}R - \frac{1}{2}R^2 g_{\mu\nu} + 2\square R g_{\mu\nu} - 2\nabla_\mu \nabla_\nu R) + \\ & - \alpha(-\frac{4}{3}R_{\mu\nu}R + \frac{1}{3}R^2 g_{\mu\nu} + \frac{4}{3}\nabla_\mu \nabla_\nu R - R_{\alpha\beta}R^{\alpha\beta} g_{\mu\nu} + \\ & + 4R_{\mu\alpha}R_\nu^\alpha - \frac{1}{3}\square R g_{\mu\nu} + 2\square R_{\mu\nu} - 4\nabla_\alpha \nabla_\mu R_\nu^\alpha)\end{aligned}\quad (2.9)$$

These are equal to the most often reported e.o.m. obtained by the action (2.1)

$$\begin{aligned}\frac{1}{2}T_{\mu\nu} = H_{\mu\nu} = & \frac{1}{\sqrt{-g}} \frac{\delta S_{G^2}}{\delta g^{\mu\nu}} = \gamma(R_{\mu\nu} - \frac{1}{2}Rg_{\mu\nu}) + \\ & + 2\beta(R_{\mu\nu}R - \frac{1}{4}R^2 g_{\mu\nu} + g_{\mu\nu}\square R - \nabla_\mu \nabla_\nu R) + \\ & - 4\alpha(\nabla^\rho \nabla^\sigma + \frac{1}{2}R^{\rho\sigma})C_{\mu\rho\nu\sigma}\end{aligned}\quad (2.10)$$

Indeed the terms in γ and β are explicitly the same. For the terms in α , if we expand the Weyl tensor, and we use the second Bianchi identity, such terms become

$$\begin{aligned} & -\alpha(2R^{\rho\sigma}R_{\mu\rho\nu\sigma} + 2R_{\mu\alpha}R_{\nu}^{\alpha} - \frac{4}{3}R_{\mu\nu}R - R_{\alpha\beta}R^{\alpha\beta} + \frac{1}{3}R^2g_{\mu\nu} + \\ & + 2\square R_{\mu\nu} - 2\nabla_{\alpha}\nabla_{\mu}R_{\nu}^{\alpha} + \frac{1}{3}\nabla_{\mu}\nabla_{\nu}R - \frac{1}{3}\square Rg_{\mu\nu}) \end{aligned} \quad (2.11)$$

Now we can use the definition of the Riemann tensor

$$[\nabla_{\alpha}, \nabla_{\mu}]R_{\beta\nu} = \nabla_{\alpha}\nabla_{\mu}R_{\beta\nu} - \nabla_{\mu}\nabla_{\alpha}R_{\beta\nu} = -R_{\beta\alpha\mu}^{\rho}R_{\rho\nu} - R_{\nu\alpha\mu}^{\rho}R_{\beta\rho} \quad (2.12)$$

and, by contracting the indexes α and β , we obtain

$$\nabla^{\alpha}\nabla_{\mu}R_{\alpha\nu} - \frac{1}{2}\nabla_{\mu}\nabla_{\nu}R = R_{\mu}^{\rho}R_{\rho\nu} - R_{\rho\nu\alpha\mu}R^{\alpha\rho} \quad (2.13)$$

By using this equation, it can be verified that the terms in α of the equations (2.9) and (2.10) are the same.

From the e.o.m. in the form (2.9) we can see that any solution of the Einstein equation in the vacuum

$$R_{\mu\nu} = 0 \quad (2.14)$$

is also a solution in the vacuum for the quadratic gravity. Instead in the (2.10) it can be seen that the trace of the e.o.m. results to be

$$H_{\mu}^{\mu} = 6\beta\square R - \gamma R = \frac{1}{2}T_{\mu}^{\mu} \quad (2.15)$$

In the following we will discuss how to find the metric $g_{\mu\nu}$ that solves the equations of motion, restricting to the static spherically symmetric case in the vacuum.

2.2 Static spherically symmetric case

We reduce here to the static spherically symmetric case. This is the simplest non-trivial case, in which the e.o.m. becomes a system of two ordinary differential equations in the radial coordinate.

The general static spherically symmetric metric can be written as

$$ds^2 = -B(r)dt^2 + \frac{1}{f(r)}dr^2 + r^2d\theta + r^2\sin^2\theta d\phi^2 \quad (2.16)$$

and it is characterized by the two functions of the one radial coordinate $B(r) = -g_{tt}$ and $f(r) = g_{rr}^{-1}$. In some cases we will refer to the spacial component as $g_{rr} = A(r) = f(r)^{-1}$, used in place of $f(r)$. In the following we will specify when this notation will be used.

As stated before, in general relativity a spherically symmetric metric in the vacuum is always static, but this does not happen in the higher derivative theory, so we assume here that the metric has both these properties.

By inserting this metric in the e.o.m. we find that $H_{\mu\nu}$ takes the same diagonal structure of the metric

$$H_{\mu\nu} = \begin{pmatrix} H_{tt} & 0 & 0 & 0 \\ 0 & H_{rr} & 0 & 0 \\ 0 & 0 & H_{\theta\theta} & 0 \\ 0 & 0 & 0 & \sin^2 \theta H_{\theta\theta} \end{pmatrix} \quad (2.17)$$

We have a system of four equations, but since $H_{\phi\phi} = \sin^2 \theta H_{\theta\theta}$ and $\nabla^\mu H_{\mu\nu} = 0$, only two equations are independent.

In $H_{\mu\nu}$ the fourth derivatives of $B(r)$ and $f(r)$ appear, but H_{rr} depends only on derivatives up to $B^{(3)}(r)$ and $f''(r)$.

The combination

$$H_{tt} - X(r)H_{rr} - Y(r)\partial_r H_{rr} \quad (2.18)$$

with

$$X(r) = \frac{(\alpha - 3\beta)B(r)}{(2(\alpha + 6\beta)B(r) - r(\alpha - 3\beta)B'(r))^2} \left(4(\alpha + 6\beta)B(r)^2(rf'(r) + 3f(r)) + \right. \\ \left. - r^2(\alpha - 3\beta)f(r)B'(r)^2 - 2r(\alpha - 3\beta)B(r)B'(r)(rf'(r) + 2f(r)) \right) \quad (2.19)$$

and

$$Y(r) = \frac{2r(\alpha - 3\beta)B(r)^2f(r)}{2(\alpha + 6\beta)B(r) - r(\alpha - 3\beta)B'(r)} \quad (2.20)$$

depends only on derivatives up to $B''(r)$ and $f^{(3)}(r)$. So in the vacuum, the e.o.m. becomes a third order system of the two following differential equations

$$\begin{aligned}
H_{rr} = & B^{(3)}(r)f(r) \frac{(r(\alpha - 3\beta)B'(r) - 2(\alpha + 6\beta)B(r))}{3rB(r)^2} + \\
& - \frac{B''(r)}{6rB(r)^2} \left((3r^2(\alpha - 3\beta)f(r)B'(r)^2 + rB(r)(f(r)(r(\alpha - 3\beta)B''(r) + \right. \\
& \left. - 12(\alpha + 3\beta)B'(r)) - 2r(\alpha - 3\beta)B'(r)f'(r)) + 4(\alpha + 6\beta)B(r)^2(rf'(r) + 2f(r)) \right) + \\
& + \frac{B'(r)}{24r^3B(r)^4f(r)} \left(-2r^2B(r)f(r)B'(r)^2(3r(\alpha - 3\beta)f'(r) + 2(5\alpha + \right. \\
& \left. + 12\beta)f(r)) + rB(r)^2B'(r)(-r^2(\alpha - 3\beta)f'(r)^2 + 4rf(r)(r(\alpha - 3\beta)f''(r) + \right. \\
& \left. + (4\alpha + 6\beta)f'(r)) - 4(\alpha - 48\beta)f(r)^2) + 7r^3(\alpha - 3\beta)f(r)^2B'(r)^3 + \right. \\
& \left. + 4B(r)^3(r^2(\alpha + 6\beta)f'(r)^2 - 2rf(r)(2r(\alpha + 6\beta)f''(r) + (\alpha + 24\beta)f'(r) + \right. \\
& \left. - 3\gamma r) + 8(\alpha + 6\beta)f(r)^2) \right) + \\
& - \frac{1}{6r^4f(r)} \left(12\beta - 4\alpha + f(r)(72\beta - 4r^2(\alpha - 12\beta)f''(r) - 6\gamma r^2) + \right. \\
& \left. + r^2(\alpha - 12\beta)f'(r)^2 + 4(\alpha - 21\beta)f(r)^2 + 6\gamma r^2 \right) = 0
\end{aligned} \tag{2.21}$$

$$\begin{aligned}
H_{tt} - X(r)H_{rr} - Y(r)\partial_r H_{rr} = & -\frac{36\alpha\beta B(r)^2 f(r) f^{(3)}(r)}{r(r(\alpha - 3\beta)B'(r) - 2(\alpha + 6\beta)B(r))} + \\
& + \frac{18\alpha\beta B(r) f''(r)}{(r(r(\alpha - 3\beta)B'(r) - 2(\alpha + 6\beta)B(r)))^2} \left(rB(r)B'(r)(2(\alpha + 6\beta)f(r) + \right. \\
& \left. - r(\alpha - 3\beta)f'(r)) - 2r^2(\alpha - 3\beta)f(r)B'(r)^2 + 2(\alpha + 6\beta)B(r)^2(2f(r) + rf'(r)) \right) + \\
& - \frac{3\beta f'(r)^2}{2(r(r(\alpha - 3\beta)B'(r) - 2(\alpha + 6\beta)B(r)))^2} \left(r^3(\alpha - 3\beta)^2 B'(r)^3 + 3r^2(\alpha^2 - 9\alpha\beta + \right. \\
& \left. + 18\beta^2)B(r)B'(r)^2 - 12\alpha r(\alpha + 6\beta)B(r)^2B'(r) + 4(\alpha^2 - 6\alpha\beta - 72\beta)^2)B(r)^3 \right) + \\
& + \frac{f'(r)}{r^3 B(r)(r(\alpha - 3\beta)B'(r) - 2(\alpha + 6\beta)B(r))^2} \left(3\beta r^4(\alpha - 3\beta)^2 B'(r)^4 f(r) + \right. \\
& \left. + 3\beta r^3(\alpha - 3\beta)f(r)B(r)B'(r)^2((11\alpha - 6\beta)B'(r) - 2r(\alpha - 3\beta)B''(r)) + \right. \\
& \left. + 2rB(r)^3(18\alpha\beta r(\alpha + 6\beta)f(r)B''(r) + B'(r)(6\beta(11\alpha^2 - 12\alpha\beta + 18\beta)^2)f(r) + \right. \\
& \left. - (\alpha - 3\beta)^2(12\beta - \gamma r^2)) + r^2 B(r)^2 B'(r)(B'(r)(\gamma r^2(\alpha - 3\beta)^2 - 12\beta(8\alpha^2 + 51\alpha\beta + \right. \\
& \left. + 18\beta^2)f(r)) - 6\beta r(\alpha^2 - 15\alpha\beta + 36\beta^2)f(r)B''(r)) - 4(\alpha + 6\beta)B(r)^4(12\beta(4\alpha - 3\beta)f(r) + \right. \\
& \left. + 2\alpha(\gamma r^2 - 6\beta) + 3\beta(12\beta + \gamma r^2)) \right) + \\
& - \frac{1}{2r^4 B(r)^2(r(\alpha - 3\beta)B'(r) - 2(\alpha + 6\beta)B(r))^2} \left(3\beta r^5(\alpha - 3\beta)^2 f(r)^2 B'(r)^5 + \right. \\
& \left. + 3\beta r^4(\alpha - 3\beta)f(r)^2 B(r)B'(r)^3((19\alpha + 6\beta)B'(r) - 4r(\alpha - 3\beta)B''(r)) + \right. \\
& \left. - 4r^2 B(r)^3 f(r)(3\beta r^2(\alpha^2 + 3\alpha\beta - 18\beta^2)f(r)B''(r)^2 - 3B'(r)^2(\beta(\alpha^2 + \right. \\
& \left. + 66\alpha\beta + 36\beta^2)f(r) + (\alpha - 3\beta)(\alpha(4\beta - \gamma r^2) - 3\beta(4\beta + \gamma r^2))) + \right. \\
& \left. + rB'(r)B''(r)(\gamma r^2(\alpha - 3\beta)^2 - 6\beta(7\alpha^2 + 48\alpha\beta + 36\beta^2)f(r)) + \right. \\
& \left. + 2r^3 B(r)^2 f(r)B'(r)(6\beta r^2(\alpha - 3\beta)^2 B''(r)^2 f(r) + B'(r)^2(\gamma r^2(\alpha - 3\beta)^2 + \right. \\
& \left. - 6\beta(13\alpha^2 + 84\alpha\beta + 36\beta^2)f(r)) - 36\alpha\beta r(\alpha - 3\beta)f(r)B'(r)B''(r)) + 8r(\alpha + \right. \\
& \left. - 3\beta)B(r)^4(\gamma r^3(\alpha + 6\beta)f(r)B''(r) + B'(r)(-6\alpha\beta + 18\beta^2 + f(r)(\alpha\gamma r^2 - 24\alpha\beta - 36\beta^2 + \right. \\
& \left. + 6\beta\gamma r^2) + 6\beta(5\alpha + 3\beta)f(r)^2 + \alpha\gamma r^2 + 6\beta\gamma r^2)) - 8(\alpha + \right. \\
& \left. + 6\beta)B(r)^5(f(r) - 1)(6\beta(5\alpha + 3\beta)f(r) + \alpha(6\beta - 2\gamma r^2) - 3\beta(6\beta + \gamma r^2)) \right) = 0
\end{aligned} \tag{2.22}$$

Clearly these equations cannot be solved analytically, so numerical methods must be used in order to obtain the solutions for $B(r)$ and $f(r)$.

Having two coupled third order equations, we expect six free parameters to fix a solution. In [7], an extensive parameters counting seems to confirm that six is the total number of parameters of the theory.

2.3 Reducing to Einstein-Weyl gravity

We show in this paragraph an important theorem which motivates our interest for a theory that contains only the scalar curvature and the Weyl squared term. This was done in [8] and then corrected in [7]. Then we give some consideration on the e.o.m. in the Einstein-Weyl theory.

We consider a static metric in the form

$$g_{\mu\nu}(x)dx^\mu dx^\nu = -\lambda^2(x)dt^2 + h_{ab}(x)dx^a dx^b \quad (2.23)$$

where $h_{ab}(x)$ is the spacial metric, that we assume positive definite, and we also consider the trace of the e.o.m. (2.15) in the vacuum

$$H_\mu^\mu = 6\beta(\square R - m_0^2 R) = 0 \quad (2.24)$$

The box operator is

$$\square R = g_{\mu\nu}\nabla^\mu\nabla^\nu R = D^a D_a R + \frac{1}{\lambda} D^a \lambda D_a R \quad (2.25)$$

with D^a the covariant derivative for the metric $h_{ab}(x)$, so the trace of the e.o.m. implies

$$\frac{1}{6\beta} H_\mu^\mu = D^a D_a R + \frac{1}{\lambda} D^a \lambda D_a R - m_0^2 R = 0 \quad (2.26)$$

If we multiply by λR and integrate in a spacial volume \mathcal{S} , we get

$$\begin{aligned} & \int_{\mathcal{S}} d^3x \sqrt{h} [\lambda R D^a D_a R + R D^a \lambda D_a R - \lambda m_0^2 R^2] = \\ &= \int_{\mathcal{S}} d^3x \sqrt{h} [D^a (\lambda R D_a R) - \lambda D^a R D_a R - \lambda m_0^2 R^2] = 0 \end{aligned} \quad (2.27)$$

In the integrand we find one boundary term, and two bulk terms.

Theorem 1. *Let $g_{\mu\nu}$ be a static metric, with $g_{00} \equiv -\lambda^2$, the spatial part $g_{ij} \equiv h_{ab}$ and D_a the covariant derivative with respect to h_{ab} . Consider a spatial volume \mathcal{S} , then if h_{ab} is positive definite in \mathcal{S}*

$$\lambda R D_a R|_{\partial\mathcal{S}} = 0 \implies R = 0 \text{ in } \mathcal{S}$$

The proof requires only m_0^2 (and so β) to be positive. With this condition the two bulk terms are both negative, having h_{ab} positive definite, so a vanishing R is the only way to satisfy the (2.27).

A similar condition was found in [8] for $R_{\mu\nu}$, but in [7] this was corrected. There it was shown that the equivalent relation of (2.27) for $R_{\mu\nu}$ contains bulk terms with opposite sign, so that the theorem is not valid for the general Ricci tensor.

In the spherically symmetric case, by setting as spatial volume \mathcal{S} the region included between two radii r^+ and r^- , the boundary contribution of the theorem becomes

$$\begin{aligned} \int_{\mathcal{S}} d^3x \sqrt{h} [D^a(\lambda R D_a R)] &= \int_{\mathcal{S}} \partial_r (\sqrt{-g_{rr}(r)g_{tt}(r)} r^2 \sin\theta R \partial_r R) dr d\theta d\phi = \\ &= 4\pi \left[\sqrt{\frac{B(r)}{f(r)}} r^2 R \partial_r R \right]_{r^-}^{r^+} \end{aligned} \quad (2.28)$$

So by defining

$$C(r) = \sqrt{\frac{B(r)}{f(r)}} r^2 R \partial_r R \quad (2.29)$$

it is sufficient having $C(r^+) = 0$, $C(r^-) = 0$ to get

$$R(r) = 0 \quad \text{for} \quad r^- < r < r^+$$

We will apply this theorem for the various solution families described in the following. Here we give the first example of an asymptotically flat solution with horizon. By its own definition, a solution with an horizon at $r = r_0$ has

$$\lambda^2(r_0) = 0 \quad (2.30)$$

so $C(r^-) = C(r_0) = 0$. When imposing asymptotic flatness, we will see that the solutions at large radius become of the form (2.46), and for $r \rightarrow \infty$ we have $B(r) \rightarrow 1$, $f(r) \rightarrow 1$, $R(r)$ goes like $O(e^{-m_0 r}) + O(e^{-m_2 r})$. This implies that we can make $C(r^+)$ arbitrary small taking a large enough radius r^+ since $r^2 R \partial_r R$ goes to zero for large radius. Then the theorem 1 states that R is zero in all the volume $r_0 < r < \infty$. The e.o.m. with $R = 0$ are

$$H_{\mu\nu} = \gamma R_{\mu\nu} - \alpha(-R_{\alpha\beta}R^{\alpha\beta}g_{\mu\nu} + 4R_{\mu\alpha}R^\alpha_\nu + 2\Box R_{\mu\nu} - 4\nabla_\alpha\nabla_\mu R^\alpha_\nu) \quad (2.31)$$

and they do not depend on β . At the same time, if we consider the Einstein-Weyl theory (i.e. we set $\beta = 0$) the trace of the e.o.m. is

$$H^\mu_\mu = -\gamma R = 0$$

and then every solution has a vanishing R . So the e.o.m. for the Einstein-Weyl theory are identical to those with $R = 0$ and this makes the theory with $\beta = 0$ of great interest. We have already seen that asymptotically flat solutions with horizon must have $R = 0$ and so all these solutions belong to the Einstein-Weyl theory. With $\beta = 0$ the differential equations (2.21, 2.22) become much simpler. In fact for the vacuum solution we can use the suitable combination

$$H_{rr} - X(r)H^\mu_\mu - Y(r)(H^\mu_\mu)^2 - Z(r)\partial_r H^\mu_\mu = 0$$

using

$$\begin{aligned} X(r) &= \frac{\alpha(2rf(r)B'(r) + B(r)(2f(r) - 2 + 3rf'(r)))}{3r^2\gamma B(r)f(r)} \\ Y(r) &= -\frac{\alpha}{6\gamma^2 f(r)} \\ Z(r) &= \frac{\alpha(rB'(r) - 2B(r))}{3r\gamma B(r)} \end{aligned} \quad (2.32)$$

that, together with $H_\mu^\mu = 0$, forms a system of two coupling second order equations

$$H_\mu^\mu = \frac{1}{2r^2 B(r)^2} \left(\gamma(-r^2 f(r) B'(r)^2 + 4B(r)^2(f(r) - 1 + rf'(r)) + rB(r)(rB'(r)f'(r) + 2f(r)(2B'(r) + rB''(r)))) \right) = 0 \quad (2.33)$$

$$\begin{aligned} H_{rr} - X(r)H_\mu^\mu - Y(r)(H_\mu^\mu)^2 - Z(r)\partial_r H_\mu^\mu &= \\ = \frac{1}{2r^4 B(r)^3 f(r)} &\left(3\alpha f(r)^2 B'(r)^3 - r^2 \alpha B(r) f(r) B'(r)^2 (3f(r) + rf(r)) + \right. \\ &- 2r^2 B(r)^2 f(r) B'(r) (-r\gamma + \alpha f'(r) + r\alpha f''(r)) + B(r)^3 (-8\alpha f(r)^2 + \right. \\ &+ r(-2r\gamma + 4\alpha f'(r) - 3r\alpha f'(r)^2) + 2f(r)(4\alpha + r^2\gamma - 2r\alpha f'(r) + \\ &\left. \left. + 2r^2\alpha f''(r)) \right) = 0 \right) \end{aligned} \quad (2.34)$$

These are still not solvable exactly so, also in this case, numerical methods must be used. Since we have two second order equations, we expect only four parameters to fix a solution for this theory.

2.4 Linearised theory and asymptotically flat solutions

In order to describe the solutions of our o.d.e. system (2.21, 2.22) we start linearising the theory. We assume that the metric can be written as $g_{\mu\nu} = \eta_{\mu\nu} + h_{\mu\nu}$, with $\eta_{\mu\nu}$ the flat Minkowski metric and $h_{\mu\nu}$ a small correction. Then we ignore the $O(h_{\mu\nu}^2)$ terms in the e.o.m. This first approach results particularly convenient since the solutions can be written in a closed form in the linearised theory.

The linearised theory is particularly suitable to describe solutions in regimes of large radius, since in such regimes we are interested in solutions that approach the flat metric, i.e. asymptotically flat solutions.

We proceed by following the derivation described in [12]. We write the metric components as

$$\begin{aligned} B(r) &= 1 + \epsilon V(r) + O(\epsilon^2) \\ f(r) &= 1 + \epsilon W(r) + O(\epsilon^2) \end{aligned} \quad (2.35)$$

and, once inserted these in $H_{\mu\nu}$, we keep only the linear order in ϵ .

In particular we use the combinations

$$H^\mu_\mu = \epsilon \left(-\frac{24\beta W(r)}{r^4} + \frac{24\beta W'(r)}{r^3} - \frac{12\beta W''(r)}{r^2} - \frac{12\beta W^{(3)}(r)}{r} + \frac{2\gamma W(r)}{r^2} + \frac{2\gamma W'(r)}{r^2} - \frac{24\beta V^{(3)}(r)}{r} - 6\beta V^{(4)}(r) + \frac{2\gamma V'(r)}{r} + \gamma V''(r) \right) \quad (2.36)$$

$$H^i_i - H^t_t = \epsilon \left(\frac{8\alpha W(r)}{3r^4} - \frac{8\alpha W'(r)}{3r^3} + \frac{4\alpha W''(r)}{3r^2} + \frac{4\alpha W^{(3)}(r)}{3r} - \frac{8\beta W(r)}{r^4} + \frac{8\beta W'(r)}{r^3} - \frac{4\beta W''(r)}{r^2} - \frac{4\beta W^{(3)}(r)}{r} - \frac{16\alpha V^{(3)}(r)}{3r} - \frac{4}{3}\alpha V^{(4)}(r) - \frac{8\beta V^{(3)}(r)}{r} - 2\beta V^{(4)}(r) + \frac{2\gamma V'(r)}{r} + \gamma V''(r) \right) \quad (2.37)$$

We now set $\epsilon = 1$ and we make the substitution

$$Y(r) = \frac{(rW(r))'}{r^2} = \frac{W'(r)}{r} + \frac{W(r)}{r^2}$$

By using the Laplacian operator for spherically symmetric functions $\nabla^2 = \frac{1}{r^2} \partial_r(r^2 \partial_r)$, the equations (2.36) and (2.37) can be written as

$$H^\mu_\mu = -12\beta \nabla^2 Y(r) + 2\gamma Y(r) - 6\beta \nabla^2 \nabla^2 V(r) + \gamma \nabla^2 V(r) \quad (2.38)$$

$$H^i_i - H^t_t = -4(\beta - \frac{1}{3}\alpha) \nabla^2 Y(r) - 2(\beta + \frac{2}{3}\alpha) \nabla^2 \nabla^2 V(r) + \gamma \nabla^2 V(r) \quad (2.39)$$

so it is possible to solve this simple form in $Y(r)$ and $V(r)$ and then come back to the metric components $B(r)$ and $f(r)$.

2.5 Vacuum solutions

For the vacuum solutions we have $H_{\mu\nu} = \frac{1}{2}T_{\mu\nu} = 0$ so the equation (2.38) can be written as

$$(\nabla^2 - m_0^2)Y(r) = -\frac{1}{2}(\nabla^2 - m_0^2)\nabla^2 V(r) \quad (2.40)$$

where we used the definition $m_0^2 = \frac{\gamma}{6\beta}$.

This is simply solved by

$$Y(r) = -\frac{1}{2}\nabla^2 V(r) + \tilde{C}_0^- \frac{e^{-m_0 r}}{r} + \tilde{C}_0^+ \frac{e^{m_0 r}}{r} \quad (2.41)$$

By inserting $Y(r)$ in (2.39) we get

$$(\nabla^2 - m_2^2)\nabla^2 V(r) = \frac{2}{3}(m_0^2 - m_2^2)(\tilde{C}_0^- \frac{e^{-m_0 r}}{r} + \tilde{C}_0^+ \frac{e^{m_0 r}}{r}) \quad (2.42)$$

where we used the definition $m_2^2 = \frac{\gamma}{2\alpha}$.

We can notice that $V(r)$ play the role of the classic gravitational potential, and the (2.42) is the generalization of $\nabla^2 V(r) = 0$.

It is easy to verify that, the solution for $V(r)$ has the form

$$V(r) = C + C_S \frac{1}{r} + C_2^- \frac{e^{-m_2 r}}{r} + C_2^+ \frac{e^{m_2 r}}{r} + C_0^- \frac{e^{-m_0 r}}{r} + C_0^+ \frac{e^{m_0 r}}{r} \quad (2.43)$$

With these solutions the metric components become

$$\begin{aligned} B(r) &= 1 + C + C_S \frac{1}{r} + C_2^- \frac{e^{-m_2 r}}{r} + C_2^+ \frac{e^{m_2 r}}{r} + C_0^- \frac{e^{-m_0 r}}{r} + C_0^+ \frac{e^{m_0 r}}{r} \\ f(r) &= 1 + C'_S \frac{1}{r} + \frac{C_2^-}{2} \frac{e^{-m_2 r}}{r} (1 + m_2 r) + \frac{C_2^+}{2} \frac{e^{m_2 r}}{r} (1 - m_2 r) + \\ &\quad - C_0^- \frac{e^{-m_0 r}}{r} (1 + m_0 r) - C_0^+ \frac{e^{m_0 r}}{r} (1 - m_0 r) \end{aligned} \quad (2.44)$$

Actually, it can be verified that the two combinations (2.36), (2.37) contain terms with $H_{rr}(r)$ and $H'_{rr}(r)$ due to the condition $\nabla^\mu H_{\mu\nu} = 0$. More precisely

$$\frac{1}{2}((2.36) + (2.37)) = H_{rr}(r) + rH'_{rr}(r) + O((W, V)^2) \quad (2.45)$$

so they form a differential equation for H_{rr} , and the solutions must be corrected with $H_{rr} = 0$ as an extra condition. This correction simply gives $C'_S = C_S$ in the (2.44).

When using the (2.44) to describe solutions in the large radius regime, in order to be consistent with the expansion (2.35) we must set,

$$C = C_0^+ = C_2^+ = 0$$

and the metric components reduce to³

$$\begin{aligned} B(r) &= 1 + C_S \frac{1}{r} + C_2^- \frac{e^{-m_2 r}}{r} + C_0^- \frac{e^{-m_0 r}}{r} \\ f(r) &= 1 + C_S \frac{1}{r} + \frac{C_2^-}{2} \frac{e^{-m_2 r}}{r} (1 + m_2 r) - C_0^- \frac{e^{-m_0 r}}{r} (1 + m_0 r) \end{aligned} \quad (2.46)$$

The potential $V(r)$ contains the classical Newtonian term, plus two Yukawa corrections.

The restriction to the Einstein-Weyl theory is obtained by setting $C_0^- = 0$ for this solution, that is equivalent to set $\beta = 0$, i.e. m_0^2 diverging.

³ $C_0^+ = 0$ and $C_2^+ = 0$ ensure asymptotic flatness, $C = 0$ corresponds to the standard time parameterization

2.5.1 Second order corrections

In order to obtain the second order corrections we proceed in the same way shown for the linearised solutions.

We use the expansion

$$\begin{aligned} B(r) &= 1 + \epsilon V(r) + \epsilon^2 V_2(r) + O(\epsilon^3) \\ f(r) &= 1 + \epsilon W(r) + \epsilon^2 W_2(r) + O(\epsilon^3) \end{aligned} \quad (2.47)$$

Once inserted it in the equation $H_{\mu\nu} = 0$, we can find the solution in a closed form ⁴, but terms like

$$C_S C_i^- e^{-m_i r} \ln(r) \quad (2.48)$$

appear, with $i = 0, 2$. These terms have a slower decrease of the Yukawa terms in (2.46), however this result is still consistent with the (2.35). Indeed, for a non-vanishing Schwarzschild coefficient C_S , the first order corrections are $O(\frac{1}{r})$ so that, when deriving the (2.46), we neglected terms of order ϵ^2 that correspond to $O(\frac{1}{r^2})$. The (2.48) has a slower decrease of the Yukawa terms but it is smaller than $\frac{1}{r^2}$ for large enough radius. When $C_S = 0$ the logarithmic terms disappear and the second order corrections reduce correctly to $O(e^{-2m_i r})$.

This discussion makes evident that the exponential corrections in the linearised solutions (2.46), with respect to the Schwarzschild term, are smaller than the terms neglected in (2.35) so that, we cannot conclude that this corrections are exactly of the exponential form reported in (2.46).

In any case some corrections to the Schwarzschild terms exist as the parameters counting suggests. Even if we do not know their exact form we have seen that, in both the first and second order solutions in ϵ , the corrections to the Schwarzschild solution decrease exponentially with r . As a matter of fact we will use anyway the (2.46) as asymptotic solutions in our numerical work since they turned out to be a powerful tool to find the behavior of the generic asymptotically flat solutions in the small radius regime.

2.6 Linearised solutions coupled with a point source and the complete linearised vacuum

In this paragraph we try to use the coupling with a point source in the linearised theory, in order to relate the solution parameters with the mass of the source.

⁴The full second order corrections are shown in [9].

The stress energy tensor of a point source is

$$T_{\mu\nu} = \begin{pmatrix} M\delta^{(3)}(\vec{r}) & 0 & 0 & 0 \\ 0 & 0 & 0 & 0 \\ 0 & 0 & 0 & 0 \\ 0 & 0 & 0 & 0 \end{pmatrix} \quad (2.49)$$

and, by using the combination (2.36), (2.37), the e.o.m. become

$$H^\mu_\mu = -12\beta\nabla^2Y(r) + 2\gamma Y(r) - 6\beta\nabla^2\nabla^2V(r) + \gamma\nabla^2V(r) = -\frac{1}{2}M\delta^{(3)}(\vec{r}) \quad (2.50)$$

$$H^i_i - H^t_t = -4(\beta - \frac{1}{3}\alpha)\nabla^2Y(r) - 2(\beta + \frac{2}{3}\alpha)\nabla^2\nabla^2V(r) + \gamma\nabla^2V(r) = \frac{1}{2}M\delta^{(3)}(\vec{r}) \quad (2.51)$$

These solutions have the same form of the (2.46), but the delta function in the origin gives the following additional constraints

$$C_S = -\frac{M}{8\pi\gamma} \quad C_0^- + C_0^+ = -\frac{M}{24\pi\gamma} \quad C_2^- + C_2^+ = \frac{M}{6\pi\gamma} \quad (2.52)$$

Once imposed asymptotic flatness, the solution becomes

$$\begin{aligned} B(r) &= 1 - \frac{M}{8\pi\gamma} \left(\frac{1}{r} - \frac{4e^{-m_2 r}}{3r} + \frac{1e^{-m_0 r}}{3r} \right) \\ f(r) &= 1 - \frac{M}{8\pi\gamma} \left(\frac{1}{r} - \frac{2e^{-m_2 r}}{3r}(1 + m_2 r) - \frac{1e^{-m_0 r}}{3r}(1 + m_0 r) \right) \end{aligned} \quad (2.53)$$

and the solutions space is reduced to one dimensional line. The physical region of the solutions should be defined as the half-line with $M > 0$. However, we cannot trust the result (2.53). The reason is that the solution form (2.46) is valid only for large radius. These functions, evaluated for small radii would give the fluctuations around the Minkowski space $\epsilon W(r) \gg 1$, $\epsilon V(r) \gg 1$ and this would be inconsistent with the method used to linearise the solution. In general relativity we have only the Schwarzschild term in the metric components, but the solution in that case is exact. In both general relativity and classical quadratic gravity we can identify the constant C_S with $-2M_N$, where M_N is the Newtonian mass that appears in the Newton's law, which is valid in the large radius regime. However, only in general relativity we can also identify C_S with $-\frac{M}{8\pi\gamma} = 2MG$, where M is the mass that appears in the stress energy-tensor that, being in the origin, is located in the small radius regime. In [11] they proposed a different method to relate the mass of the source with the Newtonian mass of the solution, giving, moreover, a new possible definition of the physical region of the solution space.

Even if the coupling with a point source is incorrect in the linearised theory, the

constraints (2.52) can be used to derive the true vacuum of the linearised theory. Indeed, the spherically symmetric solutions found till now correspond to the solutions in the vacuum for $r > 0$ and not for $r \geq 0$, since, due to the spherical symmetry we are not taking into account what happens in the origin.

In order to obtain the true vacuum solutions, it must be required that the invariant quantities are regular in the origin, or equivalently, it can be set $M = 0$ in the (2.52). In this case the linearised solutions can be used in the small radius regime and we do not impose the asymptotic flatness. The linearised metric becomes

$$\begin{aligned} B(r) &= 1 + C + 2C_0^+ \frac{\sinh(m_0 r)}{r} + 2C_2^+ \frac{\sinh(m_2 r)}{r} \\ f(r) &= 1 - 2C_0^+ \left(\frac{\sinh(m_0 r)}{r} - m_0 \cosh(m_0 r) \right) + C_2^+ \left(\frac{\sinh(m_2 r)}{r} - m_2 \cosh(m_2 r) \right) \end{aligned} \quad (2.54)$$

With an appropriate choice of the parameters this form is still consistent with (2.35) but clearly it can describe the linearised solutions only for small radius if $C_0^+, C_2^+ \neq 0$. The complete vacuum of the linearised theory has 3 free parameters. By requiring the asymptotic flatness too, the metric (2.54) simply becomes the Minkowski metric, that is the unique asymptotically flat solution in the complete vacuum.

2.7 Small radius and strong curvature regime

In this section we will see how to describe solutions in the neighborhood of a specific point. The method used is particularly adapt to describe the strong curvature regime, typically corresponding to small radii where the linearised theory fails. Together with the linearised theory, the method described in the following provides a useful tool to extract physical information without solving exactly the e.o.m.

Due to the spherical symmetry, we can distinguish between two cases: the origin $r = 0$ and any other point at $r = r_0 \neq 0$.

First we present the Frobenius method that allows us to find solutions in series form around a specific point. This was designed for linear second order differential equations, but it is also a useful way to classify the solutions of our system of coupling non-linear equations. This method was used in [12] and then in [7] to classify the static spherically symmetric solutions of classical quadratic gravity.

2.7.1 Frobenius method

We start considering a linear second order differential equation in the form

$$y''(t) + f(t)y'(t) + g(t)y(t) = 0 \quad (2.55)$$

If $f(t)$ and $g(t)$ are analytic in a neighborhood of a point t_0 , which in the following we will assume without loss of generality $t_0 = 0$, then t_0 is called an ordinary point and any solution is analytic around that point. So we can write

$$y(t) = \sum_{n=0}^{+\infty} a_n t^n \quad (2.56)$$

that converges in the same region where $f(t)$ and $g(t)$ converge.

If $f(t)$ and $g(t)$ diverge, but $F(t) = tf(t)$ and $G(t) = t^2 g(t)$ are analytic around $t = 0$, zero is called a regular singular point. Then at least one solution of the form

$$y(t) = t^s \sum_{n=0}^{+\infty} a_n t^n \quad (2.57)$$

exists, and it converges where $F(t)$ and $G(t)$ converge. a_0 is defined as the first non vanishing coefficient. We can multiply the (2.55) by t^2 , in order to remove a denominator, and we get

$$t^2 y''(t) + tF(t)y'(t) + G(t)y(t) = 0 \quad (2.58)$$

By substituting the (2.57) in (2.58), and by expanding $G(t)$ and $F(t)$, we can solve the equation order by order to fix all the coefficients, except for a_0 that remains a free parameter. The lowest order term gives

$$a_0 t^s (s^2 + s(F(0) - 1) + G(0)) = 0 \quad (2.59)$$

and, since $a_0 \neq 0$ by definition, this is a second degree equation for s , called indicial equation, and it fixes the possible series that solve the o.d.e. The indicial equation gives two roots $s_1 = \alpha, s_2 = \beta$, and we get the two series

$$y^{(\alpha)}(t) = t^\alpha \sum_{n=0}^{\infty} a_n^{(\alpha)} t^n \quad (2.60)$$

$$y^{(\beta)}(t) = t^\beta \sum_{n=0}^{\infty} a_n^{(\beta)} t^n \quad (2.61)$$

The full solution can be written as the sum

$$y(t) = C_1 y^{(\alpha)}(t) + C_2 y^{(\beta)}(t) \quad (2.62)$$

if $\beta - \alpha \notin \mathbb{Z}$. We do not give the details of the $\beta - \alpha \in \mathbb{Z}$ cases, but in such cases there are two possibilities:

- the (2.62) is still the full solution,
- assuming $\alpha \leq \beta$ only $y^{(\alpha)}(t)$ is a solution.

In the last possibility, as mentioned in [9], a second solution in series form can be found, but this time containing logarithmic term. The second solution can be written in the form

$$\begin{aligned} y(t) &= t^\alpha \sum_{n=0}^{\infty} (a_n + k_n \ln(t)) t^n \quad \text{if } \alpha = \beta \\ y(t) &= t^\alpha \left(\sum_{n=0}^{\beta-\alpha-1} d_n t^n + \sum_{n=\beta-\alpha}^{\infty} (a_n + k_n \ln(t)) t^n \right) \quad \text{if } \beta \geq \alpha, \beta - \alpha \in \mathbb{Z} \end{aligned} \quad (2.63)$$

With our system of coupled non-linear second order equations we cannot make any assumption about the convergence and uniqueness of the series obtained by this approach. However we will see that, by inserting possible solutions of the Frobenius form in our system, this will actually give a useful classification of the various families of solutions.

2.8 Solutions around the origin

In [12], they have found three main families of solutions nearby the origin using the Frobenius analysis. It has been done by inserting the series

$$\begin{aligned} A(r) &= r^s \sum_{n=0}^{\infty} a_n r^n \\ B(r) &= b_0 r^t \left(1 + \sum_{n=1}^{\infty} b_n r^n \right) \end{aligned} \quad (2.64)$$

in the e.o.m. (2.21,2.22). We proceed with the same notation, so in this paragraph we characterize the spacial component of the metric with the function $A(r) = g_{rr}(r) = f(r)^{-1}$

The indicial equation is solved for all the possible values of α and β only by the pairs

$$(s, t)_0 = \begin{cases} (0, 0)_0 \\ (1, -1)_0 \\ (2, 2)_0 \end{cases} \quad (2.65)$$

where the zero subscript indicates the solutions around the origin.

Now we give a description of the three families, their physical meaning and the number of free parameters for each of them. We expect at least one free parameter, related to the time scaling. We also use the theorem 1 to extract information about the Ricci scalar for each family.

2.8.1 The $(0, 0)_0$ family

The metric components for this family take the form

$$\begin{aligned} A(r) &= 1 + a_2 r^2 + \frac{r^4}{180\alpha\beta} (a_2(\gamma(2\alpha + 3\beta) - 36\alpha\beta b_2) + 18a_2^2\beta(10\alpha + 3\beta) - 2b_2(\gamma(\alpha - 3\beta) + 9\beta b_2(2\alpha + 3\beta))) + O(r^6) \\ B(r) &= b_0 \left(1 + b_2 r^2 + \frac{r^4}{360\alpha\beta} (54a_2^2\beta^2 + a_2(-\alpha\gamma + 108\alpha\beta b_2 + 3\beta\gamma) + b_2(\gamma(\alpha + 6\beta) + 54\beta b_2(2\alpha - \beta))) \right) + O(r^6) \end{aligned} \quad (2.66)$$

This family has 2+1 free parameters: b_0 , the time scale, and a_2 and b_2 .

It can be considered the complete vacuum of the theory. The Minkowski flat space is included in this family, as it is clearly visible by setting $b_0 = 1$, $a_2 = 0$, $b_2 = 0$. The $(0, 0)_0$ family is considered the true vacuum of the theory because it is the only one having the invariant quantities, such $R_{\mu\nu\rho\sigma}R^{\mu\nu\rho\sigma}$, regular in the origin.

For a comparison, the complete vacuum of the linearised theory (2.54) was obtained by requiring the regularity of the invariant at the origin, and it turned out to have three free parameters just like the $(0, 0)_0$ family.

We can apply the theorem 1 to this family, using as boundary only the surface of the sphere having radius $r = r_1$. By taking the limit $r_1 \rightarrow \infty$ we can say that every asymptotically flat solution of this family has $R = 0$ in the entire space, so that such solutions of the full theory must appear in the $\beta = 0$ theory too.

We report the form of the solutions for the Einstein-Weyl theory, which is equal to the (2.66) fixing $a_2 = b_2$ and taking the limit $\beta \rightarrow 0$

$$\begin{aligned} A(r) &= 1 + a_2 r^2 + \frac{(12\alpha a_2^2 + \gamma a_2)}{20\alpha} r^4 + O(r^6) \\ B(r) &= b_0 \left(1 + a_2 r^2 + \frac{(24\alpha a_2^2 + \gamma a_2)}{40\alpha} r^4 + O(r^6) \right) \end{aligned} \quad (2.67)$$

In the Einstein-Weyl theory the vacuum solutions have 1+1 free parameters and the Minkowski space is the only asymptotically flat solution of this family.

2.8.2 The $(1, -1)_0$ family

The first orders of this family are

$$\begin{aligned} A(r) &= a_1 r - a_1^2 r^2 + a_1^3 r^3 + a_4 r^4 - \frac{1}{16} (a_1(3a_1 b_2 + 19a_1^4 + 35a_4)) r^5 + O(r^6) \\ B(r) &= b_{-1} \left(\frac{1}{r} + a_1 + b_2 r^2 + \frac{1}{16} (a_1 b_2 + a_1^4 + a_4) r^3 + O(r^4) \right) \end{aligned} \quad (2.68)$$

The free parameters are 1+3: b_{-1}, a_1, b_2, a_4 . The Schwarzschild solution belongs to this family with $b_{-1} = -r_s, a_1 = -\frac{1}{r_s}, a_4 = -\frac{1}{r_s^4}, b_2 = 0$, but we will see that many other solutions belong to this family, most of them without horizon. The indicial structure makes the invariant $R_{\mu\nu\rho\sigma}R^{\mu\nu\rho\sigma}$ singular at the origin, and it goes like $O(r^{-6})$ for r going to zero.

We can use the theorem 1, this time by taking as boundary the surface of a sphere with large radius and the surface of the sphere with $r = \epsilon \ll 1$, in order to avoid the singular point $r = 0$. The boundary term $C(r) = \sqrt{B(r)A(r)}r^2R\partial_rR$ for $r = \epsilon$ goes like $O(\epsilon^3)$, so again the asymptotically flat solutions belonging to this family have $R = 0$, and we can restrict to the $\beta = 0$ theory when looking for such solutions.

In the $\beta = 0$ theory, this family reduces to

$$\begin{aligned} A(r) &= a_1r - a_1^2r^2 + a_1^3r^3 + \left(\frac{5}{3}a_1b_2 - a_1^4\right)r^4 + \left(a_1^5 - \frac{23}{6}a_1^2b_2\right)r^5 + O(r^6) \\ B(r) &= b_{-1} \left(\frac{1}{r} + a_1 + b_2r^2 + \frac{1}{6}a_1b_2r^3 + O(r^4) \right) \end{aligned} \quad (2.69)$$

which has 2+1 free parameters. It is equal to (2.68) fixing $a_4 = \frac{5}{3}a_1b_2 - a_1^4$ and taking the limit $\beta \rightarrow 0$.

2.8.3 The $(2,2)_0$ family

The first terms of this family are

$$\begin{aligned} A(r) &= a_2r^2 + a_2b_3r^3 - \frac{a_2}{6}(2a_2 + b_3^2 - 8b_4)r^4 + a_5r^5 + \\ &+ \frac{1}{1296\alpha\beta} \left(-12\alpha^2a_2^3 - 2a_2^2(b_3^2(\alpha^2 - 603\alpha\beta - 252\beta^2) + 27\alpha(20\beta b_4 + \gamma)) + \right. \\ &+ a_2(b_3^4(-16\alpha^2 + 1413\alpha\beta - 72\beta^2) + 2b_4b_3^2(19\alpha^2 - 2223\alpha\beta + 180\beta^2) + \\ &- 36b_5b_3(\alpha^2 + 45\beta^2) + 12\alpha b_4^2(\alpha + 162\beta)) + 324\beta a_5b_3(7\alpha + 3\beta) \Big) r^6 + O(r^7) \quad (2.70) \\ B(r) &= b_2 \left(r^2 + b_3r^3 + b_4r^4 + b_5r^5 + \frac{1}{216\alpha a_2} \left(a_2^2(14b_3^2(2\alpha + 3\beta) - 24\alpha b_4) + \right. \right. \\ &- 12\alpha a_2^3 + a_2(2b_3^4(67\alpha - 3\beta) + 2b_4b_3^2(-227\alpha + 15\beta) + 45b_5b_3(7\alpha - 3\beta) + \\ &\left. \left. + 180\alpha b_4^2) + 27a_5b_3(\alpha + 3\beta) \right) r^6 + O(r^7) \right) \end{aligned}$$

This is a completely new family: no G.R. solution belongs to this family. It has 5+1 free parameters, the total number of the theory: $b_2, a_2, b_3, b_4, b_5, a_5$.

These solutions were largely studied by B. Holdom, and in [5] he found that a subfamily of the $(2,2)_0$ could be the most suitable family of solutions to be coupled with a compact matter source.

The Kretschmann scalar $R_{\mu\nu\rho\sigma}R^{\mu\nu\rho\sigma}$ is singular at the origin, and goes like r^{-8} as r goes to zero.

In this case the boundary term $C(r) = \sqrt{B(r)A(r)}r^2R\partial_rR$ for $r = \epsilon$ goes like $O(\epsilon^{-1})$ and the theorem1 cannot be applied, so we expect to find $(2, 2)_0$ asymptotically flat solutions in the full theory that are not in the $\beta = 0$ restriction.

We give the form of the solutions for the $\beta = 0$ case

$$\begin{aligned} A(r) &= a_2r^2 + a_2b_3r^3 - \frac{a_2}{6}(2a_2 + b_3^2 - 8b_4)r^4 + \\ &- \frac{1}{18\alpha b_3}a_2(10\alpha a_2^2 + a_2(11\alpha b_3^2 + 45\gamma) + \alpha(12b_3^4 - 25b_4b_3^2 - 10b_4^2))r^5 + \\ &- \left(a_2(140\alpha a_2^2 + 10a_2(2\alpha b_3^2 + 12\alpha b_4 + 63\gamma) + \alpha(11b_3^4 + 144b_4b_3^2 - 356b_4^2))\right)r^6 + O(r^7) \\ B(r) &= b_2\left(r^2 + b_3r^3 + b_4r^4 + \right. \\ &- \frac{1}{18\alpha b_3}a_2(6\alpha a_2^2 + a_2(\alpha b_3^2 + 27\gamma) + \alpha(8b_3^4 - 19b_4b_3^2 - 6b_4^2))r^5 + \\ &\left.\frac{1}{36}\left(-\frac{a_2}{\alpha}(\alpha b_3^2 + 4\alpha b_4 + 90\gamma) - 22a_2^2 - 4b_3^4 - 14b_4b_2\right)r^6 + O(r^7)\right) \end{aligned} \tag{2.71}$$

which is equal to (2.70) fixing

$$\begin{aligned} a_5 &= -\frac{1}{18\alpha b_3}a_2(10\alpha a_2^2 + a_2(11\alpha b_3^2 + 45\gamma) + \alpha(12b_3^4 - 25b_4b_3^2 - 10b_4^2)) \\ b_5 &= -\frac{1}{18\alpha b_3}a_2(6\alpha a_2^2 + a_2(\alpha b_3^2 + 27\gamma) + \alpha(8b_3^4 - 19b_4b_3^2 - 6b_4^2)) \end{aligned} \tag{2.72}$$

and taking the limit $\beta \rightarrow 0$. Again, it has the total number of parameters of the theory.

2.8.4 Generalized Frobenius solutions

In [9] another family of solutions is found. Taking inspiration from the Frobenius solutions (2.63), they tried as possible form

$$\begin{aligned} A(r) &= r^s(a_0 + p_0 \ln(r) + a_1r + p_1r \ln(r) + a_2r^2 + p_2r^2 \ln(r) + ..) \\ B(r) &= r^t(b_0 + q_0 \ln(r) + b_1r + q_1r \ln(r) + b_2r^2 + q_2r^2 \ln(r) + ..) \end{aligned} \tag{2.73}$$

They found that the logarithmic terms cannot appear in the leading order, and that the indicial equation is satisfied by the same pairs of (s, t) mentioned before. In the analysis of the possible extended family, the $(2, 2)_0$ and $(0, 0)_0$ should not present any possible new term: this because the $(2, 2)_0$ family has already the total number of free parameters, while the other one has the same number of parameters of the vacuum solutions in the linearised case so again we do not expect any other

free term. On the contrary, they found that logarithmic terms can appear in the $(1, -1)_0$ family starting from the third order. If such terms are included, since our system is non-linear, also terms of the kind $\ln(r)^2$ must appear starting from the sixth order. The solutions must be generalized in order to include them. The final form of this family can be written as

$$\begin{aligned} A(r) &= r(a_0 + a_1r + a_2r^2 + \dots)(1 + c_3 \ln(r)r^3 + c_6 \ln(r)^2 r^6 + \dots) \\ B(r) &= r^{-1}(b_0 + b_1r + b_2r^2 + \dots)(1 + d_3 \ln(r)r^3 + d_6 \ln(r)^2 r^6 + \dots) \end{aligned} \quad (2.74)$$

It results that these solutions have 4+1 free parameters and the restriction to the $\beta = 0$ theory is equal to (2.69), which does not contain any logarithmic term. Indeed in [9] they checked that in the Einstein-Weyl case all the logarithmic terms must vanish till the ninth order.

In conclusion, these are all the solution families around the origin found until now. In the previous works several other ansatz have been tried. Even if many of these trials cannot be excluded at all, no other family was positively confirmed.

2.9 Solutions around $r_0 \neq 0$

Following the same method we can study the solutions as series expansion around a point corresponding to a non-zero radius. In this case we come back to the metric in the form

$$\begin{aligned} f(r) &= (r - r_0)^s \sum_{n=0}^{\infty} a_n (r - r_0)^n \\ B(r) &= b_0 (r - r_0)^t \left(1 + \sum_{n=1}^{\infty} b_n (r - r_0)^n \right) \end{aligned} \quad (2.75)$$

to classify the various families: this because in this work we will focus on describing the solutions having a singularity in $r = r_0$, which will correspond to $f(r)$ vanishing in r_0 , so it results convenient to use the metric written in terms of $f(r)$ instead of $A(r)$. We specify here that we call the point $r_0 \neq 0$ "singular", even if in this case it is about a singularity of the o.d.e. system (i.e. a singularity in this coordinate system) and it is not a singularity of the metric itself. Indeed we will see that invariants stay regular at this point.

In this case, for generic α and β , the indicial equation admits only the pairs

$$(s, t)_{r_0} = \begin{cases} (0, 0)_{r_0} \\ (1, 1)_{r_0} \\ (1, 0)_{r_0} \end{cases} \quad (2.76)$$

where the subscript indicates the expansion around $r_0 \neq 0$. The $(0, 0)_{r_0}$ family has the full number of parameters and corresponds to a regular point where nothing particular happens.

We give the details just for the last two families, and for the other non-Frobenius families found.

2.9.1 Black hole solutions

The $(1, 1)_{r_0}$ family corresponds to the solutions close to an horizon. The first terms are

$$\begin{aligned} f(r) &= f_1(r - r_0) + f_2(r - r_0)^2 + O((r - r_0)^3) \\ B(r) &= b_1 \left(r - r_0 + \frac{1}{9\beta f_1 r_0^2 (\alpha - 3\beta)} \left(\pm \left((\alpha - 3\beta)(144\beta^2(\alpha - 3\beta) + \gamma^2 r_0^4(\alpha - 3\beta) + \right. \right. \right. \right. \\ &\quad \left. \left. \left. \left. - 24\beta\gamma r_0^2(\alpha + 6\beta)) + 72\beta f_1 r_0 \left(2\beta f_1 r_0(\alpha + 3\beta)^2 - (\alpha - 3\beta)(4\beta(\alpha - 3\beta) + \right. \right. \right. \\ &\quad \left. \left. \left. + 8\alpha\beta f_2 r_0^2 + \gamma r_0^2(-(\alpha + 2\beta))) \right) \right)^{\frac{1}{2}} + r_0^2(\alpha - 3\beta)(\gamma - 3\beta f_2) + \right. \\ &\quad \left. \left. \left. \left. + 12\beta f_1 r_0(\alpha + 3\beta) \right) (r - r_0)^2 + O((r - r_0)^3) \right) \right) \end{aligned} \tag{2.77}$$

It has 3+1 free parameters: b_1 the time scale, f_1 , f_2 , and the location of the horizon r_0 . We have already seen that in r_0 the boundary term of the theorem 1 vanishes: for this reason any asymptotically flat solution with horizon has $R = 0$ outside the horizon so, again, any of these solutions of the full quadratic theory belong to the Einstein-Weyl theory too.

The Schwarzschild solution belongs to this family with $r_0 = \frac{1}{f_1} = \frac{1}{b_1} = 2GM_N$ but we will see that new solutions with horizon are present.

For the Einstein-Weyl theory, the solutions can be obtained by fixing

$$f_2 = \frac{3\gamma}{8\alpha} + \frac{\frac{-3\gamma}{8\alpha f_1} - 2f_1}{r_0} + \frac{1}{r_0^2}$$

and by taking the limit $\beta \rightarrow 0$. In this case the metric components take the form

$$\begin{aligned} f(r) &= f_1(r - r_0) + \left(\frac{3\gamma}{8\alpha} + \frac{\frac{-3\gamma}{8\alpha f_1} - 2f_1}{r_0} + \frac{1}{r_0^2} \right) (r - r_0)^2 + O((r - r_0)^3) \\ B(r) &= b_1 \left(r - r_0 + \frac{1}{8f_1^2 r_0^2 \alpha} \left(\gamma r_0 - f_1(-8\alpha + 16\alpha f_1 r_0 + \gamma r_0^2) \right) (r - r_0)^2 + O((r - r_0)^3) \right) \end{aligned} \tag{2.78}$$

We report the Kretschmann scalar only for the $\beta = 0$ case, since it has a more compact form, that is

$$R_{\mu\nu\rho\sigma}R^{\mu\nu\rho\sigma} = \frac{8 + 4f_1r_0(-4 + 5f_1r_0)}{r_0^4} + O(r - r_0) \quad (2.79)$$

It is regular in $r = r_0$ like the other invariant quantities of this family, and the same regularity is found in the general $\beta \neq 0$ case.

2.9.2 The $(1, 0)_{r_0}$ family: wormhole solutions

The $(1, 0)_{r_0}$ family corresponds to solutions close to something different from an horizon. Due to the indicial structure, at $r = r_0$ the $f(r)$ component goes to zero but the $B(r)$ component does not. The first terms of this family are

$$\begin{aligned} f(r) &= f_1(r - r_0) + \frac{1}{18\alpha\beta f_1 r_0^2(\alpha - 3\beta)} \left(12\alpha^2\beta f_1 - 72\alpha\beta^2 f_1 + 108\beta^3 f_1 + \right. \\ &\quad \pm (\gamma r_0(\alpha - 3\beta) - 6\beta f_1(2\alpha + 3\beta)) \sqrt{27\alpha\beta f_1^2 r_0^2 + 2(\alpha - 3\beta)(2\alpha - 6\beta - 3\gamma r_0^2)} + \\ &\quad + 9\alpha^2\beta f_1^2 r_0 - 3\alpha^2\gamma f_1 r_0^2 + 135\alpha\beta^2 f_1^2 r_0 + 27\beta^2\gamma f_1 r_0^2 + \\ &\quad \left. + 2\gamma r_0(\alpha - 3\beta)^2 \right) (r - r_0)^2 + O((r - r_0)^3) \\ B(r) &= b_0 \left(1 + \frac{2}{f_1 r_0^2(\alpha - 3\beta)} (r - r_0)(f_1 r_0(\alpha + 6\beta) + \right. \\ &\quad \mp \sqrt{27\alpha\beta f_1^2 r_0^2 + 2(\alpha - 3\beta)(2\alpha - 6\beta - 3\gamma r_0^2)}) + O((r - r_0)^2) \left. \right) \end{aligned} \quad (2.80)$$

It has 1+2 free parameters: b_0 , r_0 , f_1 .

For such metric the Kretschmann scalar is regular around r_0 and takes the value

$$R_{\mu\nu\rho\sigma}R^{\mu\nu\rho\sigma} = \frac{1}{4}b_1^2 f_1^2 + \frac{4 + 2f_1^2 r_0^2}{r_0^4} + O(r - r_0) \quad (2.81)$$

where

$$b_1 = \frac{2}{f_1 r_0^2(\alpha - 3\beta)} (f_1 r_0(\alpha + 6\beta) \mp \sqrt{27\alpha\beta f_1^2 r_0^2 + 2(\alpha - 3\beta)(2\alpha - 6\beta - 3\gamma r_0^2)})$$

For this solution the boundary term $C(r)$ of the theorem 1 goes as $O(\sqrt{r - r_0})$ and we can restrict to the $\beta = 0$ theory when looking for asymptotically flat solutions. The Einstein Weyl restriction of this family is

$$\begin{aligned} f(r) &= f_1 \left(r - \frac{4\alpha f_1}{2\gamma + 3\alpha f_1^2} \right) + \frac{\gamma}{4\alpha^2 f_1^2 r_0^2} (2\gamma + \alpha f_1^2) \left(r - \frac{4\alpha f_1}{2\gamma + 3\alpha f_1^2} \right)^2 + O((r - \frac{4\alpha f_1}{2\gamma + 3\alpha f_1^2})^3) \\ B(r) &= b_0 \left(1 + \left(r - \frac{4\alpha f_1}{2\gamma + 3\alpha f_1^2} \right) \left(\frac{\gamma^2}{\alpha^2 f_1^3} + \frac{\gamma}{\alpha f_1} - \frac{3f_1}{4} \right) + O((r - \frac{4\alpha f_1}{2\gamma + 3\alpha f_1^2})^2) \right) \end{aligned} \quad (2.82)$$

where r_0 and b_1 are forced to be functions of f_1 , hence only 1+1 free parameters remain: b_0 the time scaling, and f_1 . In particular

$$r_0 = \frac{4\alpha f_1}{2\gamma + 3\alpha f_1^2} \quad (2.83)$$

We can invert this relation finding

$$f_1 = \frac{2\alpha \pm \sqrt{4\alpha^2 - 6\alpha\gamma r_0^2}}{3\alpha r_0} \quad (2.84)$$

Only for $r_0 \leq \sqrt{\frac{2\alpha}{3\gamma}}$, the parameter f_1 is real, so this family can describe only objects with a radius smaller than this quantity. In the (2.80) a similar constraint on the parameters is present due to the square root, but in that case it involves f_1 too. By imposing the argument of the square root to be positive, we get

$$\begin{cases} r_0^2 \leq \frac{4(\alpha-3\beta)^2}{6(\alpha-3\beta)\gamma - 27\alpha\beta f_1^2} & \text{if } f_1^2 < \frac{6(\alpha-3\beta)}{27\alpha\beta} \\ \text{no constraint} & \text{if } f_1^2 \geq \frac{6(\alpha-3\beta)}{27\alpha\beta} \end{cases} \quad (2.85)$$

so in the full quadratic theory the solutions of this family can have r_0 arbitrary large.

The particular indicial structure of these solutions gives rise to the following interpretation. Let us consider a radial geodesic that enters in r_0 from larger radius. We use the Lagrangian formalism to derive the geodesic equation. The action of an observer in our static spherically symmetric metric is

$$\begin{aligned} S &= \int d\lambda \left(\frac{dx^\mu}{d\lambda} \frac{dx^\nu}{d\lambda} g_{\mu\nu} \right) = \\ &= \int d\lambda \left(-B(r) \left(\frac{dt}{d\lambda} \right)^2 + \frac{1}{f(r)} \left(\frac{dr}{d\lambda} \right)^2 + r^2 \left(\frac{d\theta}{d\lambda} \right)^2 + r^2 \sin(\theta)^2 \left(\frac{d\phi}{d\lambda} \right)^2 \right) \end{aligned} \quad (2.86)$$

and the equations of motion is

$$\frac{d}{d\lambda} \left(\frac{\partial L}{\partial \dot{x}^\mu} \right) = \frac{\partial L}{\partial x^\mu} \quad (2.87)$$

where the dot indicates the derivation with respect to λ . Considering a radial geodesic (i.e. $d\phi = 0$ $d\theta = 0$) we can ignore the equations for the coordinates θ and ϕ , so we must solve just the two remaining equations. Instead of the equation for the radius, we take the four-velocity condition and we restrict to the two main physical cases: the mass-less particle (null geodesic) and the massive particle (time-

like geodesic). We have to solve the system

$$\begin{aligned} \frac{d}{d\lambda}(-2B(r)\dot{t}) &= 0 \\ -B(r)\dot{t}^2 + \frac{1}{f(r)}\dot{r}^2 &= \begin{cases} 0 & \text{for a mass-less particle} \\ -1 & \text{for a massive particle if } \lambda = \tau \text{ the proper time} \end{cases} \end{aligned} \quad (2.88)$$

The first one is simply solved by

$$\dot{t} = \frac{1}{B(r)}K \quad (2.89)$$

where we choose $K > 0$ in order to have $\frac{dt}{d\lambda} > 0$ for $r > r_0$. Here we are assuming for $r > r_0$ to have the Minkowski signature, so we have $B(r) > 0$, $f(r) > 0$, $b_0 > 0$, $f_1 > 0$. The second equation becomes

$$-\frac{1}{B(r)}K^2 + \frac{1}{f(r)}\dot{r}^2 = \begin{cases} 0 & \text{if } m = 0 \\ -1 & \text{if } m > 0 \text{ and } \lambda = \tau \end{cases} \quad (2.90)$$

and it is solved by

$$\dot{r} = \begin{cases} \pm K \sqrt{\frac{f(r)}{B(r)}} & \text{if } m = 0 \\ \pm \sqrt{-f(r) + K^2 \frac{f(r)}{B(r)}} & \text{if } m > 0 \text{ and } \lambda = \tau \end{cases} \quad (2.91)$$

The sign before the root corresponds to an entering or outgoing geodesic. The constant of integration K measures the energy of the particle. This is clearly visible in the massive case. Indeed, when imposing asymptotic flatness for large radius, $f(r)$ and $B(r)$ approach 1, and the square root in the second equation of the (2.91) is real for an arbitrary large value of r only if $K^2 \geq 1$. $K^2 = 1$ clearly corresponds to the escape energy, instead, for $K^2 < 1$ an outgoing massive particle with $\dot{r} > 0$ would reach a maximum r^* where $\dot{r} = 0$, i.e. r^* would be a reversal point of the motion. For radius close to r_0 , when inserting the metric (2.80) in the (2.91) we can already see two differences with respect to usual horizons:

- $r = r_0$ is a reversal point of the motion, since $\dot{r} = 0$ in r_0 . This does not happen with the Schwarzschild metric or with the more general horizons (2.77), since for such metric the ratio $\frac{f(r)}{B(r)}$ does not vanish for $r \rightarrow r_0$.
- For the massive particle there is a minimum energy required to arrive at $r = r_0$, since, for r larger and close to r_0 , the argument of the square root is positive only if $K^2 > b_0$. On the contrary, in the horizon case, the non-vanishing and positive ratio $\frac{f(r)}{B(r)}$ ensures that the square root is real around r_0 for any value

of K . More generically, by requiring the argument of the square root to be positive, we must have $K^2 \geq B(r)$ for all the radius corresponding to the range of motion of the particle.

Considering the mass-less case, for the entering geodesic we can integrate the (2.91) to obtain

$$\lambda = -\frac{1}{K} \int dr \sqrt{\frac{B(r)}{f(r)}} + \text{cost} \quad (2.92)$$

Now we can see what happens near r_0 . By substituting the metric components with the (2.80) in the (2.92) we have

$$\begin{aligned} \lambda &= -\frac{1}{K} \int dr \sqrt{\frac{b_0(1 + b_1(r - r_0) + O((r - r_0)^2))}{f_1(r - r_0) + O((r - r_0)^2)}} + \text{cost} = \\ &= -\frac{1}{K} \int dr \sqrt{\frac{b_0}{f_1(r - r_0)}} \left(1 + O(r - r_0)\right) + \text{cost} = \\ &= -\frac{2}{K} \sqrt{\frac{b_0(r - r_0)}{f_1}} + O((r - r_0)^{\frac{3}{2}}) + \text{cost} \end{aligned} \quad (2.93)$$

We make the substitution $\rho = \sqrt{r - r_0}$, so the (2.93) becomes

$$\lambda = -\frac{2}{K} \sqrt{\frac{b_0}{f_1}} \left(\rho(\lambda) - \rho(0)\right) + O(\rho^3) \quad (2.94)$$

This equation tells us that a continuous path along increasing λ , starting from $r > r_0$ and $\rho > 0$, goes through the point $r = r_0$ i.e. $\rho = 0$, and then it continues in a region with again $r > r_0$, but with $\rho < 0$. This is why this kind of objects can be interpreted as traversable wormholes. A free-falling observer will never reach the region $r < r_0$, but he will end up in a copy of the $r > r_0$ region. The point $r = r_0$ turns out to be a reversal point of the motion for the coordinate r , but not for the coordinate ρ .

This family is invariant under the transformation $\rho \rightarrow -\rho$, so we could say that the regions $\rho < 0$ and $\rho > 0$ are the same, but we will see in the following that it exists a generalization of this family where the wormhole interpretation is still valid but the metric is not invariant under $\rho \rightarrow -\rho$. For this reason we have to consider $r > r_0$, $\rho > 0$ and $r > r_0$, $\rho < 0$ as two distinct regions. The case of a massive observer has the same interpretation, and the (2.94) becomes

$$\tau = -2 \sqrt{\frac{b_0}{f_1(-b_0 + K^2)}} \left(\rho(\tau) - \rho(0)\right) + O(\rho^3) \quad (2.95)$$

Here we can see that the observer goes through $\rho = 0$ in a finite interval of proper time. Unlike the black hole case, this also happens in a finite interval of the time coordinate t for both the mass-less particle and massive observer

$$t = \int dr \frac{\dot{t}}{\dot{r}} = \begin{cases} - \int dr \frac{1}{\sqrt{f(r)B(r)}} = -\frac{1}{\sqrt{b_0 f_1}}(\rho(t) - \rho(0)) + O(\rho^{\frac{3}{2}}) \\ - \int dr \frac{K}{\sqrt{-f(r)B(r)^2 + K^2 f(r)B(r)}} = -\frac{K}{\sqrt{(-b_0 + K^2)b_0 f_1}}(\rho(t) - \rho(0)) + O(\rho^{\frac{3}{2}}) \end{cases} \quad (2.96)$$

2.9.3 Non-Frobenius solutions

In [7] other two families of solution around a non-zero radius are found. These are a generalization of the Frobenius series, obtained by looking for solutions in series expansion of the variable $\rho = \sqrt{r - r_0}$. We give a description of this two family.

2.9.4 The $(\frac{3}{2}, \frac{1}{2})_{r_0,1/2}$ family

The metric components of this family have the form

$$\begin{aligned} f(r) &= f_{3/2}(r - r_0)^{\frac{3}{2}} + O((r - r_0)^2) \\ B(r) &= b_{1/2}\left(\sqrt{r - r_0} + O(r - r_0)\right) \end{aligned} \quad (2.97)$$

and the series proceed with semi-integer step in powers of $(r - r_0)$. It has 1+2 free parameters $b_{1/2}$, $f_{3/2}$ and r_0 . The boundary term of the theorem 1 for this family is $C(r) = O(\sqrt{r - r_0})$ but it does not appear in the Einstein-Weyl theory. Indeed the Ricci scalar is non-vanishing for $r > r_0$ for this family. To avoid contradiction with the theorem 1, if there is the Minkowski signature, this family cannot have asymptotically flat solution or, more generically, the quantity $C(r)$ cannot be zero for $r_0 < r < \infty$.

If we insert this kind of metric in equations (2.92) and (2.96), with the substitution $\sqrt{r - r_0} = \rho$, we can see that a path along increasing λ goes from $\rho > 0$ to $\rho < 0$ just like in the case of the $(1, 0)_{r_0}$ family. These two regions both correspond again to the two copies of $r > r_0$. However, the passage through $\rho = 0$ does not happen in a finite interval of the time coordinate t . Indeed with this substitution the metric take the $(1, 1)$ form written in the variable ρ

$$ds^2 = g_{\mu\nu}dx^\mu dx^\nu = -b_{1/2}(\rho + O(\rho^2))dt^2 + \frac{1}{f_{3/2}\rho + O(\rho^2)}d\rho^2 + \rho^4 d\Omega^2 \quad (2.98)$$

so that, $r = r_0$ ($\rho = 0$) can be seen as an horizon between the two region $\rho > 0$ and $\rho < 0$, and a radial geodesic in this metric has the same characteristics of that one in the Schwarzschild case. These solutions cannot be asymptotically flat:

actually this can be proved at most for one of the two region with $r > r_0$ since the signature changes from a patch to the other. We do not give any further physical interpretation for these unusual horizons. As a confirmation, no asymptotically flat solution that belongs to this family was found with our numerical methods.

2.9.5 The $(1, 0)_{r_0, 1/2}$ family: generic wormholes

The solutions of this family have the same indicial structure of the $(1, 0)_{r_0}$ family but, again, the series proceed with semi-integer step in powers of $(r - r_0)$. The first terms are

$$\begin{aligned} f(r) &= f_1(r - r_0) + f_{3/2}(r - r_0)^{\frac{3}{2}} + O((r - r_0)^2) \\ B(r) &= b_0 \left(1 + b_{1/2}(r - r_0)^{\frac{1}{2}} + b_1(r - r_0) + O((r - r_0)^{\frac{3}{2}}) \right) \end{aligned} \quad (2.99)$$

It has the full number of free parameters of the theory: $b_0, b_{1/2}, b_1, f_1, f_{3/2}, r_0$. For such metric the Kretschmann scalar is regular around r_0 and takes the value

$$\begin{aligned} R_{\mu\nu\rho\sigma}R^{\mu\nu\rho\sigma} &= \frac{b_{1/2}^2 f_{3/2}^2 r_0^4 - 2b_{1/2}(b_{1/2}^2 - 4b_1)f_1 f_{3/2} r_0^4 + f_1^2 ((b_{1/2}^2 - 4b_1)^2 r_0^4 + 128r_0^2) + 256}{64r_0^4} + \\ &+ O(\sqrt{r - r_0}) \end{aligned} \quad (2.100)$$

The boundary term $C(r_0)$ of the theorem 1 does not vanish in general, so, from this and from the full number of parameters, we expect possible asymptotically flat solutions belonging to this family that are in the $\beta \neq 0$ theory but that are not in the Einstein-Weyl theory. The restriction to the Einstein-Weyl theory is

$$\begin{aligned} f(r) &= f_1(r - r_0) + \frac{(\alpha f_1^2 r_0 (b_{1/2}^2 r_0 + 12) - 16\alpha f_1 + 8\gamma r_0)}{3\alpha b_{1/2} f_1 r_0^2} (r - r_0)^{\frac{3}{2}} + O((r - r_0)^2) \\ B(r) &= b_0 \left(1 + b_{1/2}(r - r_0)^{\frac{1}{2}} + \frac{(\alpha f_1^2 r_0 (b_{1/2}^2 r_0 - 9) + 8\alpha f_1 + 2\gamma r_0)}{3\alpha f_1^2 r_0^2} (r - r_0) + \right. \\ &\left. + O((r - r_0)^{\frac{3}{2}}) \right) \end{aligned} \quad (2.101)$$

which is equal to the (2.99) fixing

$$\begin{aligned} f_{3/2} &= \frac{(\alpha f_1^2 r_0 (b_{1/2}^2 r_0 + 12) - 16\alpha f_1 + 8\gamma r_0)}{3\alpha b_{1/2} f_1 r_0^2} \\ b_1 &= \frac{(\alpha f_1^2 r_0 (b_{1/2}^2 r_0 - 9) + 8\alpha f_1 + 2\gamma r_0)}{3\alpha f_1^2 r_0^2} \end{aligned} \quad (2.102)$$

and taking the limit $\beta \rightarrow 0$. It still has the total number of free parameters of the theory. Due to the same indicial structure, the wormhole interpretation is still valid

for this family, but this time the metric is not invariant under the transformation $\rho \rightarrow -\rho$ so we have to distinguish between the two regions. From the geodesic equations found previously, a free falling observer with $\dot{r} < 0$ inverts his motion at r_0 but he continues the motion in a different copy of $r > r_0$. We will see in section 6 it is possible to study numerically the general features of this new region of the space-time.

Imposing asymptotic flatness for both the $\rho > 0$ and $\rho < 0$ patches corresponds to two independent constraints.

When studying this family of solutions we can use the theorem 1 referred to the coordinate ρ instead of the radius. The metric signature and the equations 2.27 are invariant under change of coordinates, but when we substitute r with ρ we cannot extend the domain anymore in the $r < r_0$ region, instead we can integrate through the new $\rho < 0$ region. The theorem is still valid and, when looking for asymptotically flat solutions in both the patches, it implies that these solutions must have $R = 0$ for $r \geq r_0$ in both the regions $\rho \geq 0$ and $\rho \leq 0$, so we can restrict to the Einstein-Weyl theory when looking for such solutions.

The $(1, 0)_{r_0}$ is clearly a particular case of this wider family. From the parameters counting it seems that the asymptotically flat solutions belonging to the $(1, 0)_{r_0}$ family correspond to solutions of the $(1, 0)_{r_0,1/2}$ family, when asymptotic flatness is imposed on both patches. Indeed, in both cases we should have a unique solution: the $(1, 0)_{r_0}$ family has three free parameters that are fixed with the three conditions of asymptotic flatness, and the six parameters of the $(1, 0)_{r_0,1/2}$ family are fixed by the six conditions of asymptotic flatness on both patches. This is confirmed by our numerical study and an analogous result was found in [9], where a unique asymptotically flat solution for the $(1, 0)_{r_0}$ is obtained.

In section 6 we studied asymptotically flat solutions belonging to the $(1, 0)_{r_0,1/2}$ family in the Einstein-Weyl theory by imposing asymptotic flatness only to one patch.

It could seem that the $(1, 0)_{r_0}$ is obtained by taking $b_{1/2} \rightarrow 0$ and $f_{3/2} \rightarrow 0$ (and only $b_{1/2} \rightarrow 0$ in the Einstein-Weyl theory), since it does not contain any semi-integer order. Actually, from our numerical results in the Einstein-Weyl theory, we have seen that the correct limit of $b_{1/2} \rightarrow 0$ is a more general subfamily. In our solution space an entire line of solutions with $b_{1/2} = 0$ seems to belong to this subfamily (and only one point of this line truly belongs to the $(1, 0)_{r_0}$). We describe it in the following.

2.9.6 A new subfamily of the $(1, 0)_{r_0,1/2}$

In Einstein-Weyl gravity, taking the limit $b_{1/2} \rightarrow 0$ for the $(1, 0)_{r_0,1/2}$ family forces the parameter f_1 to be function of r_0 : in particular the relation (2.84) has to

be satisfied. If not, divergences appear due to the factor $b_{1/2}$ in the denominators of the coefficients in (2.101). More precisely, we must have

$$f_1 - \frac{2\alpha \pm \sqrt{4\alpha^2 - 6\alpha\gamma r_0^2}}{3\alpha r_0} \rightarrow 0 \quad (2.103)$$

as $b_{1/2}$ goes to 0, but actually there are no constraints on the limit of the quantity

$$\frac{f_1 - \frac{2\alpha \pm \sqrt{4\alpha^2 - 6\alpha\gamma r_0^2}}{3\alpha r_0}}{b_{1/2}} \rightarrow l \quad (2.104)$$

apart from $|l| < \infty$. The relation (2.102) for $f_{3/2}$ shows that this coefficient is proportional to the quantity in (2.104), that remains undetermined in the limit $b_{1/2} \rightarrow 0$. So in the $\beta = 0$ case a "new" family of solutions with the same indicial structure of the $(1, 0)_{r_0}$ family exists, with $f_1 = \frac{2\alpha \pm \sqrt{4\alpha^2 - 6\alpha\gamma r_0^2}}{3\alpha r_0}$, but with $f_{3/2}$ free. These solutions can be directly derived by inserting the series

$$\begin{aligned} f(r) &= f_1(r - r_0) + f_{3/2}(r - r_0)^{\frac{3}{2}} + f_2(r - r_0)^2 + f_{5/2}(r - r_0)^{\frac{5}{2}} + O((r - r_0)^3) \\ B(r) &= b_0 \left(1 + b_1(r - r_0) + b_{3/2}(r - r_0)^{\frac{3}{2}} + b_2(r - r_0)^2 + O((r - r_0)^{\frac{5}{2}}) \right) \end{aligned} \quad (2.105)$$

in the system (2.33, 2.34). Once the e.o.m. are written in power series of $\sqrt{r - r_0}$, two of the first equations that involve the coefficients f_1 and $f_{3/2}$ are not independent, and both are satisfied by (2.84), leaving $f_{3/2}$ as a free parameter. The first terms of this family are

$$\begin{aligned} f(r) &= \frac{2\alpha \pm \sqrt{4\alpha^2 - 6\alpha\gamma r_0^2}}{3\alpha r_0} (r - r_0) + f_{3/2}(r - r_0)^{\frac{3}{2}} + O((r - r_0)^2) \\ B(r) &= b_0 \left(1 + 2 \frac{2\alpha - 2\gamma r_0^2 \mp \sqrt{4\alpha^2 - 6\alpha\gamma r_0^2}}{\gamma r_0^3} (r - r_0) + \right. \\ &\quad \left. + f_{3/2} \frac{-4\alpha^2 + 3\alpha\gamma r_0^2 \pm 2\alpha\sqrt{4\alpha^2 - 6\alpha\gamma r_0^2}}{\gamma^2 r_0^4} (r - r_0)^{\frac{3}{2}} + O((r - r_0)^2) \right) \end{aligned} \quad (2.106)$$

This family has 1+2 free parameters: b_0 , r_0 , $f_{3/2}$ (we could choose f_1 instead of r_0 as we made for the $(1, 0)_{r_0}$ family). As for the $(1, 0)_{r_0}$ family in the Einstein-Weyl theory, f_1 is real only for $r_0 \leq \sqrt{\frac{2\alpha}{3\gamma}}$ so also this family can describe only objects with a radius smaller than this quantity.

The wormholes interpretation is still valid, being the indicial structure of the leading order the same.

These solutions still contain the semi-integer orders (clearly except for the order $\frac{1}{2}$ in $B(r)$). The semi-integer coefficients contain factors of $f_{3/2}$ in the numerator, such that they vanish when $f_{3/2}$ goes to zero, and the solutions become of the kind

$(1, 0)_{r_0}$. Even if this is a subfamily of the $(1, 0)_{(r_0, 1/2)}$ it is interesting to notice that in the Einstein-Weyl theory $f_{3/2}$ is not a free parameter of the $(1, 0)_{(r_0, 1/2)}$ family, instead it emerges with the limit $b_{1/2} \rightarrow 0$.

Similarly we have found the corresponding subfamily with $b_{1/2} = 0$ for the full quadratic theory. Again it can be obtained by the series (2.105), this time by inserting them in the system (2.21, 2.22). The first terms in this case are

$$\begin{aligned} f(r) &= f_1(r - r_0) + f_{3/2}(r - r_0)^{\frac{3}{2}} + O((r - r_0)^2) \\ B(r) &= b_0 \left(1 + \frac{2}{(\alpha - 3\beta)f_1^2 r_0^4} \left(\alpha f_1^2 r_0^3 + 6\beta f_1^2 r_0^3 \pm \right. \right. \\ &\quad \left. \left. \pm \sqrt{27\alpha\beta f_1^4 r_0^6 - 6\alpha\gamma f_1^2 r_0^6 + 18\beta\gamma f_1^2 r_0^6 + 4\alpha^2 f_1^2 r_0^4 + 36\beta^2 f_1^2 r_0^4 - 24\alpha\beta f_1^2 r_0^4} \right) (r - r_0) + \right. \\ &\quad \left. + b_{3/2}(r - r_0)^{\frac{3}{2}} + O((r - r_0)^2) \right) \end{aligned} \tag{2.107}$$

It has 1+4 free parameters, $r_0, b_0, f_1, f_{3/2}, b_{3/2}$. Actually what we got is that, when solving the system (2.21, 2.22) order by order in the $b_{1/2} = 0$ case, the coefficients $r_0, b_0, f_{3/2}$ can be chosen as free parameters, but one between f_1 and b_1 must be constrained, and only the other one can be free⁵. Moreover $b_{3/2}$, that is constrained by the other coefficients in the general $(1, 0)_{r_0, 1/2}$ family, emerges as a free parameter in this case.

The square root that appears in the (2.107) is proportional to the square root present in the (2.80) and it gives the same constraints to r_0 and f_1 reported in (2.85). The $(1, 0)_{r_0}$ family can be obtained by setting $f_{3/2} = 0, b_{3/2} = 0$.

2.9.7 Other possible solution families

In the previous paragraphs we have seen all the solution families around $r_0 \neq 0$ found until now. In [9] several other ansatz have been tried, including power series with fractional steps, like the $(1, 0)_{r_0, 1/2}$ and $(\frac{3}{2}, \frac{1}{2})_{r_0, 1/2}$, or power series with logarithmic terms. Again, even if many of these trials cannot be excluded at all, no other family was positively confirmed.

⁵We have reported in the (2.107) the choice with b_1 constrained, and f_1 free.

3 Numerical methods

In the previous sections we have shown the main features of the static spherical symmetric solutions in classical quadratic gravity for different regimes of the radius or of the curvature. Since we are interested in the global structure of the solutions, we have to connect these different regimes with numerical methods. Now we are going to explain which numerical methods have been used and their main features. All the numerical calculations have been done with Wolfram Mathematica.

3.1 Numerical solutions of ordinary differential equations

In this work we perform several numerical integrations of our system of differential equations. In all these calculations we use the function `NdSolve` by applying specific methods. Firstly we tried a simple Runge-Kutta method with an adaptive step size. The Runge-Kutta methods are based on the standard formulation of a Cauchy problem. Given

$$\begin{cases} y'(x) = f(x, y(x)) \\ y(x_0) = y_0 \end{cases} \quad (3.1)$$

a solution can be found as

$$y(x) = y_0 + \int_{x_0}^x dx' f(x', y(x')) \quad (3.2)$$

that, written for a small interval of the variable x , becomes

$$y(x_{n+1}) = y(x_n) + \int_{x_n}^{x_{n+1}} dx f(x, y(x)) \quad (3.3)$$

The couple $(y(x), x)$ is substituted by its discrete counter part (y_n, x_n) for the generic step n . A Runge-Kutta method calculates at each step y_{n+1} , given y_n , by substituting the integral with a discrete approximation. The Euler method is the first Runge-Kutta method, where the discrete approximation is simply

$$y_{n+1} = y_n + h f(x_n, y_n) \quad (3.4)$$

with $h = x_{n+1} - x_n$. This method has an error of order h^2 . A generic Runge-Kutta method is called of order N if it has an error of order h^{N+1} . The 4th order Runge-Kutta is considered a good trade-off between numerical efficiency and high accuracy. It is implemented by

$$y_{n+1} = y_n + \frac{k_1}{6} + \frac{k_2}{3} + \frac{k_3}{3} + \frac{k_4}{6} \quad (3.5)$$

with

$$\begin{aligned}
 k_1 &= hf(x_n, y_n) \\
 k_2 &= hf\left(x_n + \frac{h}{2}, y_n + \frac{k_1}{2}\right) \\
 k_3 &= hf\left(x_n + \frac{h}{2}, y_n + \frac{k_2}{2}\right) \\
 k_4 &= hf(x_n + h, y_n + k_3)
 \end{aligned} \tag{3.6}$$

and it has an error of the order $O(h^5)$. At each step the interval h must be chosen in order to satisfy the precision required. A constant h is often a bad choice because it could be too small where the solution is almost constant, or too high where the solution varies too rapidly. An adaptive step size takes account of this. We used the "DoubleStep" option, included with the Ndsolve function, as controller method which implements an extrapolation of the error, and adapts the step h so that the error estimation will be within the limits of the local precision required. The extrapolation of the error is made by calculating y_{n+1} with one step of size h , that we call y_1 , and with two half step of size $\frac{h}{2}$, that we call y_2 . Being the error $O(h^5)$, we can write

$$\begin{aligned}
 y(x_n + h) - y_1 &= Ch^5 + O(h^6) \\
 y(x_n + h) - y_2 &= C(2h)^5 + \mathcal{O}(h^6)
 \end{aligned} \tag{3.7}$$

where C is the proportionality constant between the real error and h^5 . The error estimation is obtained with

$$\epsilon = \frac{|y_2 - y_1|}{2^5 - 1} = Ch^5 + O(h^6) \tag{3.8}$$

This method works very well with many differential equations, but unfortunately with our system of o.d.e. the program reports the error message "the system appears to be stiff" and the results seem incorrect. A problem is called "stiff" when certain numerical methods produce instability, unless the step size is taken unacceptably small. The "StiffnessSwitching" option for the NdSolve function uses a stiffness test for changing the method when the system appears to be stiff. We set the 4th order Runge-Kutta as explicit method with the "StiffnessSwitching" option. In case of stiffness the program switches to an implicit method, that by default is the implicit Euler method. The implicit Euler method turns out to be more stable and hence more adapted to integrate stiff system. It is implemented by

$$y_{n+1} = y_n + hf(x_n, y_{n+1}) \tag{3.9}$$

where y_{n+1} appears in both the right and left hands of the equation, so it is computed after solving this algebraic equation.

All the result in this work were obtained by using the options "DoubleStep" and "StiffnessSwitching", with an high local accuracy required (10 or more digits).

3.2 Numerical roots of multivariable functions

In order to find our numerical solutions it was necessary to solve equations with multivariable functions. This was done by using the `FindRoot` function. As the `NdSolve`, this function has different options and methods that can be specified. It uses by default the Newton's method in case one initial value for the iteration is specified, or the Broyden's method (called "secant" method in the `FindRoot` options) if two initial values are specified. The Newton method is based on the iteration

$$\vec{x}_{n+1} = \vec{x}_n - \mathbf{J}(\vec{x}_n)^{-1} \vec{f}(\vec{x}_n) \quad (3.10)$$

where $\vec{f}(\vec{x})$ are the functions for which we want to find the roots, and $\mathbf{J}(\vec{x})^{-1}$ the inverse of the Jacobian matrix. When the Jacobian cannot be computed, an approximation with finite differences replaces the last term in the iteration (3.10): however this can add much numerical effort. The Broyden's method computes the Jacobian only at the first two values and then updates directly the inverse of the Jacobian with

$$J_{(n)}^{-1}{}_{ij} = J_{(n-1)}^{-1}{}_{ij} + \frac{\Delta x_{n,i} - \sum_k J_{(n-1)}^{-1}{}_{ik} \Delta f_{n,k}}{\sum_{kk'} \Delta x_{n,k} J_{(n-1)}^{-1}{}_{kk'} \Delta f_{n,k'}} \sum_k \Delta x_{n,k} J_{(n-1)}^{-1}{}_{kj} \quad (3.11)$$

where

$$\begin{aligned} \Delta \vec{x}_n &= \vec{x}_n - \vec{x}_{n-1} \\ \Delta \vec{f}_n &= \vec{f}(\vec{x}_n) - \vec{f}(\vec{x}_{n-1}) \end{aligned} \quad (3.12)$$

In our work the Jacobian has been always approximated. The Newton method with finite differences seems to work better for our calculation, even if it required more numerical effort. In particular, we specify that this method has been used for the wormhole solutions in section 6, while for the black hole solutions in section 5 the Broyden's method turned out to be more adapt.

3.3 Shooting method

The shooting method is a useful numerical tool designed to solve the boundary value problems. Given a system of ordinary differential equations, when we know all the boundary conditions at a certain point x_0 we can use the previously described methods, integrating from x_0 to a generic point x , in order to find the solution $y(x)$. But, if part of the boundary conditions are known at one point x_1 and the others at a different point x_2 , new methods must be implemented in order to find the solution.

The harmonic oscillator can be a useful example. Given the problem

$$\begin{cases} y''(x) = -\lambda^2 y(x) \\ y(x_1) = y_1 \\ y(x_2) = y_2 \end{cases} \quad (3.13)$$

there is still a unique solution, as in the case in which we know $y(x_1)$ and $y'(x_1)$. The shooting method works as follow. We start integrating from the point x_1 using the boundary conditions known (in this case $y(x_1) = y_1$), while the unknown conditions are initialized with some guessed values (in our example we have $y'(x_1) = s$). Then the integration stops at x_2 obtaining a value

$$y(x_2; y_1, s)$$

Now in x_2 we have this result obtained by the first integration, but we also have the second boundary condition $y(x_2) = y_2$. We now consider the difference

$$d = y_2 - y(x_2; y_1, s)$$

Clearly the two values will not match at the first iteration and the difference will not vanish. This difference d can be thought as a function of the arbitrary condition s given in x_1 . Now we have to find the root of $d(s)$. Once we have the root s_r such that

$$d(s_r) = 0$$

the problem becomes equivalent to the standard Cauchy problem, with the boundary conditions

$$\begin{cases} y(x_1) = y_1 \\ y'(x_1) = s_r \end{cases} \quad (3.14)$$

since we are sure that also the conditions at the point x_2 are matched. For our purpose, this procedure involves the NdSolve function, initialized with the guessed values for the unknown boundary conditions at the first point. Then the variable "difference" is passed as argument of the function FindRoot, which iterates multiple NdSolve until the conditions that make the difference vanish are found. Typically, a good estimation of the guessed condition is needed in order to help the convergence. A variant of this method has been used in this work, and it is implemented as follow. We perform two numerical integrations to obtain the solution, one from x_1 and the other from x_2 , to a certain fitting point x_{fit} . In both points the NdSolve is initialized with guessed values for the unknown conditions. Then the obtained functions and their derivatives are compared in the fitting point x_{fit} . In our example

of the harmonic oscillator we guess the two values

$$\begin{aligned} y'(x_1) = s_1 &\quad \text{obtaining} \quad \vec{f}_1 = \left(y(x_{fit}; y_1, s_1), y'(x_{fit}; y_1, s_1) \right) \\ y'(x_2) = s_2 &\quad \text{obtaining} \quad \vec{f}_2 = \left(y(x_{fit}; y_2, s_2), y'(x_{fit}; y_2, s_2) \right) \end{aligned} \quad (3.15)$$

where we compare the functions till the first derivative since we are solving a second order differential equation. Then, we define $\vec{s} = (s_1, s_2)$, and the vector difference

$$\vec{d}(\vec{s}) = \vec{f}_1 - \vec{f}_2 \quad (3.16)$$

is used as the argument of `FindRoot`, which returns the correct values for the guessed parameters (s_1, s_2) . In this work we always use a similar approach with our system of o.d.e.

Why do we need the shooting method?

What we are going to do is to connect the solutions close to the origin, or close to a singularity of the o.d.e. (wormhole or black hole type, at a radius r_0), with the asymptotically flat solutions at large radius.

We could write the solutions at large radius with the linearised solutions (2.46) and then use these functions as boundary conditions at large radius. The parameters of these boundary conditions are the two parameters of the asymptotically flat solutions in the Einstein-Weyl theory, C_S and C_2^- . So, fixed the couple (C_S, C_2^-) , we could integrate, from large radius to the origin, in order to identify the behavior of the solution at the origin (or at r_0 if it encounters a singularity at this radius), i.e. we want to understand to what family the solutions belong. This does not need the shooting method for the families that occupy a surface on the plane (C_S, C_2^-) . But if we are interested in solutions that will occupy a line (or a point) on the plane (C_S, C_2^-) we need the shooting method to determine the precise parameterization of the curve (or the coordinates of the specific point). This is exactly what we will do for the black hole solutions.

Moreover, if we want the precise values of the parameters that characterize the family we cannot use the result of just one single integration because, typically, the parameter estimations that we can construct are affected by substantial errors. Instead, with the shooting method, we can fix the form of a particular family with all its free parameters as boundary conditions close to the origin (or r_0 if it is one of the families around $r \neq 0$), and then select only the subspace of parameters that correspond to asymptotically flat solutions.

We will give the details for the black holes and wormholes case in the following sections.

4 Numerical results and physical discussion

Once introduced the main aspects of the classical quadratic gravity, found the solutions in different regimes, described the numerical methods, we are finally able to show our numerical results, as well as the physical information that we get from them.

The numerical analysis has been made only for the Einstein-Weyl theory, due to two reasons:

- the simpler form of the corresponding o.d.e. system, and the related minor number of parameters;
- the existence of the theorem 1, which ensures that certain solutions of the full quadratic theory must belong to Einstein-Weyl gravity too;

Every reference to the solution families and the linearised theory in the following is intended to their form in the Einstein-Weyl case, unless otherwise specified.

We want to understand how the solutions at large radius are connected with the small radius regime, in particular we will analyze the asymptotically flat solutions case. The large radius regime will be described by the linearised theory with the metric (2.46), in which we set $C_0^- = 0$. Instead, in the small radius regime, we will try to understand to what families, described in series form around the origin or $r_0 \neq 0$, the solutions integrated from larger radius correspond. In particular for the black holes case and the wormholes case, we will show what is the subspace of free parameters of such families, which corresponds to asymptotically flat solutions.

In this section we firstly specify the units chosen for the numerical algorithms and the corresponding physical scale; then we show the phase diagram of the asymptotically flat solutions; finally we show the results for black hole and wormhole solutions. Moreover, the parameters of the asymptotically flat solutions obtained for these two families are used to explore the interior of both the black holes and wormholes, and also to explore the new copy of $r > r_0$ in the wormholes case.

4.1 Ghost unit and physical scale

When reducing to the Einstein-Weyl theory, a natural energy scale emerges

$$m_2^2 = \frac{\gamma}{2\alpha} = 1 \quad (4.1)$$

It can be checked that the solutions of the linearised theory and the solution families around the origin and r_0 depend on α and γ only through m_2 in their Einstein-Weyl restriction. The choice $m_2 = 1$ is numerically implemented by simply setting $\alpha = \frac{1}{2}$

and $\gamma = 1$. Regarding the physical scale corresponding to this unit, it is related to the physical value of γ and α , i.e. the Newton's constant and the coupling of the Weyl square term. Unfortunately there are no experiments to evaluate the latter. Possible theoretical values can be found in the various attempts of constructing a consistent quantum theory with the quadratic action (2.1). The ghost mass is related to the Planck mass by

$$m_2^2 = \frac{\gamma_0}{2\alpha} = \frac{1}{32\pi G\alpha} = \frac{m_P^2}{32\pi\alpha} \quad (4.2)$$

so that, for α of order 10^{-2} , we have that a radius of order 1 in our solution space corresponds to a radius of order of the Planck length

$$l_P \simeq 1.616 \times 10^{-35} m \quad (4.3)$$

In any case, the structure of the solution space does not depend on the values of α if we keep it with positive sign. Changing this parameters affects only the solutions that must have a radius smaller than a certain quantity which depends on α (the solutions of the subfamily with $b_{1/2} = 0$).

4.2 Solution space

We show here the analysis of the generic asymptotically flat solutions. In order to study the solutions space, we take the linearised theory (2.46) at large radius as boundary conditions and then we integrate to small radius. Initializing the integration with the (2.46) ensures the asymptotic flatness of the solutions.

We explored the plane (C_S, C_2^-) starting the integration from $r = 15$. The range of C_S should be chosen in such a way that $\frac{|C_S|}{r} << 1$, in order to be consistent with the assumption that the correction to the Minkowski space is small (2.35). We pushed our range of C_S to the interval $(-2, 2)$ so we have $\frac{|C_S|}{15} \leq 0.133$. The same reasoning puts a limit on the Yukawa term but since we explored only the interval $(-2, 2)$ for C_2^- we have a Yukawa correction $|C_2^-|e^{-15} \leq 6.12 \times 10^{-7}$ already small enough.

Then the numerical integration of the system (2.33,2.34) has been performed from $r = 15$ to $r = 10^{-5}$.

The NdSolve gives an error message if the integration encounters a singularity ⁶ at a radius $r_0 \neq 0$: in those cases we can consider only the integration till that radius as correct solution. Actually, in order to study our solution space, we decided to consider a solution with singularity when $f(r) < 10^{-5}$ occurs, so that to stop the integration a little before the singularity, since this reduces a lot the time required

⁶We recall it would be a singularity of our o.d.e. system and not a true metric singularity

for the numerical integration.

We have evaluated the quantities

$$I_f = \begin{cases} r \frac{f'(r)}{f(r)}|_{r=10^{-5}} & \text{if no singularities are detected} \\ (r - r_0) \frac{f'(r)}{f(r)}|_{r=r_0+10^{-3}} & \text{if there is a singularity at } r = r_0 \end{cases}$$

$$I_A = -I_f \quad (4.4)$$

$$I_B = \begin{cases} r \frac{B'(r)}{B(r)}|_{r=10^{-5}} & \text{if no singularities are detected} \\ (r - r_0) \frac{B'(r)}{B(r)}|_{r=r_0+10^{-3}} & \text{if there is a singularity at } r = r_0 \end{cases}$$

that represent the estimations of the powers that appear in the leading order of the series expansion around the origin or $r_0 \neq 0$. The estimations in case of singularity are taken at $r_0 + 10^{-3}$ instead of $r_0 + 10^{-5}$ because the way in which we have chosen to detect singularities puts a limit on the precision of this estimation. On the contrary, in case of no singularity before the origin, we can push these estimations to very small radius, until we trust the precision of the NdSolve. The theoretical values of these quantities change with discrete steps when there is a transition from a family to another, but with our numerical results this will appear with a continuous change of the quantities I_B, I_f .

Generically we expect to find that: the families with four free parameters appear as surfaces, those with three parameters as lines, and those with two parameters as points. However we will see that there could be exceptions.

In figure 1 the phase diagram of our solution space is shown. In this figure the level sets of the function $I_B(C_S, C_2^-)$ are plotted. First we divide the data into solutions with and without singularity, then we analyze the families that we encounter in our diagram.

In the following we will refer to the region with $C_S \leq 0$ as the physical region since, having $C_S = -2MG$ for the solution in general relativity, the condition $C_S \leq 0$ corresponds to the physical condition $M \geq 0$. We use this identification even if it is not properly correct in Einstein-Weyl gravity. However, since C_S can be correctly interpreted as

$$C_S = -2M_N G$$

where M_N is the Newtonian mass that appears in the Newton's law, the condition $M_N \geq 0$ excludes the half-plane $C_S < 0$.

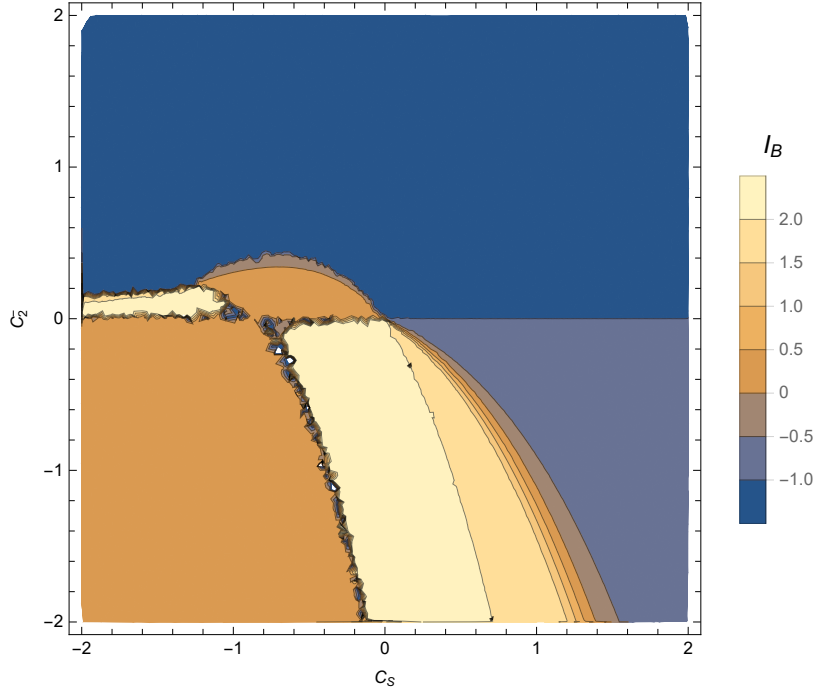


Figure 1: Phase diagram of asymptotically flat solutions

Some boundaries between different families appear quite irregular: this happens because the phase diagram has actually been plotted by evaluating $I_B(C_S, C_2^-)$ for 20,000 points taken randomly in the square $(-2, 2) \times (-2, 2)$.

4.3 Solutions without singularity

In figure 2a the level sets of $I_B(C_S, C_2^-)$ are plotted again, but now we are excluding the cases where singularities have been encountered. The values of I_B are approximately in the interval $(-1.31, 2.05)$. We have identified two sets of solutions that occupy most of this surface, with typical values

$$-1.31 < I_B < -0.7$$

$$1.9 < I_B < 2.05$$

with just a little area in which we found a gradual transition between these two behaviors (figures 2c, 2b, 2d). Due to the presence of a transition area, the upper bound of the first interval, and the lower bound of the second one, are actually qualitative and we have chosen values so that we have two well distinct families. A more precise investigation with a shooting method could reduce the transition area to a one dimensional line. The first region (the wider one, shown in figure 2b) seems to be filled with functions belonging to the $(1, -1)_0$ family. These solutions occupy most of the unphysical region, but also a large surface in the physical region. This

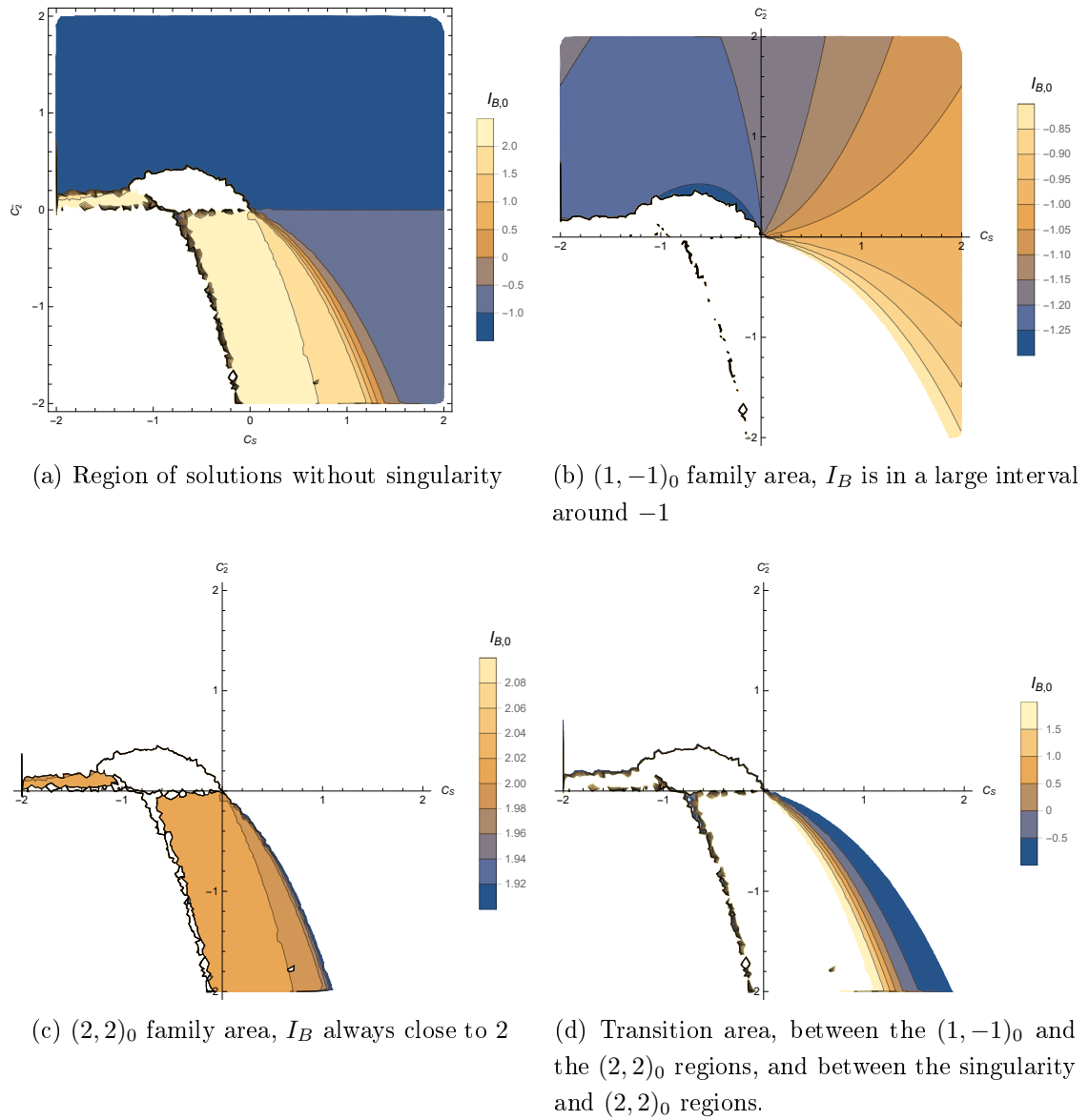


Figure 2: Families found without singularity

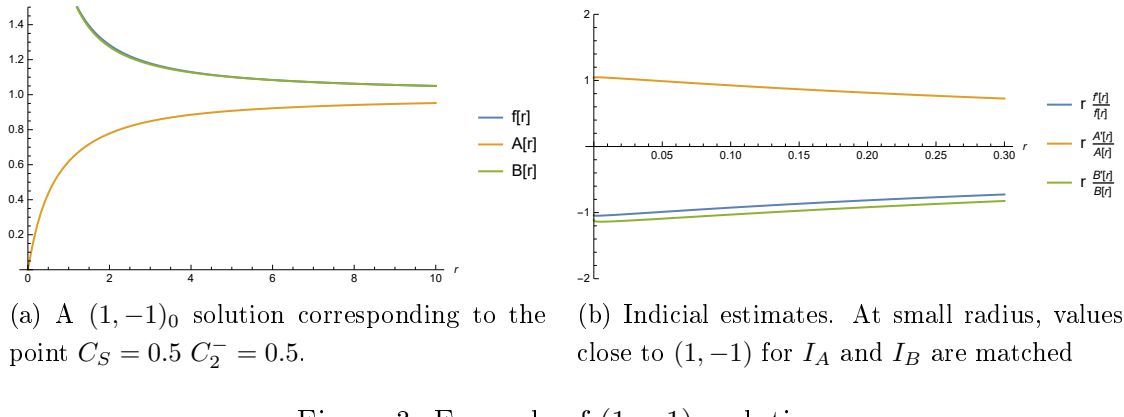
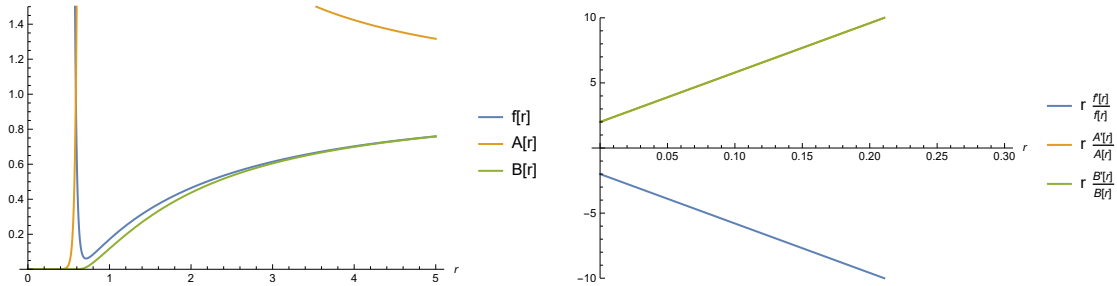


Figure 3: Example of $(1, -1)_0$ solution

is different from our expectation since a family with three free parameters should appear as a line in our phase diagram. There are several possible explanation. Leaving aside the time scaling, i.e. if, for now, we ignore the b_{-1} parameter for the $(1, -1)_0$ family and the parameter C in the full solution of the linear theory (2.44), the subspace of the other two parameters of the $(1, -1)_0$ family should correspond to a surface in the three dimensional space (C_S, C_2^-, C_2^+) of the linearised theory. There are the following possibilities:

- This surface lies on the plane (C_S, C_2^-) i.e. every solution of this family is asymptotically flat. However this seems to be excluded because non asymptotically flat solutions of this family have been found.
- The intersection between this surface and (C_S, C_2^-) is a one dimensional line, and what we see as surface is actually a new kind of solution that shares the same leading order of the $(1, -1)_0$ family.
- The intersection between this surface and (C_S, C_2^-) is a one dimensional line, but what occupy the surface are actually functions belonging to the $(2, 2)_0$ family. This can appear unexpected but, as showed in figure 5, a $(2, 2)_0$ solution close to the transition area typically has $B(r)$ that, when $r \rightarrow 0$, grows similarly to $\frac{1}{r}$, then it reaches a maximum and goes to zero as r^2 . If this maximum corresponds to a radius less than 10^{-5} the solution will appear as a member of the $(1, -1)_0$ family for our phase diagram. We expect that this is true at least for the solutions close to the transition area, but it could happen that a very large surface that appears occupied by $(1, -1)_0$ solutions it is actually filled by $(2, 2)_0$ solutions.
- There is an extra free parameter that appears only at a certain order of the series expansion.



(a) A $(2, 2)_0$ solution corresponding to the point of the physical region $C_0 = -1.25$ $C_2^- = 0.1$. Notice the minimum of $f(r)$. When this minimum reaches zero the solution becomes a black hole.

(b) Indicial estimates. At small radius, the values $(2, 2)$ for I_A and I_B are matched

Figure 4: Example of a $(2, 2)_0$ solution

The values of I_B for the $(1, -1)_0$ solutions are in a larger interval around the correct value -1 than those found for the others better identified families. An even more precise analysis has been done for few points where the NdSolve has been pushed to a radius $r = 10^{-24}$. We have seen that the values of I_B , for the solutions with $C_2^- > 0$, were very close to -1 , giving more credit to the hypothesis that there is a new family that share the same leading order of the $(1, -1)_0$ family. On the contrary, for the solutions that apparently belong to the $(1, -1)_0$ family with $C_2^- < 0$, we have seen, from this deeper analysis, that lots of them actually seem belong to the $(2, 2)_0$ family. The solutions on the half line $C_2^- = 0$, $C_0 > 0$ show almost exactly the parameter $I_B = -1$ as we would expect since on this line we know the exact solution, that is a Schwarzschild solution with negative mass, i.e. with no horizon. Apart from the transition region, the rest of the surface is filled with solutions that belong to the $(2, 2)_0$ family: an example is shown in figure 4. This is exactly what we expected since this family has the maximum number of parameters allowed in the theory. We find two areas of this solution in both the physical and unphysical regions.

The solutions of the transition area have clearly an hybrid behavior, probably due to the integration limited to $r > 10^{-5}$. As shown in figure 5, a more detailed integration should better identify the two families and reduce the transition area to a one dimensional line. We can notice here that this transition appears clearly between the $(2, 2)_0$ and the $(1, -1)_0$ area, but it appears also in a little surface along the $(2, 2)_0$ regions that are close to the surface with singularity. We will see that this last result is consistent with what we have found in the black holes analysis. In the last part of this work we will see that $(1, -1)_0$ solutions are characterized by a repulsive potential in the origin, since they are similar to a Schwarzschild solution

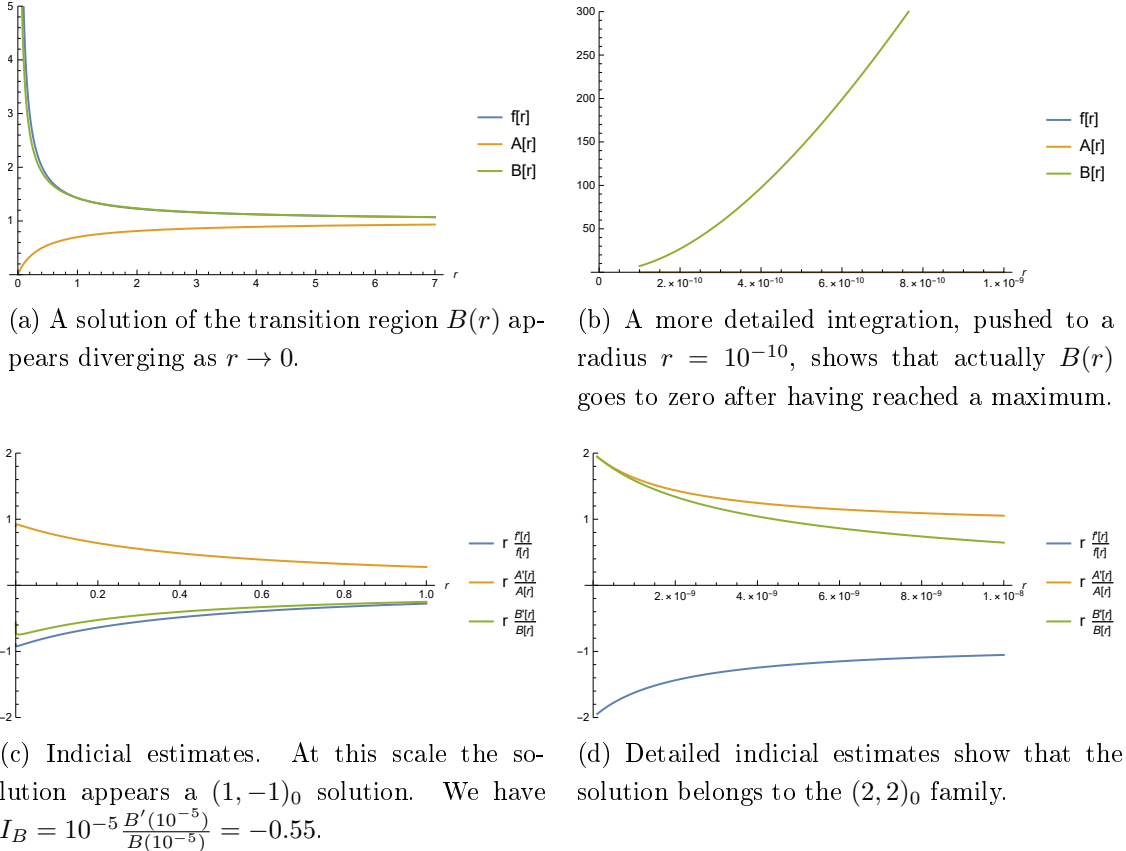


Figure 5: Example of solution in the transition region, corresponding to the point $C_S = 0.5$ $C_2^- = -0.3$

with negative mass, as well as $(2, 2)_0$ solutions are characterized by an attractive potential in the origin.

4.4 Solutions with singularity

We do not give too much details in this section about these solutions since they are the main argument of the following sections, where there will be a deeper analysis of their structure.

In figure 6a we can see that the entire surface is filled by solution with $I_B \simeq 0$ and in the following sections the shooting method will confirm that these solutions correspond to the non-Frobenius wormholes, i.e. the $(1, 0)_{(1/2, r_0)}$ family. We can see an example in figure 6b. As expected, with four free parameters, this family occupies a two dimensional region.

The other family found is clearly the $(1, 1)_{r_0}$ family, i.e. the black holes family. This is not well visible in our phase diagram since these solutions lie on a one-dimensional region. They seem to be located on the border of this singularity region. Indeed

we can see a small transition area where I_B changes from 0 to higher values. We already know that the Schwarzschild line $C_2^- = 0$, $C_S < 0$ belongs to the black holes family, but in [7] a second line of new black holes has been found, and then it has been further studied in [11] and [2]. Similarly to the Schwarzschild line, it separates the wormholes region from the Holdom solutions. The fact that these solutions are located on one-dimensional regions is what we expect from the parameters counting. An example of non-Schwarzschild black hole is shown in figure 7.

5 Black hole solutions

In this section we report the general analysis of the black hole solutions. We give a description of: how we have found these solutions on the (C_S, C_2^-) plane, the general dependence of the parameters on the radius of the horizon, and how to explore the solutions inside the horizon.

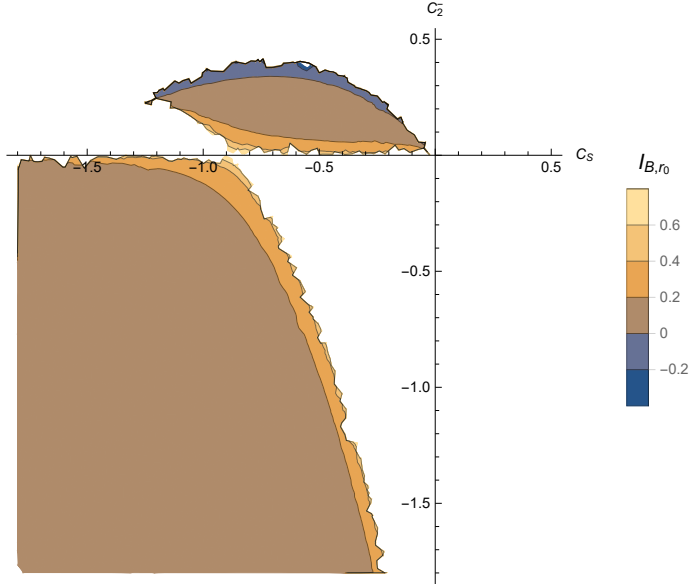
5.1 Shooting method for black hole solutions

We start by describing the structure of shooting method for these solutions. We used the variant of the shooting method in which two numerical integrations are performed from two different starting points and then compared at a fitting point. In both points the boundary conditions are only partially given. Our aim is to obtain the four continuity conditions matched at the fitting point r_{fit} , where we compare the vector defined as

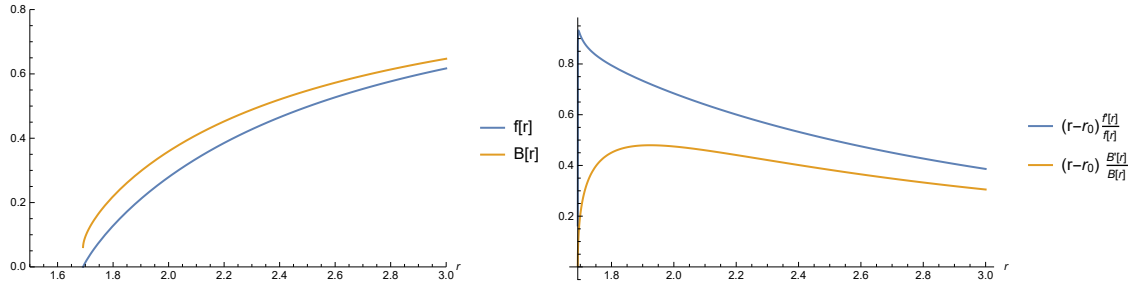
$$\vec{c}(r) = \begin{pmatrix} f(r) \\ f'(r) \\ B(r) \\ B'(r) \end{pmatrix} \quad (5.1)$$

since we are integrating the second order system (2.33,2.34). In the black holes case, the two set of boundary conditions are defined as follows. One set has been taken close to the singularity at the point $r = r_0 + \delta$, where r_0 is the radius of the singularity and δ a small quantity, typically $\delta = 0.001$. The other set is defined at large radius $r = r_1 = 15$ where we can use the linearised theory. These sets of boundary conditions are generated through the evaluation of the vector $\vec{c}(r)$ with the black holes expansion (2.78) at $r = r_0 + \delta$ and with the linearised solutions (2.46) at $r = r_1$.

Now we have a total of five parameters that we have to fix: three of them from the black hole series and the others two from the asymptotically flat linearised solutions. We fix one parameter in order to have a unique solution: let it be the radius of the



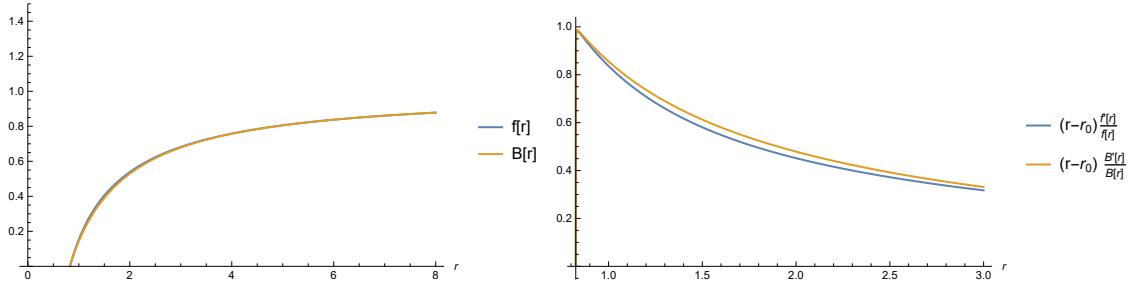
(a) Solutions with singularity



(b) Example of wormhole solution. The $B(r)$ component ends at a non-vanishing value, with an almost vertical tangent, i.e. $B'(r)$ is diverging for $r \rightarrow r_0$. This is what we expect for solutions of the $(1, 0)_{(1/2, r_0)}$ family

(c) The indicial estimates match the values $(1, 0)$

Figure 6: Phase diagram of solutions with singularity, and an example of wormhole solution corresponding to the point $C_S = -0.98$ $C_2^- = -0.5$



(a) Example of the new kind of black holes found, with different first derivatives for the two metric component at the horizon
(b) The indicial estimates match the values (1, 1)

Figure 7: Example of non-Schwarzschild black hole solution corresponding to the point $C_S = -0.975$ $C_2^- = 0.1$.

singularity $r = r_0$. Then the continuity conditions at the fitting point will determine the other four parameters.

The two integrations with the NdSolve are performed, one from $r_0 + \delta$ to larger radius, stopped at the fitting point, and the other from r_1 to smaller radius, stopped at the fitting point too. This fitting point is typically taken closer to the horizon ($r_{fit} \approx r_0 + 0.3$). This because a small deviation of the parameters of the black holes expansion from the correct asymptotically flat values always brings instability if used for the numerical integration from the horizons to too large radius. The algorithm proceeds defining the vector difference at the fitting point

$$\vec{d}(r_{fit}) = \begin{pmatrix} f(r_{fit}; \vec{c}(r_0 + \delta)) - f(r_{fit}; \vec{c}(r_1)) \\ f'(r_{fit}; \vec{c}(r_0 + \delta)) - f'(r_{fit}; \vec{c}(r_1)) \\ B(r_{fit}; \vec{c}(r_0 + \delta)) - B(r_{fit}; \vec{c}(r_1)) \\ B'(r_{fit}; \vec{c}(r_0 + \delta)) - B'(r_{fit}; \vec{c}(r_1)) \end{pmatrix} = \begin{pmatrix} \Delta f(r_{fit}) \\ \Delta f'(r_{fit}) \\ \Delta B(r_{fit}) \\ \Delta B'(r_{fit}) \end{pmatrix} \quad (5.2)$$

Now r_0 is a fixed input that will parameterize the asymptotically flat black holes on the plane (C_S, C_2^-) . The vector $\vec{d}(r_{fit})$ depends only on C_S, C_2^- through $\vec{c}(r_1)$, and on f_1, b_1 through $\vec{c}(r_0 + \delta)$.

$\vec{d}(r_{fit})$ is passed to FindRoot that returns the vector

$$\vec{p}(r_0) = \begin{pmatrix} C_S(r_0) \\ C_2^-(r_0) \\ f_1(r_0) \\ b_1(r_0) \end{pmatrix} \quad (5.3)$$

such that $\vec{d}(r_{fit}; \vec{p}) = 0$. Once fixed r_0 and matched all the boundary conditions, only one asymptotically flat solution should be found. Actually there are two solutions for each value of r_0 , and this is why we have two lines of black holes on the plane

(C_S, C_2^-) .

Regarding the initialization of the guessed value, for the black hole case we used a first integration before starting the proper shooting. This has been done from large radius with the starting values (C_S, C_2^-) , corresponding to a point close to where we expected a non-Schwarzschild black hole on the phase diagram, that we recall to be located on the border between the solutions with and without singularity. With this preliminary integration we have estimated the parameters (f_1, b_1, r_0) to initialize the first shooting. We used the detection of the singularity of the NdSolve for r_0 , and took the quantity $f'(r)$ and $B'(r)$ close to the horizon as estimations for f_1 and b_1 . Once obtained the convergence of the FindRoot for this first black hole, the others have been generated by moving along the black holes line: we have varied the radius with small steps δr_0 , and we used the solution vector $\vec{p}(r_0)$ defined in 5.3, obtained for the previous black hole, as initial value for the shooting of the new black hole.

5.2 General features of black hole solutions

The general behavior of the black hole solutions is shown in figure 7, having both the metric components vanishing at the same non-zero radius, with finite first derivatives.

In figure 8a the position of the black holes found on the phase diagram is shown. The shooting has confirmed that the black holes are located along two lines: as we expected one is the half line $C_S < 0, C_2^- = 0$, while the other one is a curve that starts at a critical point of coordinates $(C_S, C_2^-) \simeq (-1.246, 0.217)$. The non-Schwarzschild black holes line crosses the Schwarzschild one in $(C_S, C_2^-) \simeq (-0.876, 0)$, continues in a region with $C_S < 0$ and $C_2^- < 0$, and then enters in the unphysical region $C_S > 0$ through the point $(C_S, C_2^-) \simeq (0, -2.8)$. This new line shows an increasing radius of the horizon when going from the critical point towards the direction of the unphysical region. It is not clear if the radius vanishes at the critical point since we had difficulties with the convergence of the code for $r_0 < 0.35$. Even if the convergence is lost for $r_0 < 0.35$, the existence of a critical point can be inferred by observing that, changing the radius with uniform steps, the non-Schwarzschild black holes have not a uniform distribution on the phase diagram and, for decreasing r_0 , it seems that the line stops approximately at the point $(C_S, C_2^-) \simeq (-1.246, 0.217)$ (figure 8b). This seems to be a point of coexistence of all the solution families found, as shown in figure 8c. This plot shows also that the results of the shooting method for black holes agree with the qualitative results obtained by the phase diagram, and that both the black holes lines are a phase transition between solutions of the $(2, 2)_0$ family and wormholes. This will be helpful to determine the border of the

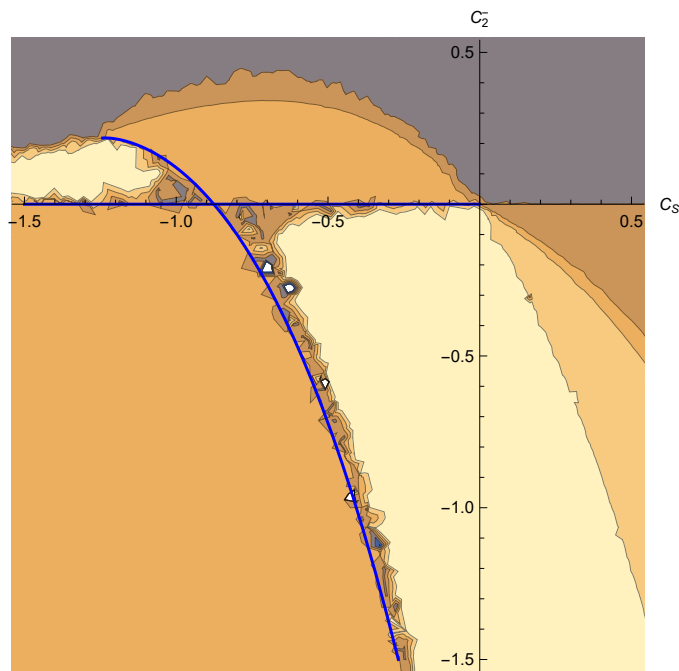
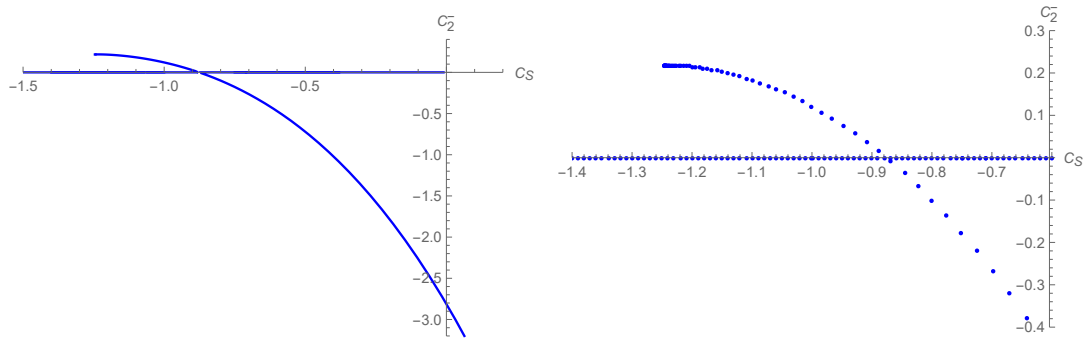


Figure 8

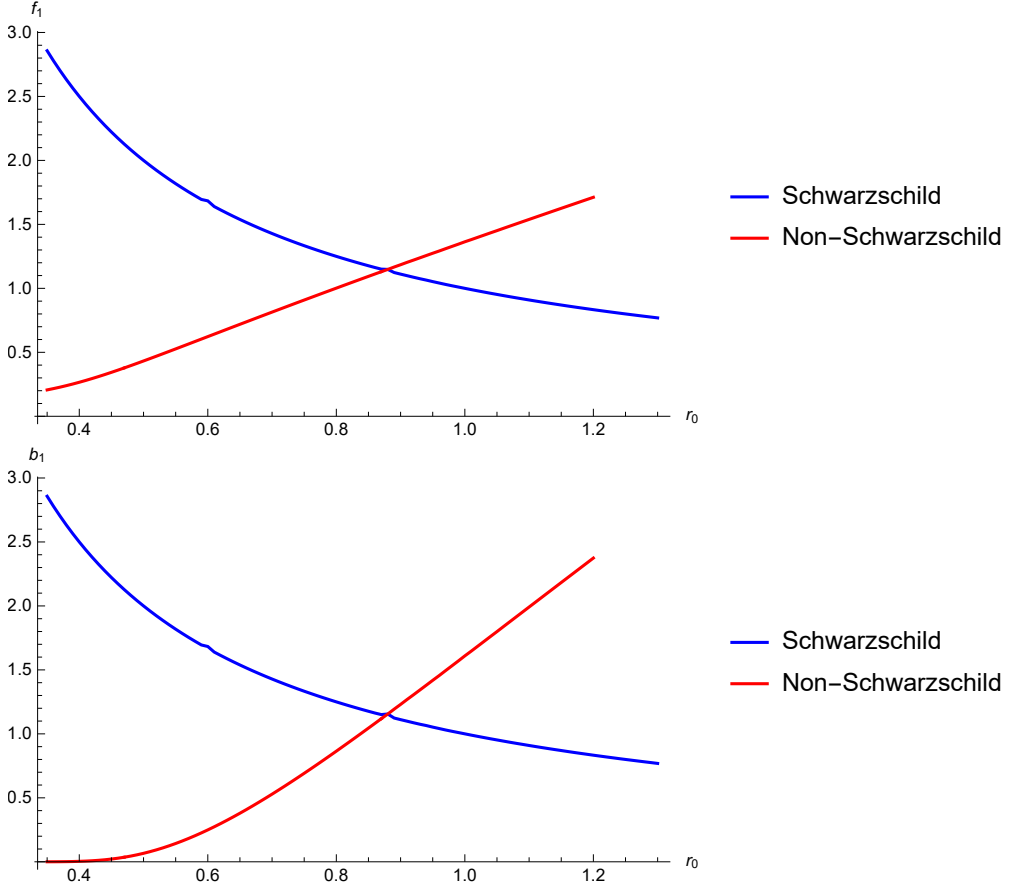


Figure 9: The parameters f_1 , b_1 in function of r_0 for the black hole solutions

wormholes region in the following section.

In figure 9 the parameters $f_1(r_0)$, $b_1(r_0)$ for both the of black holes lines are plotted. The dependence of the parameters with respect to the horizon is completely different for the two kinds of black holes. In [11] and [2] they made a similar analysis of these solutions, in which interesting properties of these new black holes has been studied. Since it can be proved that the surface gravity k for generic black hole solutions is

$$k = \frac{1}{2} \sqrt{b_1 f_1}$$

and that the Hawking temperature is related to the surface gravity by

$$T_H = \frac{k}{2\pi}$$

they found that the non-Schwarzschild black holes have always a lower temperature than the Schwarzschild ones.

The results obtained by the shooting method have been also used to explore the interior of the black holes. We have used the expansion (2.78) as boundary conditions at a point both inside and close to the horizon $r = r_0 - \delta$, and then we have integrated

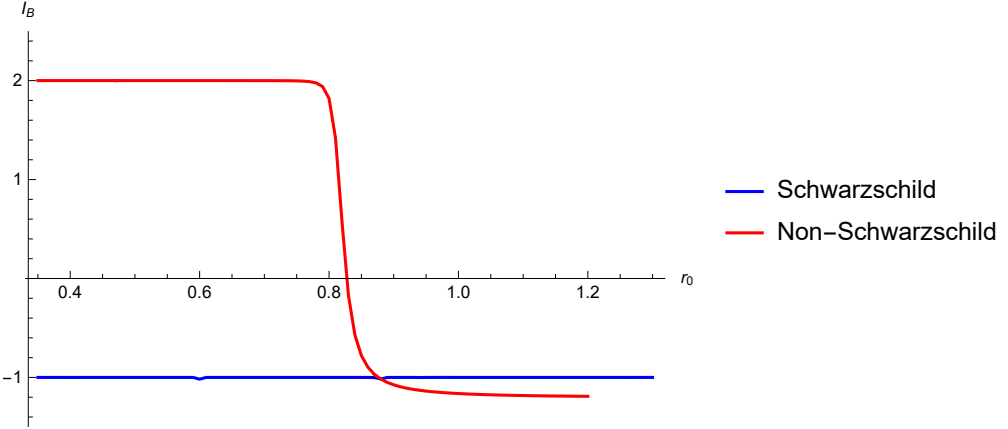


Figure 10: Estimates of I_B at the origin versus the radius of the horizon r_0 , for both the black holes lines

to smaller radius. In order to match the external asymptotically flat solution it is sufficient to initialize the integration with the same parameters (b_1, f_1, r_0) found outside the horizon. The same values of r_0 for the internal and the external solutions ensure the continuity of the metric components at the horizon, and the same values of f_1, b_1 make the first derivatives continuous. Actually, the spacial metric written in this coordinate system is not continuous, since $g_{rr} = f(r)^{-1}$. If we write our o.d.e. system (2.33,2.34) in terms of $g_{rr} = A(r) = \frac{1}{f_1(r-r_0)+O((r-r_0)^2)}$ we could not match the continuity conditions at $r = r_0$. However, with the same o.d.e. system written in terms of $B(r)$ and $f(r)$ of the (2.78), we can match the continuity condition in r_0 for both the functions involved. The Schwarzschild solution in general relativity presents the same situation. Moreover the continuity of f_1 is required in order to have the same invariant quantities in r_0 (such the Kretschmann scalar (2.79)) for both the internal and external expansion.

We explored the interior of our black hole solutions by analyzing the indicial estimate of the $B(r)$ close to the origin (again at $r = 10^{-5}$), as we did in section 4.2.

In figure 10 the behavior at the origin of our numerical solutions is shown. The Schwarzschild black holes have $I_B \simeq -1$ as we expect by its exact form. The non-Schwarzschild solutions instead present a $(2, 2)_0$ behavior for almost all the solutions with $C_2^- > 0$ (i.e. $r_0 < 0.876$), and a $(1, -1)_0$ behavior for the solutions with $C_2^- < 0$. We have seen a similar but opposite behavior for the solutions in the unphysical region $C_S > 0$ when we moved from the $C_2^- < 0$ to the $C_2^- > 0$ region. We recall that, in figure 2d a little area of transition, between $I_B \simeq -1$ and $I_B \simeq 2$, is also visible in the region of solutions without singularity close to the non-Schwarzschild black holes with $C_2^- < 0$. This exactly agrees with what we have found for the black holes with $C_2^- < 0$, in the sense that, moving on the phase diagram, the $(2, 2)_0$

behavior starts to become more similar to the $(1, -1)_0$ behavior till it becomes of the $(1, -1)_0$ kind when the solution becomes a black hole.

5.3 Precision of the method and errors estimation

We discuss here about the precision of our shooting method. There is not a specific way to determine the errors on our results but we can make some consideration about them.

The linearised solutions bring theoretical errors related to the expansion (2.35) where we ignore the $O(\epsilon^2)$ terms. We recall that this theoretical error disappears when $C_2^- = 0$, and the linearised solutions become exact for the full non linear theory along this line. Similarly when $C_S = 0$ the Yukawa corrections to the flat metric are of order $O(e^{-r})$ and the terms neglected in the (2.46) become of order $O(e^{-2r})$, so, also in this case, the theoretical error is considerably reduced for $r = 15$. For the general $C_S \neq 0$, $C_2^- \neq 0$ case, we simply consider that we are looking for asymptotically flat solutions belonging to a specific family (in this section the black hole solutions, in the next one the wormhole solutions). However we can renounce their exact position on the phase diagram: the connection of the solutions at small radius with the expansion (2.46) ensures asymptotic flatness despite the finite precision of the linearised solutions .

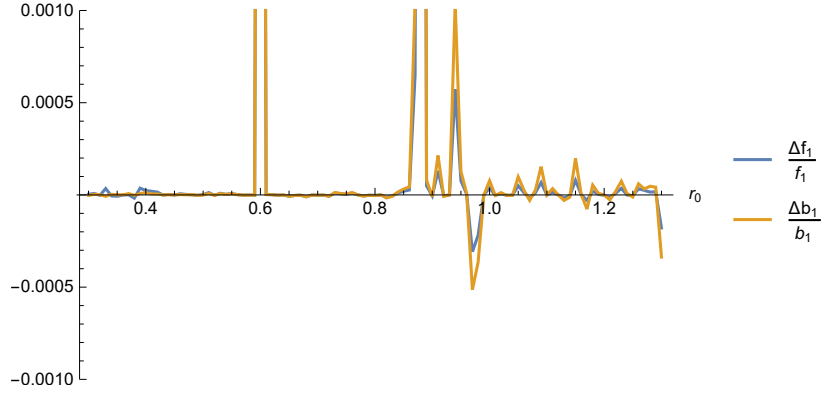
Another theoretical error comes from the truncation of the series expansion (2.78), but we have truncated these series at the eighth order in $(r - r_0) = \delta = 10^{-3}$ making this contribution negligible.

For the numerical aspects, the Schwarzschild line provides a useful check since we have obtained the black hole solutions on this line with the same numerical procedure of the other solutions. The numerical data of this solutions can be used to show the discrepancy between $f_1(r_0)$, $b_1(r_0)$ and their expected values $f_{1,S} = \frac{1}{r_0}$, $b_{1,S} = \frac{1}{r_0}$, which comes only from the numerical precision of our shooting code, since there are no theoretical errors on this line. The relative errors on these parameters are plotted in 11a. They are almost always less than 10^{-3} and their averages on the data are

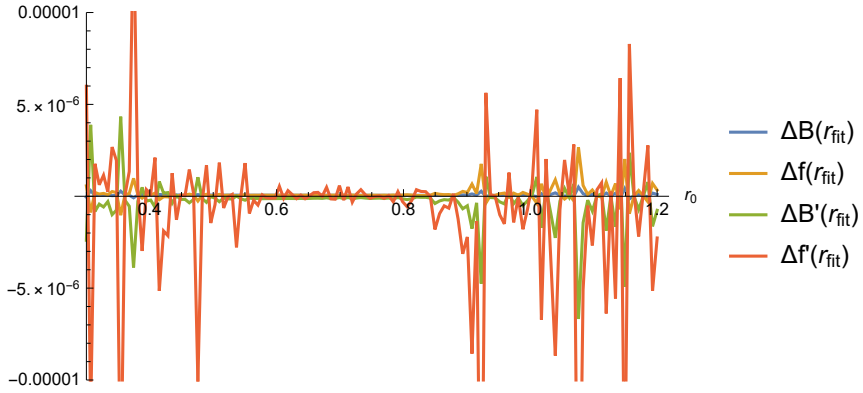
$$\langle \frac{\Delta f_1}{f_1} \rangle = 2.8 \times 10^{-4}$$

$$\langle \frac{\Delta b_1}{b_1} \rangle = 2.2 \times 10^{-4}$$

giving an idea of the precision of the shooting. On the other hand, in figure 11b the values of the vector $\vec{d}(r_{fit})$, defined in (5.2), are plotted. They were obtained by initializing the two integrations from $r = 15$ and from $r = r_0 + \delta$, with a Schwarzschild



(a) Relative errors on f_1 and b_1 along the Schwarzschild line



(b) Discrepancy at the fitting point, obtained by using the exact set of Schwarzschild parameters

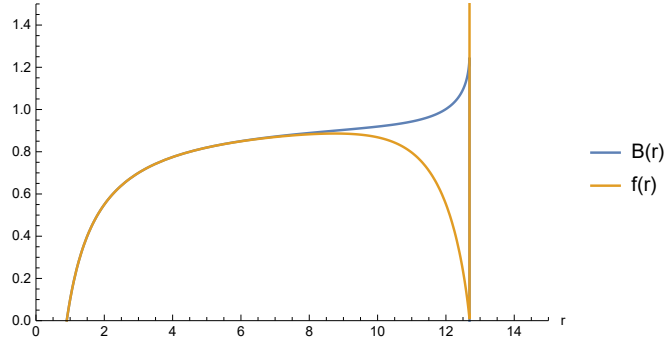
Figure 11

set of parameters

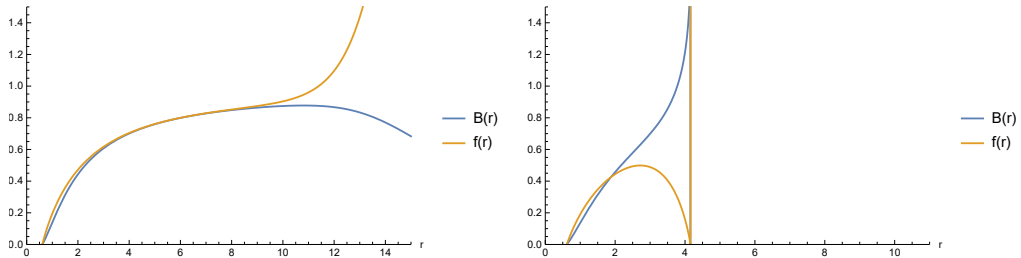
$$\begin{aligned}
 C_S &= -r_0 \\
 C_2^- &= 0 \\
 f_1 &= \frac{1}{r_0} \\
 b_1 &= \frac{1}{r_0}
 \end{aligned} \tag{5.4}$$

and by varying r_0 . The deviation from zero of these values gives an estimation of the error on the metric components that comes only from the numerical integration.

We make a last consideration on what happens when we integrate from a point close to the horizon to larger radius, not stopping at $r = r_{fit}$ but initializing the boundary conditions with the Schwarzschild parameters $f_1 = \frac{1}{r_0}$, $b_1 = \frac{1}{r_0}$. We show an example in figure 12a but we encountered the same behavior for a large set of Schwarzschild black holes. The solutions integrated from the horizon to larger radius stay flat till $r \simeq 8$ and then encounter another singularity or they diverge (figure 12a). Again



(a) An exact Schwarzschild solution integrated from the horizon to large radius



(b) One of our non-Schwarzschild numerical solutions integrated from the horizon to large radius

(c) The same solution plotted in 12b, with r_0 varied by 1%, integrated from the horizon to large radius

Figure 12: Level of flatness of different parameters set for the black hole solutions

this comes only from the finite precision of the NdSolve. However a little deviation from the correct asymptotically flat set of parameters brings divergences way before $r \simeq 8$ (figure 12c). This feature of the numerical integrations from the singularity helps us to distinguish the correct asymptotically flat solutions from the other ones. Our data show the same behavior for the non-Schwarzschild black holes (figure 12b) that stay flat till large radius, so we are quite confident that the parameters found with the shooting code describe the correct asymptotically flat black holes. We will have a similar level of flatness for the wormhole solutions presented in the next section.

6 Wormhole solutions

We present here the asymptotically flat solutions that we identified as wormholes. As stated before, the peculiarity of these solutions is the behavior of the metric components close to the singularity: the inverse of the spacial component $f(r)$ vanishes at the singularity $r = r_0$, but the temporal component $B(r_0)$ does not vanish. These solutions seem to cover a surface on the phase diagram. Consistently with this, we look for solutions belonging to the $(1, 0)_{r_0, 1/2}$ family that, having four free parameters, is the most adapt family to describe solutions located on a two-dimensional region. With the wormhole interpretation a new copy of the region $r > r_0$ emerges for these solutions. We specify here that we impose the asymptotic flatness only for one of the two patches with $r > r_0$. Asymptotically flat solutions are obtained with the shooting method, as we made for black hole solutions.

We show the behavior of the parameters found with the shooting method, specifically commenting on how they vary close to the transition with other families. Moreover we give a description of the line of solutions with $b_{1/2} = 0$, looking for asymptotically flat solutions belonging to the subfamily 2.9.6. In addiction, we use the results of the shooting code to explore both the new copy of $r > r_0$ and the interior $r < r_0$ of the wormhole solutions found.

6.1 Shooting method for wormhole solutions

The shooting code used for these solutions is similar to the black holes one. As before, it is implemented performing two integrations: one starting close to the singularity, typically from $r = r_0 + 10^{-3}$, stopped at $r = r_{fit}$ and the other one starting from $r = 15$ to $r = r_{fit}$. This time the conditions around r_0 have been initialized with the expansions (2.101). We set the fitting point typically at $r_{fit} = r_0 + 0.05$ in order to limit the instabilities of the integration from the singularity to larger radius, as well as we did for the black holes case. The four parameters of the expansions (2.101) with the two parameters of the linearised solutions make a total of six variable to fix: C_S , C_2^- , r_0 , b_0 , f_1 , $b_{1/2}$. We have to find the set of parameters that make the metric components and their first derivatives continuous at the fitting point. This gives a total of four conditions and it implies that we have to specify two parameters to fix a unique solution. We chose to specify C_S and C_2^- due to reasons related to the convergence of the code. Indeed, as usual, we must initialize the code with a set of parameters that are not too far from the correct set which we are looking for. In order to initialize correctly the shooting we proceeded as follows. With our phase diagram 1 we have already an idea of the values of C_S and C_2^- that correspond to wormhole solutions. Once fixed these

values, a preliminary integration can be performed till the NdSolve encounters the singularity. The other four parameters of the (2.101) can be estimated by using the singular radius detected by the NdSolve as estimate for r_0 , and

$$\begin{aligned} f'(r)|_{r=r_0+\delta} &\text{ as estimate for } f_1 \\ B(r)|_{r=r_0+\delta} &\text{ as estimate for } b_0 \\ 2\sqrt{r-r_0}\frac{B'(r)}{B(r)}|_{r=r_0+\delta} &\text{ as estimate for } b_{1/2} \end{aligned} \quad (6.1)$$

These estimations should be close to the correct values that we are looking for, only if the behavior around the singularities is truly described by the expansion (2.101). We have analyzed a large set of points in the wormhole region fixing C_S , C_2^- and initializing the shooting code with the estimates (6.1). The precise borders of this region have been delimited by the points for which the preliminary integration did not encounter any singularity.

Regarding the accuracy level of this method and its results, we give some comment in the following.

6.2 General features of wormhole solutions

We show here our numerical results for the asymptotically flat wormhole solutions. The solutions found have a general behavior of the kind 6b. The borders of the wormhole region on the plane (C_S, C_2^-) correspond to the black holes lines found in the previous section, and to the transition with the $(1, -1)_0$ solutions, in agreement with the general phase diagram (as shown in figure 13).

The parameters of the wormholes are shown with their contour plots with respect to the coordinates (C_S, C_2^-) of the phase diagram. In figure 14 the contour lines of the radius r_0 are plotted. For the region explored we have approximately $r_0 \in (0.02, 3)$. The wormholes with $0 < r_0 < 0.876$ are located in the $C_2^- > 0$ region, while the wormholes with $r_0 > 0.876$ are located in the $C_2^- < 0$ region, just like the non-Schwarzschild black holes. The r_0 parameter seems to be continuous at the transition black holes/wormholes as its contour lines connect the two black holes lines to their respective points having the same r_0 value. This implies that we have an increasing radius of the singularity even in the physical region: indeed r_0 has not an upper bound for $C_S < 0$, as for black hole solutions in general relativity.

In figure 15 the level sets of $\log_{10}(b_0)$ are plotted. For our data, we have approximately $b_0 \in (10^{-4}, 10)$. We can see that there is a continuity for the parameter b_0 too, in the sense that it seems to vanish at the transition with the black holes lines. On the contrary, this parameter grows close to the transition with the $(1, -1)_0$ solutions. The increasing of b_0 is in agreement with the behavior of $B(r)$ for the

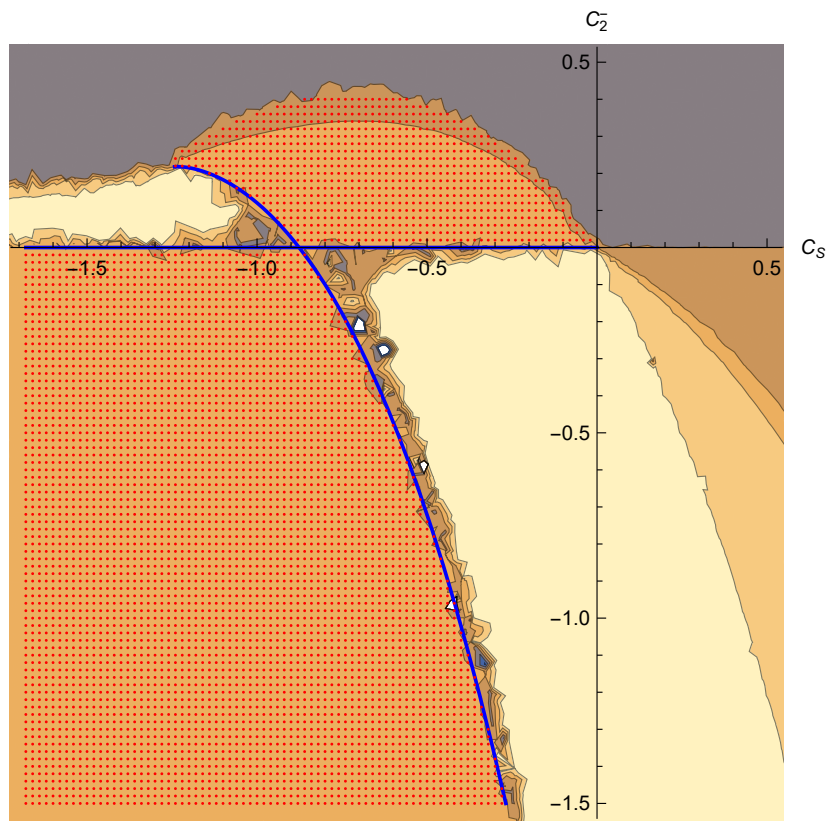


Figure 13: Wormholes region obtained by the shooting method.

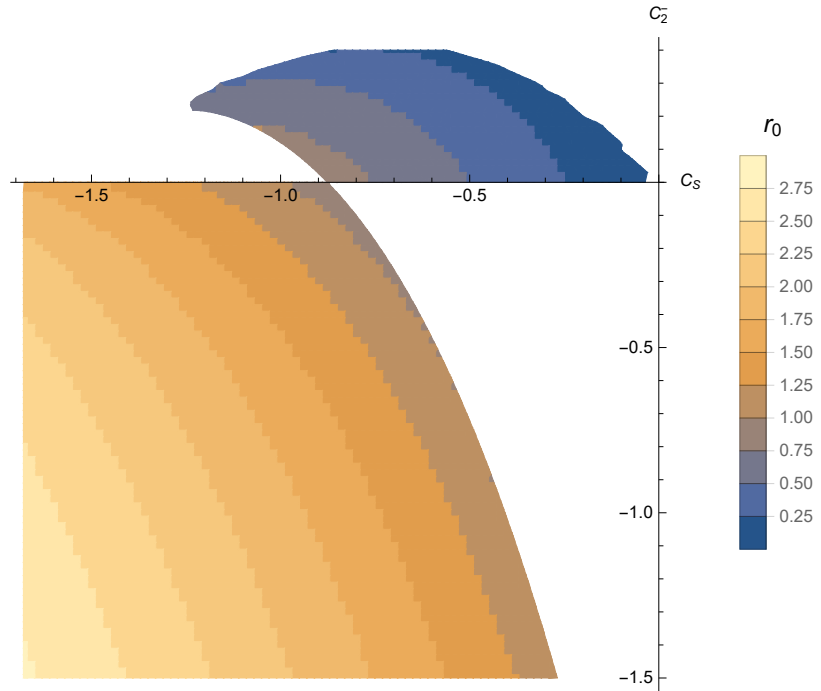


Figure 14: Contour lines of r_0

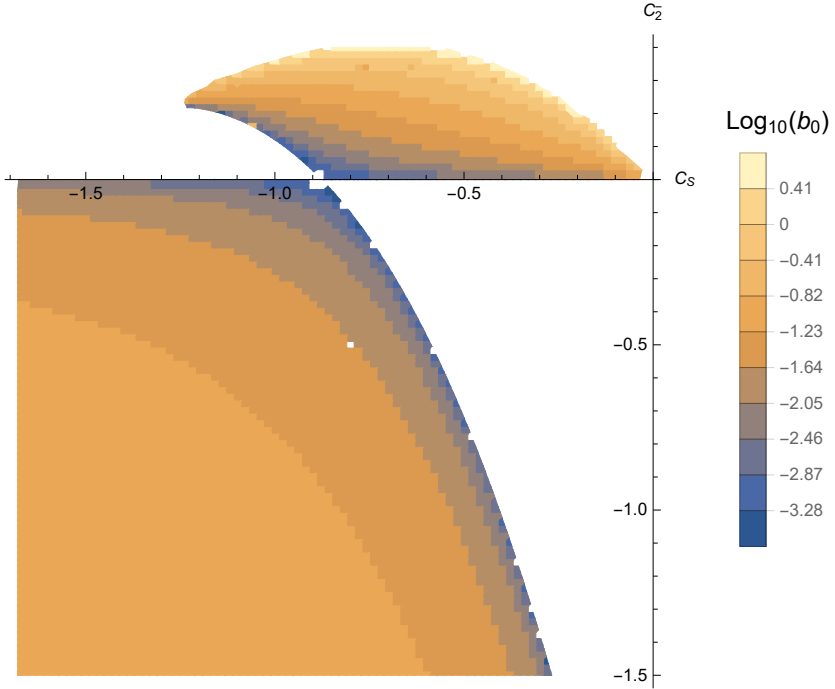


Figure 15: Contour lines of b_0

$(1, -1)_0$ solutions, that must grow in the small radius regime. We recall that from the (2.91) b_0 is related to the potential energy of a massive observer close to the wormhole, and only if $K^2 > b_0$ the observer will pass through the wormhole. Generically if we have an observer located in $r > r_0$ we must have $K^2 \geq B(r)$. $K^2 = B(r)$ corresponds to an observer that starts the motion with $v = 0$. For $C_2^- < 0$ we have always $B(r) > b_0$ if $r > r_0$; more precisely for these solutions $B(r)$ results to be monotonic. For such solutions, any observer initially located in $r > r_0$ with $v = 0$ will cross $r = r_0$ reaching the new patch $r > r_0$, $\rho < 0$. On the contrary, for a portion of the $C_2^- > 0$ region, we have solutions for which $B(r) > b_0$ is not valid for all the radius $r > r_0$ (an example in figure 18), and part of these solutions also have $b_0 > 1$. This portion of the phase diagram corresponds to solutions with $b_{1/2} < 0$ as we discuss in the following.

The values of the parameter f_1 are shown in figure 16. For our data we have approximately $f_1 \in (1, 40)$, corresponding to $\log_{10}(f_1) \in (0, 1.60)$. The curves of the two disconnected region seem to belong to a unique set of curves. f_1 takes large values for C_S going to zero and it could diverge in this limit, exactly like for the Schwarzschild black holes. Actually this parameter shows a discontinuity at the transition with the black holes: an example is the curve $\log_{10}(f_1) = 0.3$, $f_1 \simeq 1.995$ that in the lower region ends close to the black hole solution $(C_S, C_2^-) = (-1, 0)$, which instead has $f_1 = 1$. In this sense, at the transition black holes/wormholes, the metric components are continuous at the singularity, but with the first derivatives

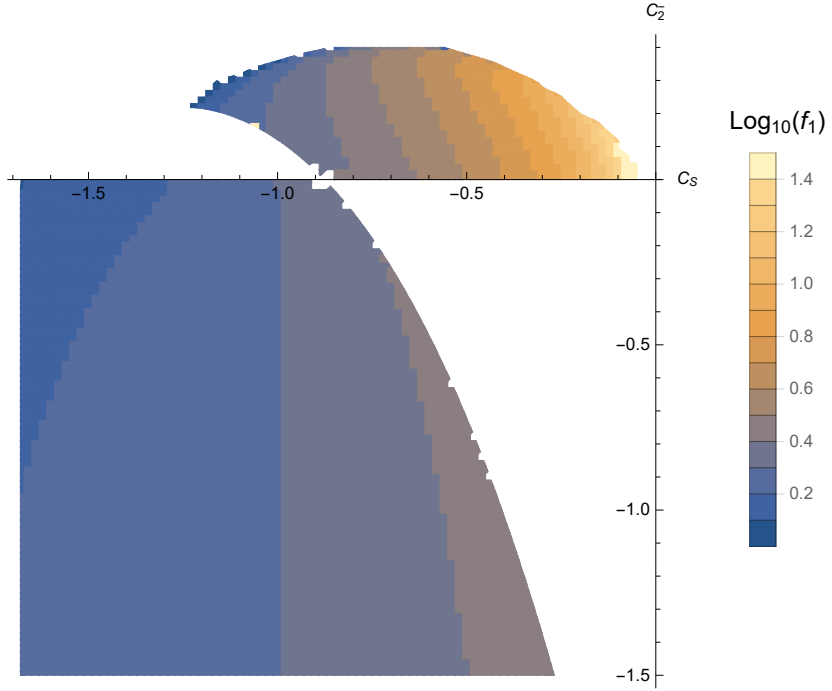


Figure 16: Contour lines of f_1

discontinuous, in particular diverging for the temporal component of the wormholes.

The level curves of $b_{1/2}$ in figure 17 show that this parameter is always positive for $C_2^- < 0$, but that it also takes negative values in a portion of the region $C_2^- > 0$, giving rise to the behavior plotted in figure 18. Indeed, for our data we have approximately $b_{1/2} \in (-10, 80)$. The wormholes with negative $b_{1/2}$ correspond with the wormholes with b_0 large, i.e. the region close to the $(1, -1)_0$ solutions. In the upper region we have also found the line with $b_{1/2} = 0$ that we will describe in the following section. From the families described in section 2.9.2 and 2.9.6 we expect to find only solutions with $r_0 \leq \sqrt{\frac{1}{3}}$ on the line with $b_{1/2} = 0$. Indeed we can see that the level sets of r_0 cross the line $b_{1/2} = 0$ only for $r_0 \leq \sqrt{\frac{1}{3}}$ (figure 20). From this plot it results that the condition $r_0 \leq \sqrt{\frac{1}{3}}$ is also valid for the asymptotically flat solutions with $b_{1/2} < 0$.

At the transition with the black holes, $b_{1/2}$ takes large values and it could diverge approaching the black hole lines. At the transition with the $(1, -1)_0$ solutions, instead, $b_{1/2}$ takes large negative values.

In figure 19a the contours plot of the quantity defined as

$$\Delta = \sqrt{\frac{\Delta f(r_{fit})^2 + \Delta B(r_{fit})^2 + \Delta f'(r_{fit})^2 + \Delta B'(r_{fit})^2}{4}} \quad (6.2)$$

are shown. This quantity gives an estimate of how much precise the results obtained are. For our data we have approximately $10^{-16} < \Delta < 1$

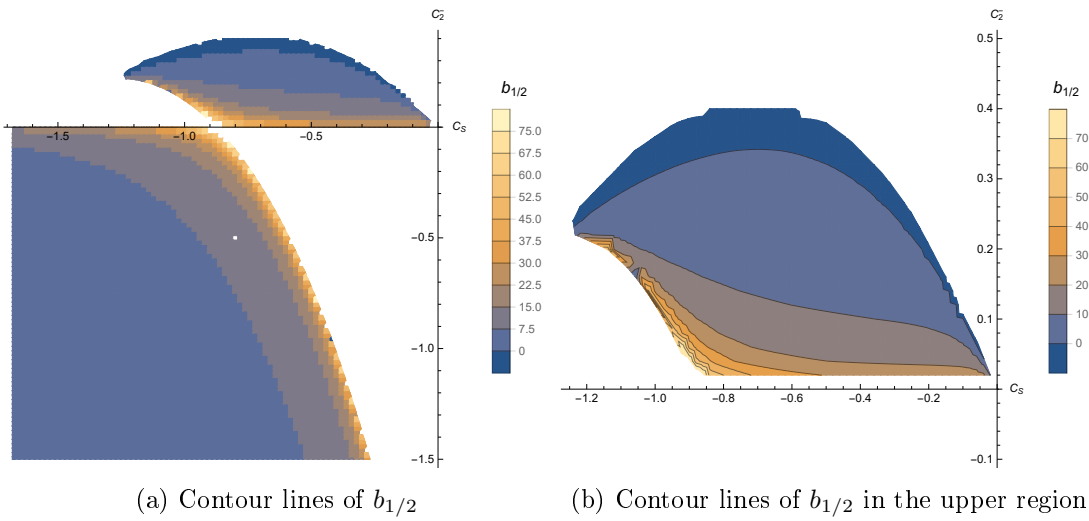


Figure 17

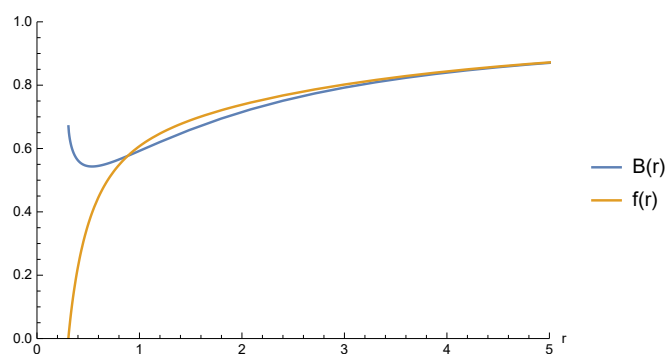
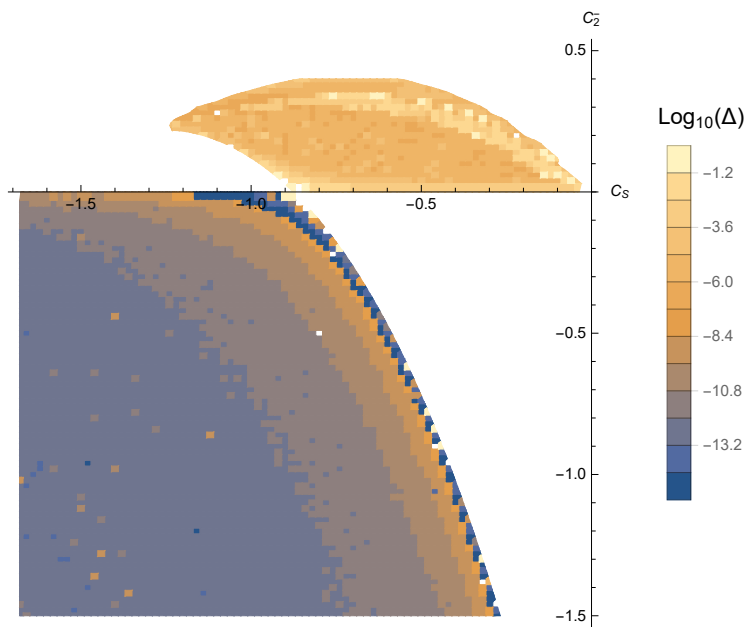
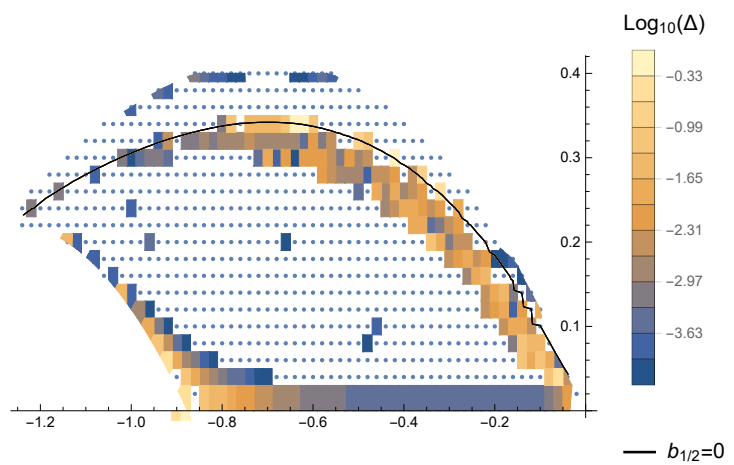


Figure 18: Wormhole solution with $b_{1/2} < 0$ corresponding to the point $(C_S, C_2^-) = (-0.65, 0.35)$



(a) Contour lines of Δ



(b) Contour lines of $\Delta > 10^{-4}$

Figure 19

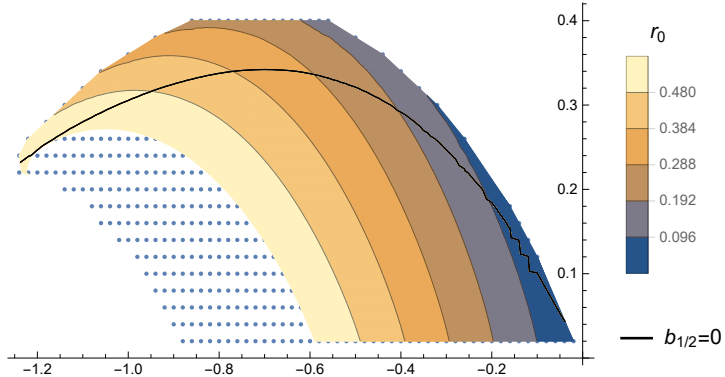


Figure 20: Contour lines of $0 < r_0 < \frac{1}{\sqrt{3}}$

For the black hole solutions in the section above we had this quantity always minor than 10^{-4} . In this section the solutions are of a different kind, and r_{fit} has been taken closer to the singularity than the black holes case. For these reasons we have to choose again a value of Δ that define a good level of accuracy for our solutions. We consider as good level of precision the values of Δ such that the corresponding solutions integrated from the singularity to large radius stay flat at least till $r \simeq 8$, just like we have for the black holes. For our data the solutions with $\Delta < 10^{-4}$ show this regular behavior, so $\Delta < 10^{-4}$ discriminates the solutions with good precision, for both wormhole and black hole solutions. On the contrary within the range $\Delta < 10^{-4}$, a minor Δ does not mean a better behavior of the solutions, indeed almost all the solutions within this range stay flat till $r \simeq 8$.

In figure 19b only the data with $10^{-4} < \Delta < 1$ are shown, and it is easy to see that we have three regions with less precision all in the upper side. We have two regions with less precision located close to the transition with the other families, and one around the level curve $b_{1/2} = 0$. This agrees with what we have described in section 2.9.5 and 2.9.6: by calculating the various order of the expansion (2.101) it can be noticed that $b_{1/2}$ is in the denominator of all the coefficients of the higher order, and some divergences appear when taking the limit $b_{1/2} \rightarrow 0$, unless the relation (2.84) is satisfied. This clearly complicates the convergence of the shooting code around this line, so the precision gets lost in this area. However it is possible to describe the solutions on the line $b_{1/2} = 0$ using the appropriate expansion at r_0 .

6.3 Solutions with $b_{1/2} = 0$

The first trial we made to find the solutions on this line involved the expansion (2.82): we did not get a good accuracy level, and we also had problems with the number of free parameters. Instead, by inserting the series (2.105) in our o.d.e. system we have noticed a new free parameter $f_{3/2}$ emerging, and the new more

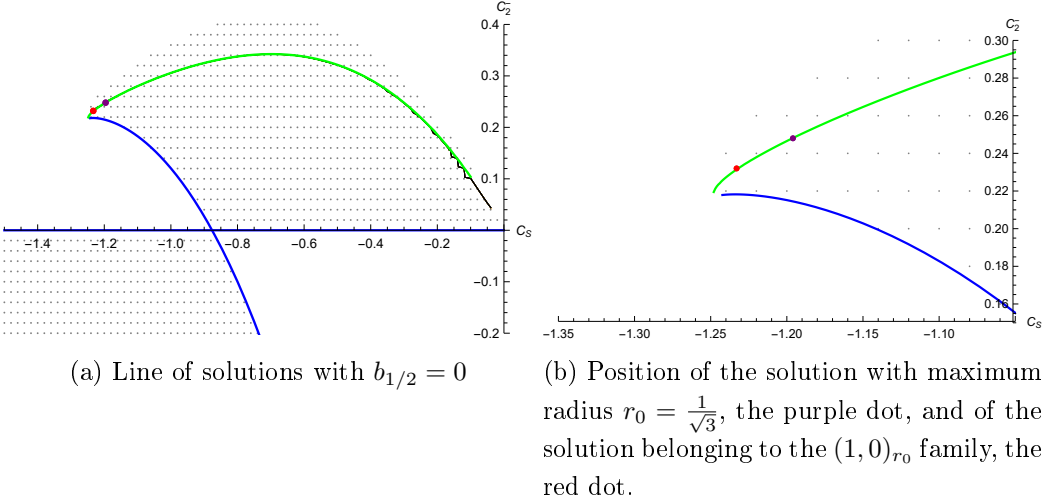


Figure 21

general subfamily of solutions (2.106) was obtained. It has the correct number of free parameter to describe a line on the phase diagram. Another shooting code has been initialized with this expansion, obtaining the correct solutions for $b_{1/2} = 0$ with positive result in terms of precision on the parameters.

The location of these wormholes is shown by the green line in figure 21, and it coincides with the level curve $b_{1/2} = 0$ obtained by the interpolation of the previous data.

We got a good precision for the points on the green line with $-1.247 < C_S < -0.210$. For $-0.210 < C_S < 0$ the shooting code does not converge with a good precision, but this is simply due to the high values of the gradient of the parameters in this region (i.e. high variability for small deviation from the correct position). For C_S decreasing we have an increase of r_0 till $r_0 \simeq \frac{1}{\sqrt{3}} \simeq 0.57735$, corresponding to the solution located in $(C_S, C_2^-) \simeq (-1.196, 0.248)$ (the purple dot in figure 21). After this maximum, r_0 start to decrease and the line seems to end on the same critical point of the non-Schwarzschild black holes. The maximum of r_0 found is in agreement with the constraint found for this family $r_0 \leq \sqrt{\frac{2\alpha}{3\gamma}}$ or, in our unit $r_0 \leq \sqrt{\frac{1}{3}}$.

The relation (2.84) is satisfied by two values of f_1 for every r_0 , but we have used

$$f_1 = \frac{2\alpha + \sqrt{4\alpha^2 - 6\alpha\gamma r_0^2}}{3\alpha r_0} \quad (6.3)$$

for the solutions before the maximum of r_0 , i.e. $-1.196 < C_S < 0.210$, and

$$f_1 = \frac{2\alpha - \sqrt{4\alpha^2 - 6\alpha\gamma r_0^2}}{3\alpha r_0} \quad (6.4)$$

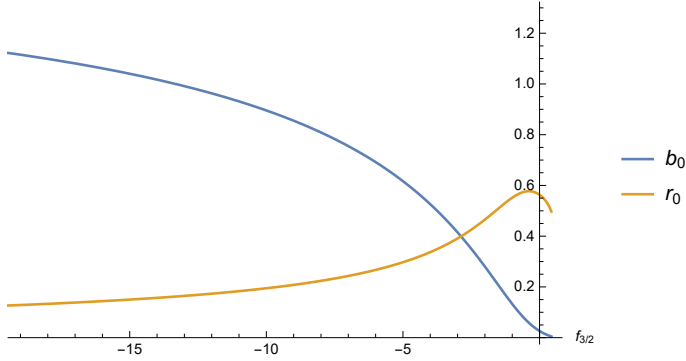


Figure 22: Relations between the parameters of the solutions with $b_{1/2} = 0$

for the solutions with $-1.247 < C_S < -1.196$. There were no other choices to obtain a good convergence. In our unit we have

$$f_1 = \frac{2 \pm 2\sqrt{1 - 3r_0^2}}{3r_0} \quad (6.5)$$

and we have f_1 continuous along the entire line, since the change of sign in the relation (2.84) happens when $r_0 = \frac{1}{\sqrt{3}}$, i.e. when the two choices coincide. The new parameter $f_{3/2}$ takes negative values for $-1.233 < C_S < 0.210$, it vanishes in $(C_S, C_2^-) \simeq (-1.233, 0.232)$ (the red dot in figure 21), and it becomes positive for $-1.247 < C_S < -1.233$.

The point $f_{3/2} = 0$ coincides with the unique asymptotically flat solution found for the $(1, 0)_{r_0}$ family: indeed the two families coincide for this point, since $f_{3/2}$ appears only in the numerator of the semi-integer coefficient of the (2.106). So, when it vanishes, we get the same expansion of the (2.82). A shooting code with the expansion (2.82) confirmed this data. In [9] they found with different numerical methods that the unique solution belonging to the $(1, 0)_{r_0}$ family has $r_0 \simeq 0.577198$, i.e. the wormholes with $f_{3/2} = 0$ and maximum r_0 almost coincide, so it is unclear if the point $f_{3/2} = 0$ is actually different from the solution with $r_0 = \frac{1}{\sqrt{3}}$, or if the difference obtained with our method is due to numerical errors.

In figure 22 the behaviors of r_0 and b_0 with respect to $f_{3/2}$ are shown; they corresponds to moving along the line with C_S decreasing.

Having $b_{1/2} = 0$, these solutions have the first derivatives finite of both the metric component at the singularity. This makes them more suitable to go behind the singularity in the $r < r_0$ region, even if a problem occurs also in that case as we will see in the following section.

We conclude with a comment regarding the behavior of the gravitational potential of these solutions, codified in the component $B(r)$. We have two possibilities similarly to the generic wormholes case:

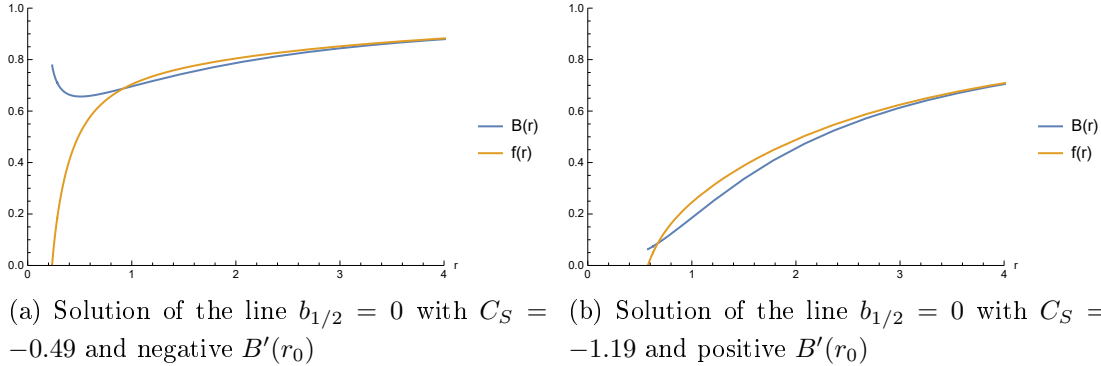


Figure 23

- for $C_S > -0.99$ (corresponding to $b_0 > 0.22$, $f_{3/2} < -1.59$) the solutions are of the kind shown in figure 23a, and the gravitational potential has a minimum in $r^* > r_0$, similarly to the generic wormholes case with $b_{1/2} < 0$;
- for $C_S \leq -0.99$ the solutions have $B(r)$ monotonic, as shown in figure 23b, and they are similar to the generic wormholes with $b_{1/2} > 0$.

The solution with $C_S \simeq -0.99$ is the unique solution with the first derivative of $B(r)$ vanishing in $r = r_0$, it has $b_0 \simeq 0.22$, $r_0 \simeq 0.50$, and it is monotonic too.

6.4 Interior of wormholes

The generic solutions of the $(1, 0)_{r_0, 1/2}$ family show the following property: they do not want to be explored inside $r = r_0$ by an observer initially located outside of $r = r_0$. We have seen that this is physically due to the radial geodesic that proceeds in a region with $\rho = \sqrt{r - r_0}$ with inverted sign, corresponding to a copy of $r > r_0$. This property is also present in a mathematical sense, since the expansion (2.101) takes real values only for $r \geq r_0$.

Actually we have seen that a similar expansion for the interior of the wormholes satisfies our e.o.m. of the Einstein-Weyl theory. It is possible to change variable by defining $\rho' = \sqrt{r_0 - r}$, and it is easy to verify that the expansion

$$\begin{aligned}
 f(r) &= f_1(r_0 - r) + \frac{16\alpha f_1 + 8\gamma r_0 + 12\alpha f_1^2 r_0 - \alpha b_{1/2}^2 f_1^2 r_0^2}{3\alpha b_{1/2} f_1 r_0^2} (r_0 - r)^{3/2} + O((r_0 - r)^2) \\
 B(r) &= b_0(1 + b_{1/2}(r_0 - r)^{1/2} + \frac{8\alpha f_1 - 2\gamma r_0 + 9\alpha f_1^2 r_0 + \alpha b_{1/2}^2 f_1^2 r_0^2}{3\alpha f_1^2 r_0^2})(r_0 - r) + \\
 &\quad + O((r_0 - r)^{3/2})
 \end{aligned} \tag{6.6}$$

is a solution of our o.d.e system for $r < r_0$ and close to r_0 . It is the most reasonable candidate to describe the interior of the wormholes since it is the unique solution

valid for $r < r_0$ with 4 free parameters and $f(r_0)$ vanishing.

For black hole solutions we used the same expansion for both the interior and the exterior of the singularity, and we have used the continuity of the metric components and of their first derivatives to fix the internal parameters, knowing the values of the external ones. If we use this procedure here, with the (2.101) for the outside and the (6.6) for the inside, we can fix just the parameters r_0 , b_0 and f_1 for $r < r_0$, knowing the respective parameters for $r > r_0$. Indeed, if $b_{1/2} \neq 0$, the first derivative of $B(r)$ is diverging for both the expansion in the limit $r \rightarrow r_0$, so the continuity of $B'(r)$ is not well defined and it seems reasonable just to require that $b_{1/2} \neq 0$ outside implies $b_{1/2} \neq 0$ inside. This problem could seem related to the divergence of the first derivative of $B(r)$, and the description of the space-time with the (6.6) could appear incorrect. However something similar happens in the more suitable $b_{1/2} = 0$ case. One can find the corresponding expansion of the (2.106) that describes such solutions for $r < r_0$. In this case the continuity of the metric would fix the corresponding b_0 and r_0 in the inside, once fixed all the parameter for $r > r_0$, but the continuity of the first derivatives of the metric would be automatically satisfied, leaving the coefficient $f_{3/2}$ undetermined in the interior of the wormhole.

An alternative procedure could be using a more physical condition such as imposing the continuity of an invariant quantity in $r = r_0$. We take again the Kretschmann scalar as example. With the metric of the form (2.101) we get

$$K(r) = R_{\mu\nu\rho\sigma}R^{\mu\nu\rho\sigma} = \frac{8 - 8f_1r_0 + 6f_1^2r_0^2}{r_0^4} + O(\sqrt{r - r_0}) \quad (6.7)$$

valid for $r > r_0$, and for the metric (6.6)

$$K(r) = R_{\mu\nu\rho\sigma}R^{\mu\nu\rho\sigma} = \frac{8 + 8f_1r_0 + 6f_1^2r_0^2}{r_0^4} + O(\sqrt{r_0 - r}) \quad (6.8)$$

valid for $r < r_0$. The condition $K(r_{0,e}) = K(r_{0,i})$ can be satisfied by the two conditions

$$r_{0,i} = r_{0,e}$$

$$f_{1,i} = -f_{1,e}$$

where the subscript indicates the internal and external set of parameters, respectively of the expansions (6.6) and (2.101). The two conditions correspond to make continuous $f(r)$ and its first derivative. Again we have nothing to fix the $b_{1/2}$ parameter for the internal expansion. In the general quadratic theory the Riemann tensor squared for the wormhole solutions is the (2.100). Instead in the interior,

with a parameterization analogous to the (6.6), the Kretschmann scalar is

$$R_{\mu\nu\rho\sigma}R^{\mu\nu\rho\sigma} = \frac{b_{1/2}^2 f_{3/2}^2 r_0^4 - 2b_{1/2}(b_{1/2}^2 - 4b_1)f_1 f_{3/2} r_0^4 + f_1^2((b_{1/2}^2 - 4b_1)^2 r_0^4 + 128r_0^2) + 256}{64r_0^4} + O(\sqrt{r_0 - r}) \quad (6.9)$$

that is the same expression of the (2.100), but the coefficients are referred to the powers of the variable $\rho' = \sqrt{r_0 - r}$. We could fix again $r_{0,i} = r_{0,e} = r_0$, $-f_{1,i} = f_{1,e} = f_1$, and the condition $K(r_{0,e}) = K(r_{0,i})$ would become equivalent to

$$(f_1(b_{1/2,i}^2 - 4b_{1,i}) + b_{1/2,i}f_{3/2,e})^2 = (f_1(b_{1/2,e}^2 - 4b_{1,e}) - b_{1/2,e}f_{3/2,e})^2 \quad (6.10)$$

that clearly has more than a unique solution for the internal parameters once fixed the external ones. Since in all the cases encountered the internal solutions seem not determined by the external ones, perhaps an ambiguity could appear when a wormhole singularity of the o.d.e. is encountered, and such ambiguity could bring interesting features of the coupling with matter of the wormhole solutions. Maybe a change of coordinates or a different combinations of $B(r)$ and $f(r)$ could make clearer the correct junction conditions at $r = r_0$.

In any case we tried to explore the interior of our solutions using the expansion (6.6) with the following choices

$$\begin{aligned} r_{0,i} &= r_{0,e} \\ b_{0,i} &= b_{0,e} \\ f_{1,i} &= -f_{1,e} \\ |b_{1/2,i}| &= |b_{1/2,e}| \end{aligned} \quad (6.11)$$

As stated before, the first two conditions make $f(r)$ and $B(r)$ continuous at the singularity, and the third makes $f'(r)$ continuous in r_0 . We recall that there are no reason for the last choice, that remains unjustified.

We integrated our solutions from $r = r_0$ to $r = 10^{-5}$, in both the cases $b_{1/2,i} = \pm b_{1/2,e}$, obtaining the two behavior shown in figure 24. Again, we evaluated

$$I_B = r \frac{B'(r)}{B(r)}|_{r=10^{-5}}$$

for each solution. The results are shown in figure 25. The choice $b_{1/2,i} = -b_{1/2,e}$ makes almost all the wormholes of the $(2,2)_0$ kind at the origin. However, it is not clear what happens to the solutions close to the black hole lines: the results for these solutions show a negative $B(r)$ too, and the solutions has an I_B close to zero, but all of this seems due to numerical errors related to the choice $b_{1/2,i} = -b_{1/2,e}$.

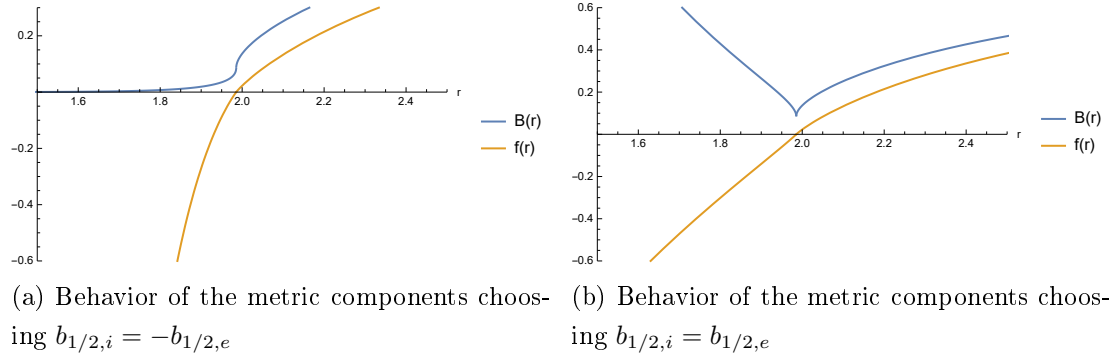


Figure 24: Behavior of the metric components with the conditions (6.11) for the solution corresponding to the point $(C_S, C_2^-) = (-1.08, -1.14)$

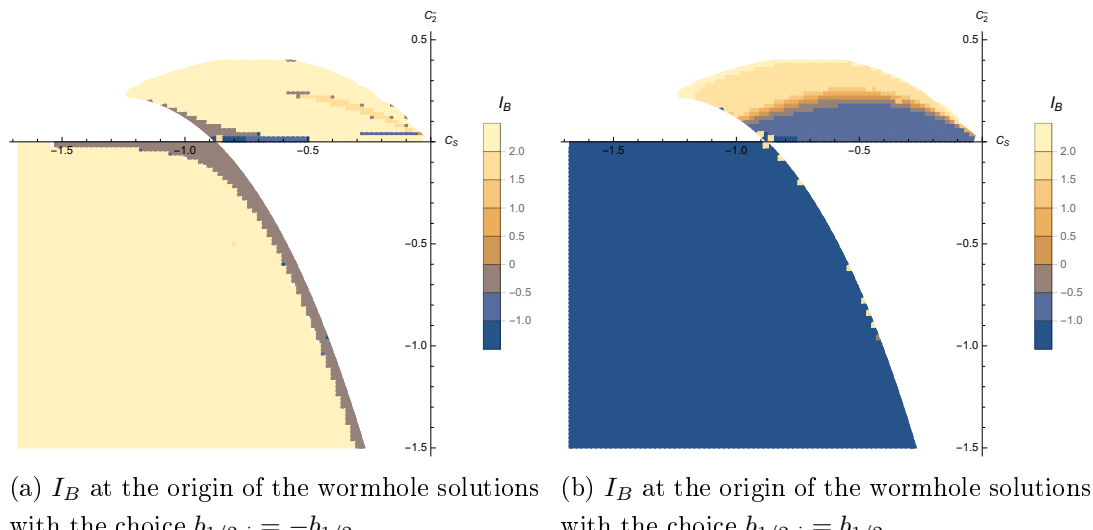


Figure 25: Internal behavior of the wormhole solutions

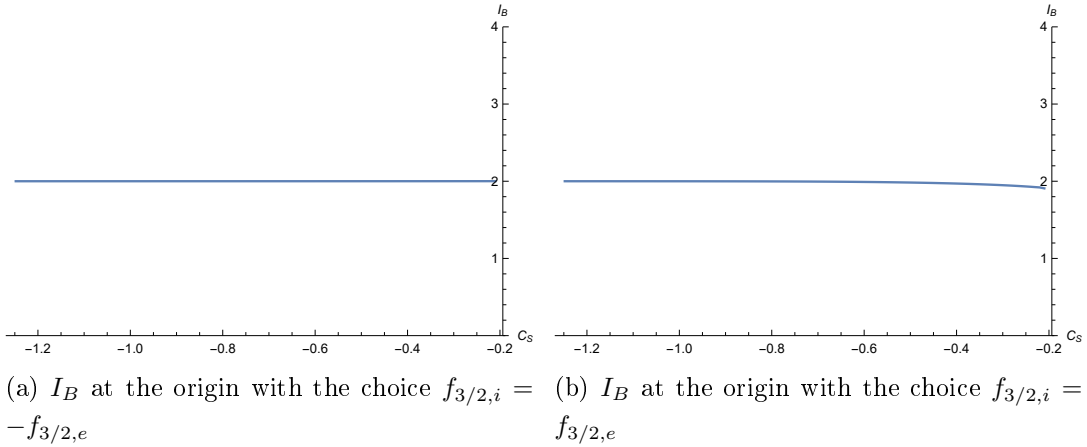


Figure 26: Internal behavior of the wormhole solutions with $b_{1/2} = 0$

The results for $b_{1/2,i} = b_{1/2,e}$ are little bit more interesting. The upper region with $C_2^- > 0$ seems to be filled by wormholes that at the origin go like the $(2, 2)_0$ solutions, but in the lower region $C_2^- < 0$ they seem to go like the $(1, -1)_0$ solutions. Actually in figure 25b almost half of the wormholes of the upper region seems to have the $(1, -1)_0$ behavior too, but again a deeper analysis showed that for very small radius they go as the $(2, 2)_0$ solutions ⁷. Instead for $C_2^- < 0$ the $(1, -1)_0$ behavior has been confirmed by the deeper analysis. This result matches with continuity what we have found for the interior of the non-Schwarzschild black holes. In this sense the choice $b_{1/2,i} = b_{1/2,e}$ (corresponding to the behavior 24b) could be the correct one (or close to the correct choice) in order to continue the solutions behind $r = r_0$, even if we have no theoretical reasons to justify it. In any case this must be taken carefully. The same behavior of $B(r)$ at the origin for black holes and wormholes does not imply any continuity for $B(r)$ when the common behavior is of the $(1, -1)_0$ kind: $B(r)$ diverges like $O(\frac{1}{r})$ in both cases, but with negative sign for black holes and positive sign for wormholes.

For completeness we also report in figure 26 the results for the $b_{1/2} = 0$ case. This time we impose the conditions

$$\begin{aligned} r_{0,i} &= r_{0,e} \\ b_{0,i} &= b_{0,e} \\ |f_{3/2,i}| &= |f_{3/2,e}| \end{aligned} \tag{6.12}$$

In both cases $f_{3/2,i} = \pm f_{3/2,e}$, the functions $f(r)$ and $B(r)$ have both the first derivative continuous, and the solutions around the singularity show the behaviors reported in figure 27. In agreement with what we found for the generic wormholes

⁷Exactly like the transition area described in the general analysis of the phase diagram

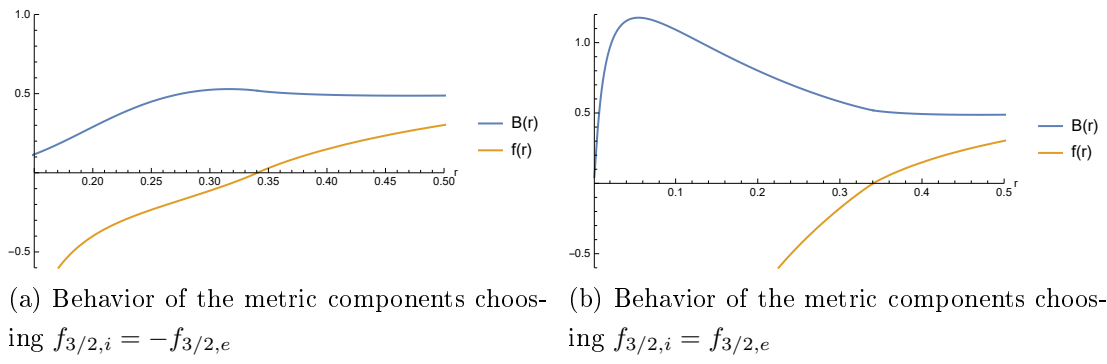


Figure 27: Behavior of the metric components with the conditions (6.12) for the solution with $b_{1/2} = 0$ corresponding to the point $(C_S, C_2^-) = (-0.690, 0.342)$

around the $b_{1/2} = 0$ line, the behavior at the origin for $b_{1/2} = 0$ is of the $(2, 2)_0$ kind for both the choices $f_{3/2,i} = \pm f_{3/2,e}$.

We conclude considering that by imposing the continuity of $B(r)$ at r_0 a change of signature of the metric occurs for $r < r_0$. Such signature change is clearly different from the one happening in black hole solutions since this time we get two temporal components for $r < r_0$. We do not discuss here the implications of such change of signature. It could be asked if a discontinuity of the temporal component $B(r)$ can be admitted at $r = r_0$ since the first derivative of this function is diverging, however in the $b_{1/2} = 0$ case the continuity condition seems inevitable.

6.5 Coupling with matter

Regarding the coupling with matter we give only some general points. In [7] the coupling with matter has been studied analytically in the linearised theory in both the case $\beta \neq 0$ and $\beta = 0$, instead in [5] a numerical study of the coupling in the full non-linear theory has been done. The most suitable matter source is a thin shell source, indeed it has been used in both the mentioned works. This because the stress-energy tensor $T_{\mu\nu}$ of such source is characterized by a delta function $\delta(r - l)$ and by the total mass M , so the connection with the vacuum solutions is obtained by simply introducing specific finite discontinuities in the metric components or in their derivatives for $r = l$. Indeed we have to satisfy the equation

$$H_{\mu\nu} = \frac{1}{2} T_{\mu\nu} \quad (6.13)$$

where the discontinuities of the metric are represented by the Heaviside function $\theta(r - l)$. Then the derivatives of the Heaviside function bring the correct delta functions on the left hand side of the (6.13) in order to be equal to the delta function in the stress-energy tensor on the right hand side.

The main point found in both the previous works is that the solutions depend on both the parameters M and l , and not only on the total mass as in GR. In general, the solutions in the $\beta = 0$ theory can depend on up to two parameters of the matter source, and up to three parameters in the general $\beta \neq 0$ case. We refer now only to the Einstein-Weyl theory, but the general quadratic theory shares the same details. In [7] it is suggested that the solution inside the thin shell source must be specified by the $(0, 0)_0$ family since we expect the metric to be regular in the origin, having no source in $r = 0$. Then, in the exterior, the solution should take a form similar to solutions of the $(2, 2)_0$ family, since this family has the maximum number of parameters. Indeed, from the counting of parameters we got that the $(0, 0)_0$ family has two free parameters, while the $(2, 2)_0$ family has a total of four, and, at the same time, we have four junction conditions at $r = l$. In this way, we have a total of two free parameters that are fixed by imposing asymptotic flatness at large radius. If the external solution had less than four parameters the system would be over constrained, or more precisely, only for a subspace of the possible values of M and l we can find a solution.

On the contrary, in [5] they found numerical solutions that in the interior of the source are of the $(0, 0)_0$ family only when l is greater than the would be horizon⁸. Instead, for l smaller than the would be horizon, the interior is described by a subfamily of the $(2, 2)_0$ family having the same number of parameters of the $(0, 0)_0$ one. Holdom suggests that, even if this subfamily has a singularity in the origin, having $\sqrt{-g}$ proportional to r^4 , the Weyl squared proportional to r^{-4} , and in particular the R^2 regular, the Lagrangian density for this $(2, 2)_0$ subfamily is regular in all the space-time. Both the works suggest that the $(2, 2)_0$ family is the most suitable family to be coupled with matter.

More precisely, in order to understand the form of the solutions at the exterior of the mass distribution, we need to take the limit of $l > 0$, since we recall that the $(2, 2)_0$ family or the $(1, -1)_0$ correspond to expansions around the origin. Actually, we have seen that, even if the $(1, -1)_0$ family has three free parameters, the $(1, -1)_0$ solutions found in the phase diagram behave as they had four. For this reason, we cannot exclude the possibility that, in the limit $l \rightarrow 0$, the solution becomes of the $(1, -1)_0$ form rather than of the $(2, 2)_0$ one.

Moreover, the possibility that in the exterior (and eventually also in the interior) of the thin shell source there is a singularity of the wormhole kind has never been taken into account. Since the wormhole family has the maximum number of parameters allowed, it can be coupled with the thin shell model, and from the parameters counting a unique solution can still be found. However, the problem shift again on

⁸Fixed M the would be horizon is $r_0 = 2GM$

determining how the solutions must be connected from the interior to the exterior of the wormhole. Taking inspiration from what happens in general relativity, we expect that, if it is possible to couple a matter source with a wormhole solution, the wormhole singularity should be at the exterior of the matter distribution, i.e. $r_0 > l$; we also expect that the interior of the mass distribution is actually described from the $(0, 0)_0$ family around the origin, in order to ensure the regularity of the metric where there is no mass. This will certainly be object of a future work, once better understood how the wormhole solution have to be connected from the interior to the exterior.

What we can state now, in general, about the coupling with matter is that specifying the two parameters M and l corresponds to fixing the exterior of the solution as one of the possible solutions found on our phase diagram 1, i.e. the values (M, l) fix a point on the (C_S, C_2^-) plane. In the theories with higher derivatives, as previously said, we cannot identify the mass of the source with the Newtonian mass that appear at large radius, but we can affirm quite confidently that with the former increasing, the latter grows too. In this way, the increase of the parameter M should correspond to moving away from the origin $(C_S, C_2^-) = (0, 0)$ in the direction of negative C_S on our phase diagram, but the precise value of C_S and C_2^- should be determined by both the parameter l and M . If we consider a collapsing thin shell with constant mass, i.e. fixed M and l decreasing, this could roughly correspond to varying C_2^- , keeping C_S fixed, so that, by varying the localization of the mass we could obtain for $r > l$ a solution similar to the $(2, 2)_0$ kind, that reach a transition point where becomes a black hole, and then a wormhole. This would not be too much different than the same situation in general relativity, in which, while l decreases the exterior solution does not change but for $l < 2GM$ an horizon appears in $r = 2GM$.

On the contrary, in [5] Holdom suggested that the $(2, 2)$ holes can be the actual final states of a collapsing star, proving the presence of a trapping mechanism for these solutions that would appear really similar to black holes in general relativity at large radius.

6.6 The new region $\rho < 0$

Unlike the $r < r_0$ region, exploring the new copy $r > r_0$, $\rho < 0$ does not present any particular problem. Indeed, switching from the r to the $\rho = \sqrt{r - r_0}$ variable makes the metric regular in $\rho = 0$. We have that our metric components become

Taylor series

$$\begin{aligned} g_{\rho\rho}^{-1}(\rho) &= \frac{f(r(\rho))}{4\rho^2} = \frac{f_1}{4} + \frac{(\alpha f_1^2 r_0(b_{1/2}^2 r_0 + 12) - 16\alpha f_1 + 8\gamma r_0)}{12\alpha b_{1/2} f_1 r_0^2} \rho + O(\rho^2) \\ -g_{tt}(\rho) &= B(r(\rho)) = b_0 \left(1 + b_{1/2} \rho + \frac{(\alpha f_1^2 r_0(b_{1/2}^2 r_0 - 9) + 8\alpha f_1 + 2\gamma r_0)}{3\alpha f_1^2 r_0^2} \rho^2 + \right. \\ &\quad \left. + O(\rho^3) \right) \end{aligned} \quad (6.14)$$

valid for both the patches $\rho < 0$, $\rho > 0$.

In this form it is visible that all the free parameters f_1 , b_0 , $b_{1/2}$, r_0 , (or b_0 , $f_{3/2}$, r_0 , for the $b_{1/2} = 0$ case) fix the metric components and the first derivatives with respect to ρ in $\rho = 0$.

Having $H_{\mu\nu}$ in a covariant form, the equivalent e.o.m. written in terms of ρ , are obtained by contracting both the indices μ and ν with the inverse of the Jacobian

$$H'_{\alpha\beta}(\rho) = H_{\mu\nu}(r(\rho)) \frac{dx^\mu}{dx'^\alpha} \frac{dx^\nu}{dx'^\beta} \quad (6.15)$$

which in our case modifies only H_{rr} , obtaining $H_{\rho\rho} = 4H_{rr}\rho^2$. It is clear that the solution for $\rho < 0$, $r > r_0$ must satisfy the same o.d.e. system valid in $\rho > 0$. Once the parameters for the asymptotically flat solutions in $\rho > 0$ are obtained, they can be used for $\rho < 0$. This is exactly what we have done. Then we have integrated again to the large radius regime corresponding to $\rho \rightarrow -\infty$. Since all the semi integer terms of the (2.101) are odd functions in $b_{1/2}$ and the integer terms are even functions in $b_{1/2}$, the expansion written for $\rho < 0$ has been obtained by changing the sign of $b_{1/2}$ in the (2.101), and then integrated to large radius by using the same o.d.e. system (2.33,2.34) written in terms of the r coordinate. In the $b_{1/2} = 0$ case, we have a similar property: the semi integer terms of the (2.106) are odd function in $f_{3/2}$, and the integer terms are even function in $f_{3/2}$, so for these solutions the $\rho < 0$ region has been described by changing the sign of this parameter.

The results show a strongly non-flat behavior in the $\rho < 0$ region for almost all the solutions. We have a typical exponential growth for $f(r)$ and a corresponding exponential descent for $B(r)$ such that both g_{tt} and g_{rr} become exponentially small for large radius (figure 28a). More precisely, the behavior of $\frac{f'(r)}{f(r)}$ and $\frac{B'(r)}{B(r)}$ is not exactly constant as it should be for a perfect exponential, but we have noticed that the derivative of these quantities shows a behavior of the kind

$$\begin{aligned} \frac{d}{dr} \left(\frac{f'(r)}{f(r)} \right) &= - \left(\frac{f'(r)}{f(r)} \right)^2 + \frac{f''(r)}{f(r)} = -\frac{2}{r^2} \\ \frac{d}{dr} \left(\frac{B'(r)}{B(r)} \right) &= - \left(\frac{B'(r)}{B(r)} \right)^2 + \frac{B''(r)}{B(r)} = \frac{2}{r^2} \end{aligned} \quad (6.16)$$

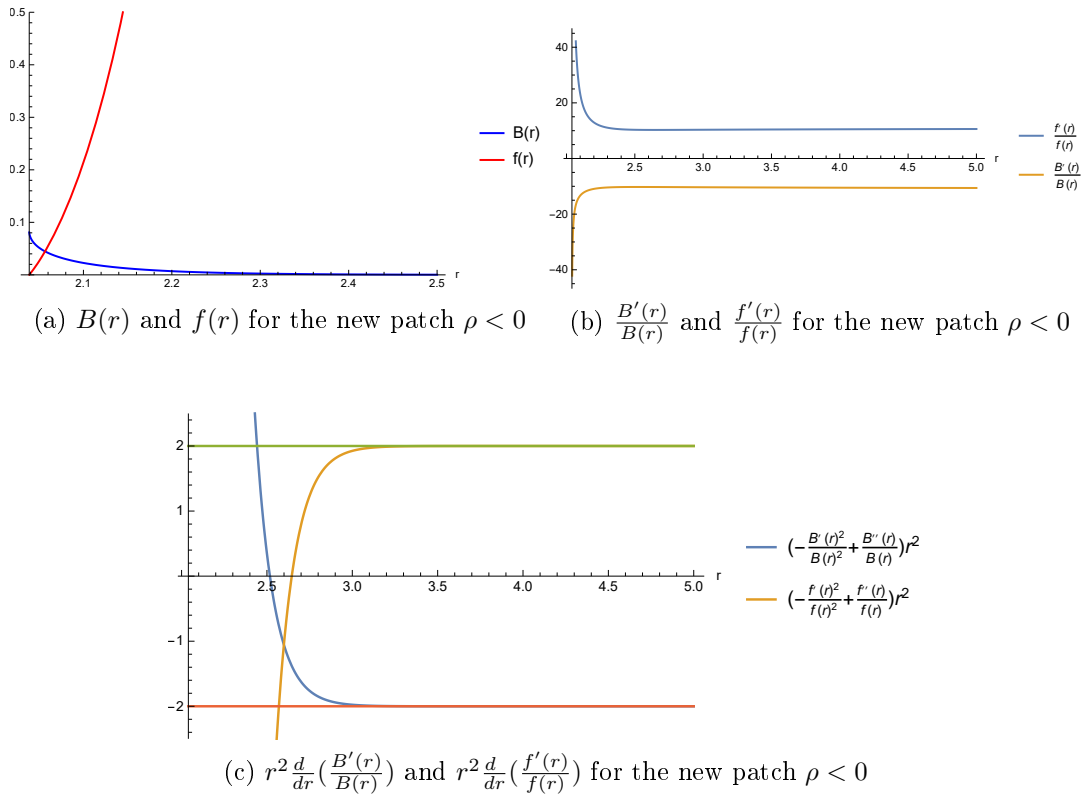


Figure 28: Typical behavior of the metric in the $\rho < 0$ region for the wormhole solution corresponding to $(C_S, C_2^-) = (-1.18, -1.00)$.

as shown in figure 28c. The previous equations can be easily integrated, finding

$$\begin{aligned} f(r) &= C_f \frac{e^{ar}}{r^2} \\ B(r) &= C_B e^{-ar} r^2 \end{aligned} \tag{6.17}$$

that correctly fit the solutions obtained for $\rho < 0$ at large radius. Indeed these functions turned out to be asymptotic solutions of our o.d.e. system.

This is one of two really general behavior, since by integrating the (2.101) from r_0 to large radius with a random set of parameters, two cases are typically encountered: one has $f(r)$ that reaches a maximum and then goes to zero encountering another singularity, the other one has $f(r)$ that, for large enough radius, grows exponentially and shows the behavior (6.17). The set of asymptotically flat parameters is in the middle of these two behaviors.

What we get from our analysis is that all the asymptotically flat solutions for $\rho > 0$, corresponding to $C_2^- < 0$, are non flat for $\rho < 0$ with the metric components described by the (6.17), and that almost all the asymptotically flat solutions for $\rho > 0$, corresponding to $C_2^- > 0$, show the same behavior for $\rho < 0$.

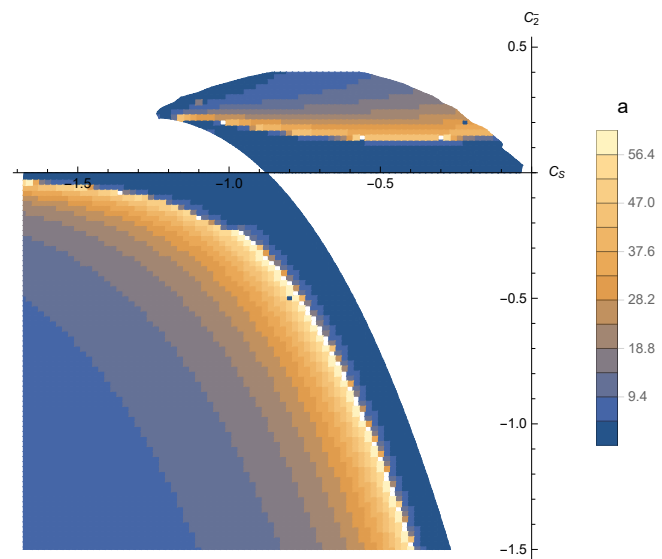
The solution of the $(1, 0)_{r_0}$ family is clearly an exception, since the asymptotic flatness for one patch implies the asymptotic flatness for the other. The solutions of the $b_{1/2} = 0$ line on the left of the $(1, 0)_{r_0}$ point represents another exception, as well as some of the generic wormhole solutions with $b_{1/2} \neq 0$ in a very small area close to this point. These two last exceptions, instead, display the aforementioned behavior with $f(r)$ vanishing again at certain point, encountering a second singularity of the o.d.e system.

We are going to try to give a physical interpretation of this new copy of $r > r_0$ in the following. The request for the asymptotic flatness for $\rho > 0$ seems to select a specific non flat behavior for $\rho < 0$. The few exceptions to this behavior are located in a very small region of our phase diagram, corresponding to the solutions on the left of the red dot in figure 21. We are not going to examine what physically happens into these solutions.

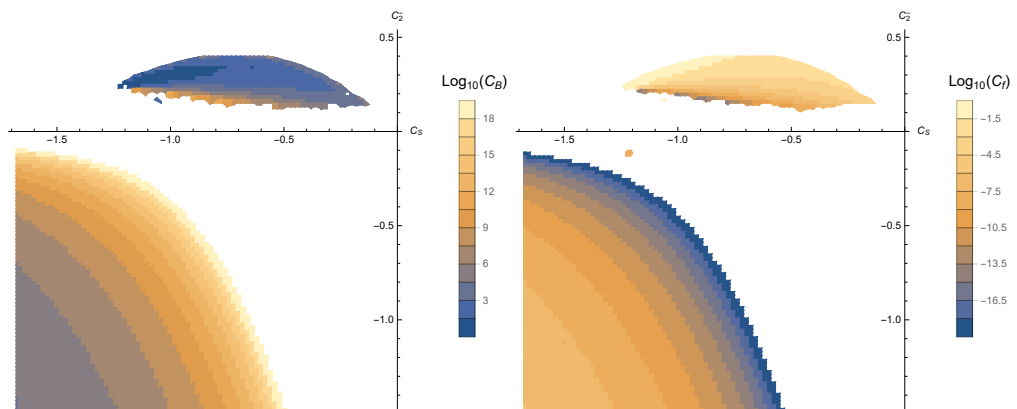
We give the results of a quick analysis made for our solutions. In figure 29 the contour plot of a , C_B , and C_f are shown. In this regime of very large $f(r)$ and very small $B(r)$ we do not know how much we can trust on the precision of the numerical integration, so the following results must be taken qualitative.

The blue region in figure 29a close to the black holes lines should not be considered, since the behavior of the metric is too extreme and the numerical integration fails after a certain radius. From the rest of the data it can be seen that the parameters a and C_B grow while approaching to the black holes region, instead C_f decreases.

For completeness we report the same analysis made for the $b_{1/2} = 0$ case. The results are shown in figure 30. They seem to agree with the results found for the



(a) Contours of the parameter a



(b) Contours of the parameter C_B

(c) Contours of the parameter C_f

Figure 29: Contour plots of the metric parameters in the $\rho < 0$ region

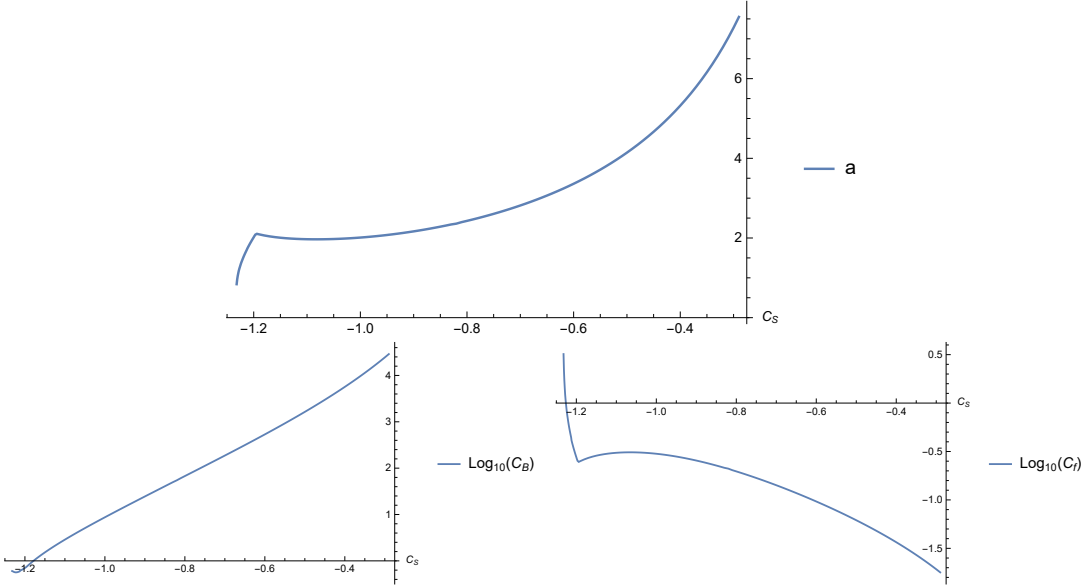
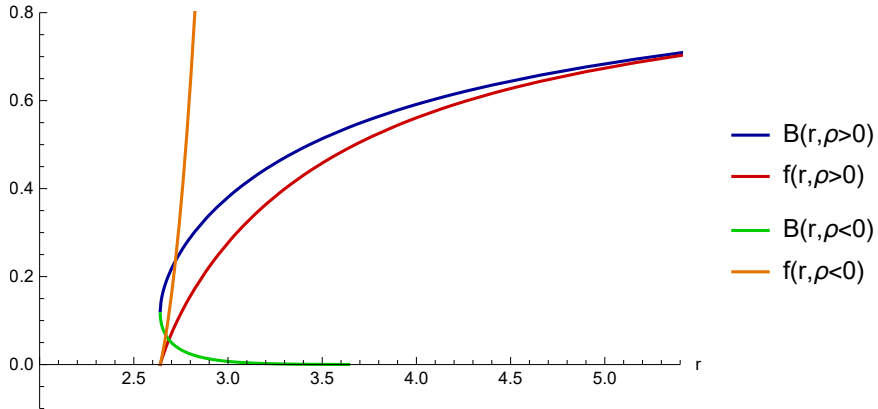
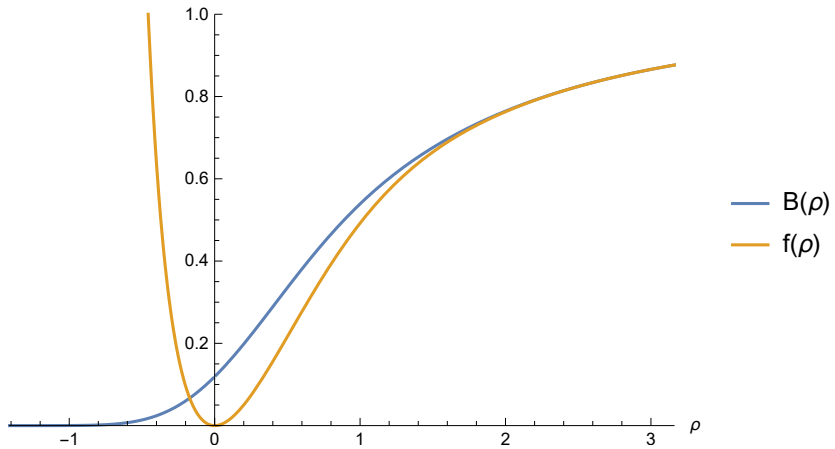


Figure 30: Behavior of the metric parameters in the $\rho < 0$ region for the $b_{1/2} = 0$ case

wormhole solutions around that line. The parameters of the metric in the $\rho < 0$ region present a smooth behavior in function of C_S , till the solution with maximum r_0 , i.e. for $-1.196 < C_S < 0$. Then all the parameters change rapidly and the exponential behavior becomes weaker till it disappears at the $(1, 0)_{r_0}$ solutions, i.e. for $-1.233 < C_S < -1.196$. As stated before, for the few solutions with $-1.247 < C_S < -1.233$ we find that, when integrating to large radius in the $\rho < 0$ region the NdSolve encounters a second singularity (we excluded these points from the plots 30). The rapid change of behavior of these quantities happens at the same point with $r_0 = \sqrt{\frac{1}{3}}$ ($C_S = -1.196$), where we changed the sign of the (2.84). This could suggest that we chose incorrectly the sign of this relation, but we checked many times that such choice was the only one correct to describe the solutions on that portion of the $b_{1/2} = 0$ line. Indeed, apart from these quantities related to the $\rho < 0$ region, all the other parameters vary smoothly when crossing the point $C_S = -1.196$.



(a) Metric of the wormhole solutions in both the regions with $r > r_0$



(b) Metric of the wormhole solutions in function of the ρ coordinate

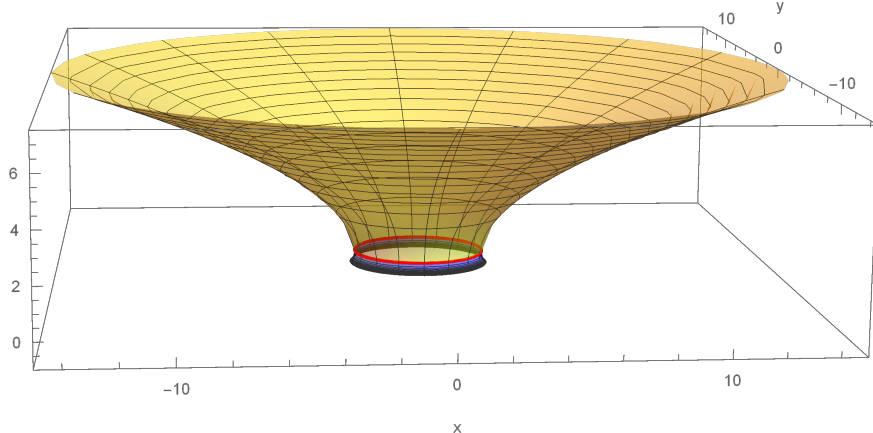
Figure 31

6.7 Physical discussion

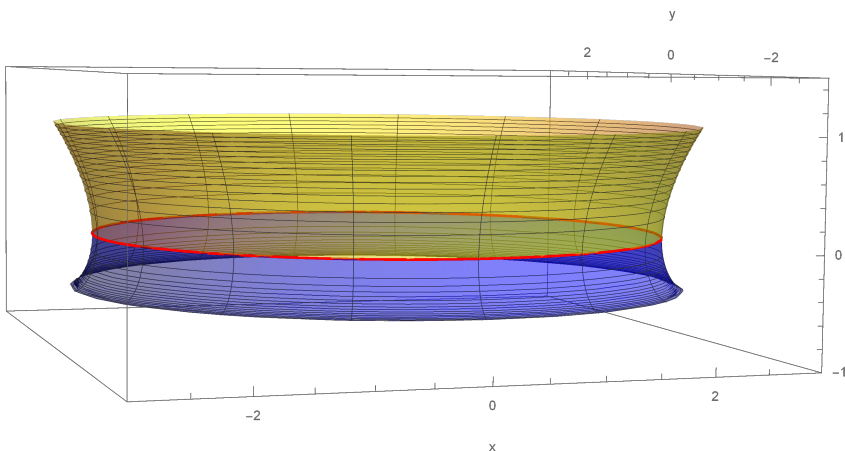
We now put together what we have obtained for both the patches and we discuss the main physical points of a massive observer that crosses a wormhole. We take as example for the wormholes with $b_{1/2} > 0$ the solution corresponding to $C_S = -1.56$, $C_2^- = -1.44$, since its characteristics are better visible than the other, but all the solutions of this region have the same following structure. We recall that this kind of wormholes cover most of the physical region of our solution space 1.

In figure 31a the components $B(r)$, $f(r)$, of both the patches, are plotted in function of the radius r . The same are plotted in function of $\rho = \sqrt{r - r_0}$ in figure 31b⁹. Summarizing what we got from the previous sections, for $\rho > 0$ the solution at large radius is described by the linearised theory (2.46), for ρ close to zero the solution goes like the wormhole expansion (2.101), and for $\rho < 0$ the solution at large radius is described by the exponential functions (6.17). $B(r)$ results to be monotonic in all

⁹In figure 31b, the function $f(r(\rho)) = g_{rr}^{-1}$ is plotted, and not the function $\frac{f(r(\rho))}{4\rho^2} = g_{\rho\rho}^{-1}$



(a) Embedding diagram of the wormhole solutions



(b) Embedding diagram around $r = r_0$

Figure 32

the space $-\infty < \rho < \infty$ so, a massive observer at any point would experience an attractive force in direction of negative ρ .

In figure 32 the embedding diagram of our wormhole solution is shown: our three-dimensional space (r, θ, ϕ) is represented by the bi-dimensional plane (x, y) and the third dimension is used to show the spatial curvature in such a way that, moving in a radial direction of a distance dr in the horizontal plane corresponds to moving on the surface embedded of a proper distance $d\tilde{r} = \frac{dr}{\sqrt{f(r)}}$. In our embedding diagram the yellow part represents the $\rho > 0$ region, the red curve corresponds to $r = r_0$, the blue part represents the $\rho < 0$ region. This type of diagram are a really convenient representation of the space curvature when we have $f(r) < 1$ for all the radius $r > r_0$ (like the Schwarzschild case). Unfortunately, this is true for the patch $\rho > 0$, but for $\rho < 0$ the exponential growth of $f(r)$ implies $f(r) > 1$ for $r > 2.951$. After this radius the proper distance $d\tilde{r}$ is shorter than dr and the region with $f(r) > 1$ cannot be represented on this diagram. This is why the blue region is much shorter

then the yellow one. However the main point of what happens to the space around $r = r_0$ is visible in this diagram. Our wormhole solutions are not so different from the Einstein-Rosen bridge in GR for r close to r_0 . This because in both wormholes and black holes we have $f(r) = O(r - r_0)$ for $r \rightarrow r_0$. The main difference is the dynamics of a free falling observer crossing the wormhole solution. In black hole solutions radial geodesics proceed in $r < r_0$. Instead for our wormhole solutions, from (2.95) we can see that this is not the case, and in particular from (2.91) we get $\dot{r} = 0$ when $r = r_0$. On the contrary, the derivative of the proper distance with respect to the proper time is

$$\frac{d\tilde{r}}{d\tau} = \frac{1}{\sqrt{f(r)}}\dot{r} = \pm\sqrt{-1 + \frac{K^2}{B(r)}} \quad (6.18)$$

which is finite for $r = r_0$ using the wormhole expansion (2.101). This corresponds to go down on the surface represented in figure 32 with a finite "velocity"¹⁰, but with a vanishing horizontal projection when $r = r_0$. The same happens to the distances derived with respect to the coordinate t .

The exponential behavior of $f(r)$ implies that the proper volume in the $\rho < 0$ region is finite. Indeed the proper volume is

$$V_p = 4\pi \int_{r_0}^{\infty} dr \frac{r^2}{\sqrt{f(r)}} \quad (6.19)$$

that converges when $f(r)$ goes like the (6.17). Similarly the proper radial distance \tilde{r} has a finite maximum for $\rho < 0$

$$\tilde{r}_{max} = \int_{r_0}^{\infty} \frac{dr}{\sqrt{f(r)}} \quad (6.20)$$

From figures 30, 14, 15, we can see that, moving in direction of negative C_S and negative C_2^- , the radius of the wormholes increases, as well as the temporal component at the wormhole radius (b_0 increasing), and the volume of the new region $\rho < 0$ (a decreasing): actually, while a decreases, C_f rapidly increases, but we checked numerically that the proper volume of the new region grows.

In the limit $r \rightarrow \infty$, $\rho \rightarrow -\infty$, the Kretschmann scalar diverges as $O(\frac{e^{2ar}}{r^6})$ as well as the squared Ricci tensor $R_{\mu\nu}R^{\mu\nu}$. Instead, the Ricci scalar and the squared Weyl tensor $C_{\mu\nu\rho\sigma}C^{\mu\nu\rho\sigma}$ result to be asymptotically vanishing as $O(\frac{1}{r^2})$. In this regime the equation (2.91) for the massive observer becomes

$$\frac{dr}{d\tau} = \pm\sqrt{-C_f \frac{e^{ar}}{r^2} + \frac{C_f K^2 e^{2ar}}{C_B r^4}} \quad (6.21)$$

¹⁰We recall that $\frac{d\tilde{r}}{d\tau}$ is not exactly the velocity experienced by the observer since $d\tilde{r}$ and $d\tau$ are distance and time interval defined in different frame of reference

In order to have a more precise physical comparison, we rewrite this relation in terms of the proper distance, but before doing this for the wormhole case, we show the behavior of $\frac{d\tilde{r}}{d\tau}$ around the origin in the $(2, 2)_0$ and in the $(1, -1)_0$ case. For the $(1, -1)_0$ family we have

$$\frac{d\tilde{r}}{d\tau} = \frac{1}{\sqrt{f(r)}} \frac{dr}{d\tau} = \pm \sqrt{-1 + \frac{K^2 r}{b_{-1}}} \quad (6.22)$$

Since for these solutions the proper distance around the origin is

$$\tilde{r}(r) = \int_0^r \frac{dr'}{\sqrt{f(r')}} = \sqrt{a_1} \int_0^r dr' \sqrt{r'} = \frac{2}{3} a_1^{\frac{1}{2}} r^{\frac{3}{2}} \quad (6.23)$$

the (6.22) becomes

$$\frac{d\tilde{r}}{d\tau} = \pm \sqrt{-1 + \frac{K^2 (3\tilde{r})^{\frac{2}{3}}}{b_{-1} (4a_1)^{\frac{1}{3}}}} \quad (6.24)$$

We can see that, as might be expected, the $(1, -1)_0$ solutions corresponds to a repulsive potential close to $r = 0$. For a finite energy K^2 the observer can't reach the origin since the square root is real only for $r > \frac{b_{-1}}{K^2}$. On the contrary, in the $(2, 2)_0$ case we have

$$\frac{d\tilde{r}}{d\tau} = \pm \sqrt{-1 + \frac{K^2}{b_2 r^2}} \quad (6.25)$$

Since for these solutions the proper distance around the origin is

$$\tilde{r}(r) = \int_0^r \frac{dr'}{\sqrt{f(r')}} = \sqrt{a_2} \int_0^r dr' r' = \frac{\sqrt{a_2} r^2}{2} \quad (6.26)$$

the (6.25) becomes

$$\frac{d\tilde{r}}{d\tau} = \pm \sqrt{-1 + \frac{\sqrt{a_2} K^2}{2 b_2 \tilde{r}}} \quad (6.27)$$

from which it is clear that these solutions are characterized by an attractive gravitational potential in the origin such that $\frac{d\tilde{r}}{d\tau} = O(\frac{1}{\sqrt{r}})$. For the wormhole solutions, we can see that the point at $r = +\infty$, corresponding to the proper distance \tilde{r}_{max} , also behaves as an attractive point. This can be seen by writing the function $\tilde{r}(r) - \tilde{r}_{max}$ in the neighborhood of $r = +\infty$, where this time

$$\tilde{r}(r) = \int_{r_0}^r \frac{dr'}{\sqrt{f(r')}} \quad (6.28)$$

. In order to do this, we write $\tilde{r}(r) - \tilde{r}_{max}$ in function of the suitable variable

$$z = r e^{-\frac{ar}{2}}$$

that goes to 0 in the limit $r \rightarrow \infty$, and we approximate this function at the first order in Taylor series. We get

$$\begin{aligned}\tilde{r}(z) - \tilde{r}_{max} &\simeq \frac{d\tilde{r}}{dz} \Big|_{z=0} z = \left(\frac{d\tilde{r}}{dr} \frac{dr}{dz} \right) \Big|_{z=0} z = \left(\frac{r}{\sqrt{C_f} e^{\frac{ar}{2}}} \frac{1}{(1 - \frac{ar}{2}) e^{-\frac{ar}{2}}} \right) \Big|_{r \rightarrow \infty} z = \\ &= \frac{-2}{a\sqrt{C_f}} z\end{aligned}\tag{6.29}$$

where we simply used $\frac{d\tilde{r}}{dr} = \frac{1}{\sqrt{f(r)}}$ and the derivative of an inverse function. Since for wormhole solutions we have

$$\frac{d\tilde{r}}{d\tau} = \pm \sqrt{-1 + \frac{K^2}{C_B e^{-ar} r^2}}\tag{6.30}$$

we can use $z = r e^{-\frac{ar}{2}}$ in the relation (6.29) and substitute it in (6.30), so that, we finally obtain the behavior of $\frac{d\tilde{r}}{d\tau}$ in function of the proper distance

$$\frac{d\tilde{r}}{d\tau} = \pm \sqrt{-1 + \frac{4K^2}{a^2 C_B C_f (\tilde{r} - \tilde{r}_{max})^2}}\tag{6.31}$$

In a neighborhood of \tilde{r}_{max} the gravitational potential is not only attractive but also stronger than the one found in the case of $(2, 2)_0$ solutions around the origin, since we have $\frac{d\tilde{r}}{d\tau} = O(\frac{1}{\tilde{r}_{max} - \tilde{r}})$.

6.7.1 Solutions with $b_{1/2} \leq 0$

We conclude showing the same physical discussion for the less abundant solutions with $b_{1/2} \leq 0$. We recall that these solutions are confined in the wormhole region with $C_2^- > 0$ above the green line in figure 21. The typical behavior of the metric for $b_{1/2} < 0$ is plotted in figure 33. The main difference with respect to the more abundant $b_{1/2} > 0$ solutions is the presence of the local minimum of the $B(r)$ component in the $\rho > 0$ region.

For $b_{1/2} = 0$ the metric becomes of the form plotted in 34. In general, some of these solutions are not monotonic but all of them are characterized by $B(\rho)$ stationary in $\rho = 0$. It can be proved that a massive observer would feel a vanishing gravitational force in $\rho = 0$.

The last solution that we show is the $(1, 0)_{r_0}$, plotted in 35. This is clearly characterized by the asymptotic flatness in both the regions $r > r_0$ since it is symmetric under the transformation $\rho \rightarrow -\rho$ ¹¹.

Again, apart from exceptions mentioned in section 6.6, for $\rho \rightarrow -\infty$ the solutions

¹¹The small difference visible for large ρ is due only to errors of the numerical integration.

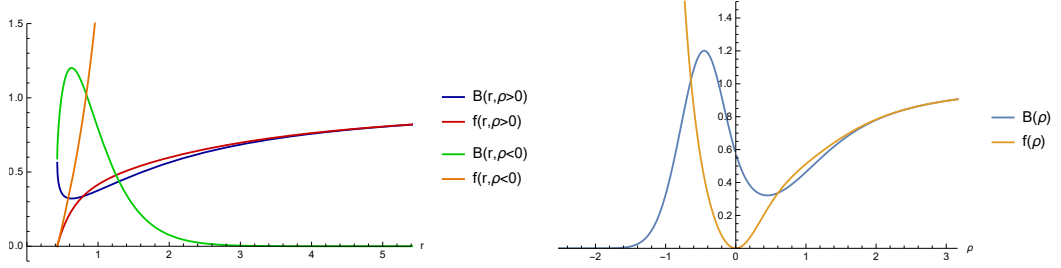


Figure 33

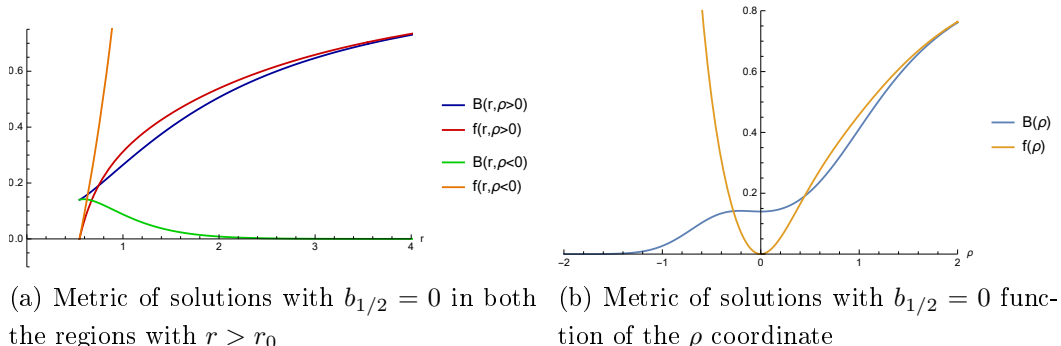


Figure 34

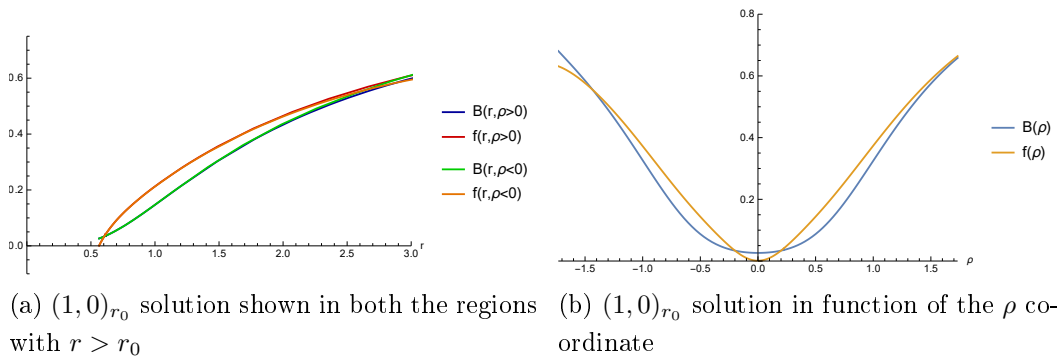
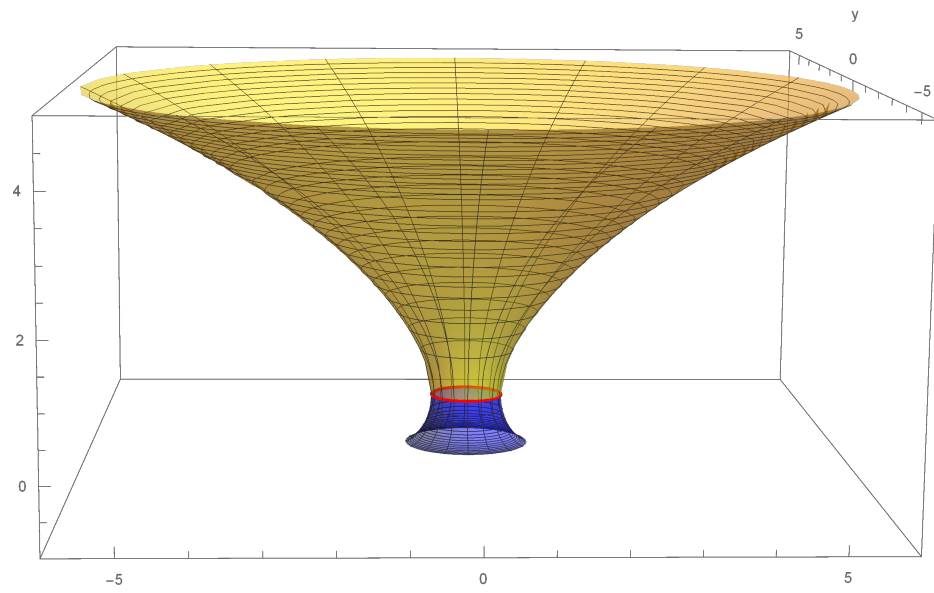
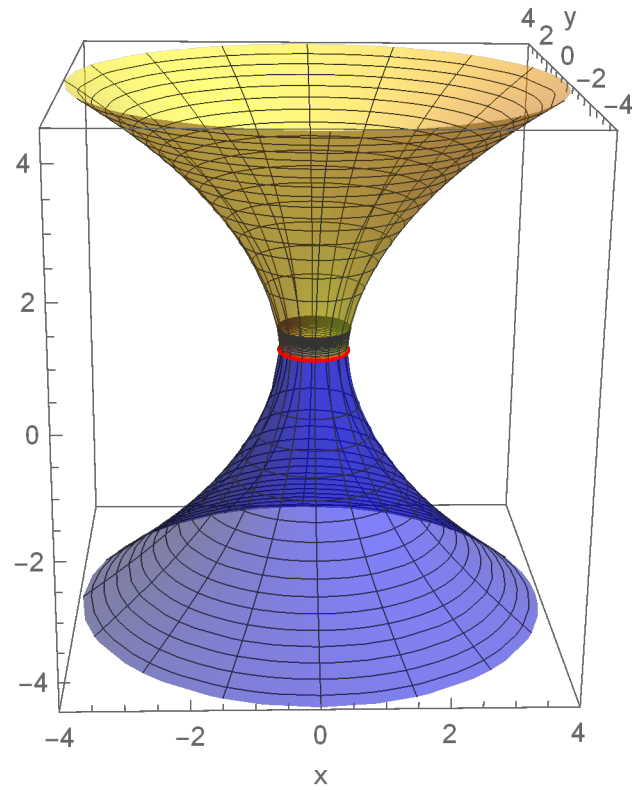


Figure 35

with $b_{1/2} \leq 0$ are described by the exponential functions (6.17). The exponential behavior is generically weaker than the $b_{1/2} > 0$ solutions, so the proper volume of the $\rho < 0$ region results to be greater, until diverging for the $(1, 0)_{r_0}$ solution. The corresponding embedding diagrams are shown in figure 36a and 36b respectively for an example of solution with $b_{1/2} \leq 0$ and the $(1, 0)_{r_0}$ solution. Except for the $(1, 0)_{r_0}$ solution, the characteristics of the invariants for $\rho \rightarrow -\infty$ are the same of the wormholes with $b_{1/2} > 0$, as well as the dynamical features of a massive observer that reaches this region.



(a) Embedding diagram of the solution with $b_{1/2} < 0$ corresponding to the point $(C_S, C_2^-) = (-0.98, 0.34)$



(b) Embedding diagram of the $(1, 0)_{r_0}$ solution

Figure 36

7 Conclusions

Our aim in this work was to study wormhole solutions in Einstein-Weyl gravity. Such solutions emerge in the context of classical quadratic gravity when looking for static spherically symmetric asymptotically flat solutions in the vacuum. The correspondent solutions in general relativity are the Schwarzschild black holes, solutions with horizons that are always asymptotically flat, but we have seen that in classical quadratic gravity many other solutions are present and in general they can be non-flat for large radius.

The study of the quadratic theory is motivated by the presence of quadratic corrections to the Einstein-Hilbert action in almost all the theories that attempts a description of quantum gravity.

In the first part we presented the state of art of classical quadratic gravity, by following the works [12] and [7]. First we solved the equations of motion when including quadratic terms in the Lagrangian, noticing that a solution in the vacuum in general relativity is also a solution in the vacuum of the theory with higher derivatives.

Then we restricted to the case of static spherically symmetric solutions which is the simplest non-trivial case but that gives an idea of what happens when including quadratic corrections in the Lagrangian. In the case of static spherically symmetric solutions the equations of motion reduce to a system of o.d.e. in the radial coordinate r of the third order for the general quadratic theory, and of the second order in the Einstein-Weyl theory. Such system turns out to be non-linear and it cannot be analytically solved, while the solutions can be described in exact form only under certain approximations.

It is further shown the theorem 1 that motivates the interest in restricting to the Einstein-Weyl case. Then we show the solutions of the linearised theory which will be used to describe our asymptotic flat solutions at large radius. Such solutions correspond to the Schwarzschild solutions in general relativity with two Yukawa corrections.

We proceeded in describing the Frobenius method, exploited to describe the solutions in series expansion around the origin or around $r_0 \neq 0$. The various families that describe the solutions around the origin have been shown, and they correspond to:

- the $(0, 0)_0$ family, i.e. the true vacuum of the theory, that clearly contains the flat Minkowski space;
- the $(1, -1)_0$ family, containing the Schwarzschild solution of general relativity, but also several others without horizon;

- the $(2, 2)_0$ family, which describes a new kind of solutions that are not present in general relativity.

We also reported a generalization of the $(1, -1)_0$ family, found in [9], which contains logarithmic terms, but that appears only in the $\beta \neq 0$ theory and not in the Einstein-Weyl restriction.

After that, the various families that describe the solutions around $r_0 \neq 0$ have been illustrated, except for the $(0, 0)_{r_0}$, which represents the series expansion of the solutions around a regular point in which nothing special happens. The families that have been found for the solutions around r_0 are:

- the $(1, 1)_{r_0}$ family, corresponding to black hole solutions;
- the $(\frac{3}{2}, \frac{1}{2})_{1/2, r_0}$ family, which constitutes an unusual horizon, but that cannot be asymptotically flat;
- the $(1, 0)_{1/2, r_0}$ family, representing wormhole solutions.

The peculiarities of the wormhole solutions are that they have a vanishing $f(r) = g_{rr}(r)^{-1}$ at $r = r_0$ but a non-vanishing $B(r) = -g_{tt}(r)$ at the same point, and that the series expansion that describe this solution is written in power of the variable $\rho = \sqrt{r - r_0}$. The wormhole interpretation is related to the solution of the equation of a radial geodesic. We have shown how to solve such equation, which shows that an observer passing through $r = r_0$ ends up into a new copy of $r > r_0$ instead that in $r < r_0$. The two patches $r > r_0$ correspond to the values of the variable $\rho = \sqrt{r - r_0}$, once taken with positive sign and then with negative.

We also reported the particular case of the $(1, 0)_{r_0}$ family that represents wormhole solutions in which the two patches $r > r_0$ are identical. Moreover, we discovered that the particular case of the solutions belonging to the $(1, 0)_{1/2, r_0}$ family with the parameter $b_{1/2} = 0$ does not strictly correspond to the $(1, 0)_{r_0}$ family, although it is properly described by a more generic subfamily with an additional free parameter w.r.t the $(1, 0)_{r_0}$.

In the second section we illustrated the numerical methods that we used to connect the linearised solutions at large radius with the solution families in the small radius regime. All the computations have been made with Wolfram Mathematica. The general solutions have been obtained thanks to the numerical integration made with the NdSolve function. Such function has been extensively used to integrate the solutions from large radius regime to small radius regime, by varying the parameters of the linearized solutions. For the specific wormhole and black hole solutions, the shooting method has been implemented, the most suitable numerical method to solve our boundary values problem. This method made it possible to find, with

optimal precision, the parameters characterizing both the black hole and wormhole solutions around the singularity of the o.d.e. system $r = r_0$.

The third section is dedicated to the numerical results obtained and to the related physical discussion.

First, we briefly commented to which length scale our solutions correspond to, that depends on the mass of the spin-two ghost.

Then we displayed the phase diagram of the asymptotically flat solutions of the Einstein-Weyl theory. Almost all the families of solutions made an appearance. As in the previous works, $(1, -1)_0$ solutions occupy a surface of our phase diagram, in contrast to what the number of free parameters suggests. The remaining surface turns out to be filled of $(2, 2)_0$ solutions and wormhole solutions. The origin of the phase diagram clearly corresponds to the flat Minkowski space, while the half-line $C_S < 0$ corresponds to the Schwarzschild solutions of general relativity.

Later we exposed the results obtained for the black hole solutions with the shooting method. Despite these solutions are not the main topic of this work, the shooting method was anyway necessary to learn their exact position (that actually constitutes the border of the wormhole region), and to understand how the parameters of the black hole solutions are related to the ones of the wormhole solutions. One paragraph of the black hole solutions is devoted to the description of the shooting method accuracy.

Next, we have outlined the numerical results obtained for the main topic of this thesis: the wormhole solutions. These are completely new results.

Wormhole solutions cover most of the physical region of the phase diagram. We characterized the asymptotically flat wormhole solutions through the trend of the parameters of the expansion (2.101) with respect to the position of the solutions on the phase diagram. The solutions can be divided in three main categories, corresponding to:

- solutions with $b_{1/2} > 0$, that occupy the majority of the wormhole region, corresponding to the whole region with $C_2^- < 0$, and a small portion with $C_2^- > 0$. These solutions have a temporal component $B(r)$ monotonic, that is equivalent to a gravitational potential decreasing with r . They have no theoretical upper bound on the value of r_0 , and they present the typical behavior shown in figure 6b;
- solutions with $b_{1/2} < 0$, which are all located in a small portion of the $C_2^- > 0$ region, together with the $b_{1/2} = 0$ solutions. These solutions have no theoretical constraint on the radius. However, the $b_{1/2} = 0$ solutions are constrained to have $r < \frac{1}{\sqrt{3}}$ (see (2.84)), and from the level sets of r_0 it appears that this property is extended to the asymptotically flat solutions with $b_{1/2} < 0$. For

$b_{1/2}$ negative we obtained solutions with the non-monotonic $B(r)$ component that typically goes like the solution plotted in figure 18;

- solutions with $b_{1/2} = 0$, that occupy the line in the wormhole region with $C_2^- > 0$ plotted in figure 21. They are described by the new subfamily (2.106). One point of this line corresponds to the unique asymptotically flat solution of the $(1, 0)_{r_0}$ family, in accordance with a similar result found in [9]. This is the unique wormhole solution found that is asymptotically flat in both the patches $\rho > 0$ and $\rho < 0$.

For all the solutions, the r_0 parameter is continuous at the transition with the black hole, and similarly we have $b_0 \rightarrow 0$ at the same transition. On the contrary, the f_1 parameter, which plays the same role both in the wormhole and in the black hole solutions, presents a discontinuity at the transition.

Then we proceeded in trying to figure out how to correctly extend the wormhole solutions for $r < r_0$. Indeed the expression for general wormholes is a power series in the variable $\sqrt{r - r_0}$ which is real only for $r > r_0$.

We proposed the expansion (6.6) as solution for the $r < r_0$ region, and an equivalent one for the $b_{1/2} = 0$ case. Such expansions result to be solutions of our ode system, but it is not clear how the internal and external solutions must be connected. In the general case $b_{1/2} \neq 0$ this is due to the divergent first derivative of $B(r)$, but also in the case $b_{1/2} = 0$ the presence of the new free parameter $f_{3/2}$ does not allow a precise linking between the internal and the external solutions. In any case, we must have $f(r)$ and its first derivative continuous at $r = r_0$, in order to obtain the continuity of the invariant quantities such as the Kretschmann scalar. An analysis of the interior of the wormhole solutions has been performed by initializing the (6.6) with some "reasonable" but non-theoretically justified conditions. With a particular choice of the parameters of the internal solution, we obtained a behavior of the wormhole solutions at the origin which shows a continuity with the well-determined behavior at the origin found for the black hole solutions.

Next, we summarized the key points of the coupling with matter, mentioning the earlier related works. We commented upon the possibility of coupling wormhole solutions with matter, since they have the condition required by the parameters counting. This will be object of future works, but, in any case, it will be necessary to understand how wormhole solutions have to be linked from $r < r_0$ to $r > r_0$.

The last two parts are devoted to the exploration of the space-time in the new region $\rho < 0$ which emerges for the wormhole solutions, and to the analysis of what happens to an observer passing through such solutions. In contrast to the interior $r < r_0$, the new region $\rho < 0$, $r > r_0$ can be easily explored. Indeed the metric written in terms of the coordinate ρ is regular in $\rho = 0$, and the wormhole expansion in

$\rho > 0$ completely determines the solution in $\rho < 0$. This is essential since an observer that falls into the wormhole reaches this new region instead of the region $r < r_0$. From our numerical results, it emerged that the behavior of the metric in the new region $r > r_0$ is strongly non-flat. We fitted this behavior with the functions (6.17) corresponding to an increasing exponential for $f(r)$ and a decreasing one for the $B(r)$ component. Such functions turned out to be asymptotic solutions, once inserted in the o.d.e. system (2.33,2.34). We encountered this behavior for almost all the wormhole solutions, except for the wormhole corresponding to the $(1,0)_{r_0}$ family, that is asymptotically flat in both the patches by its own definition, and except for those wormhole that are located in the very small region of the phase diagram on the left of the $(1,0)_{r_0}$ solution. We reported the results obtained by a quick numerical analysis about the parameters which characterize such non-flat behavior of the metric components, however a rigorous quantitative is still to be done.

Finally we put everything together in order to give a complete description of this kind of solutions. We illustrated the complete behavior of the metric in both the regions $\rho < 0$ and $\rho > 0$. We displayed the embedding diagram in such a way to visualize the space curvature around $r = r_0$. We noticed that the exponential behavior of $f(r)$ determines a finite volume for the whole region $-\infty < \rho < 0$, with a finite maximal proper radial distance \tilde{r}_{max} . We have shown the trend of the velocity of a free-falling observer, determined by 2.91 once known the metric components for $r \rightarrow \infty, \rho \rightarrow -\infty$. We remarked that the surface $\tilde{r} = \tilde{r}_{max}$ ($r = \infty, \rho = -\infty$) acts as a strongly attractive surface, even more than the origin in the $(2,2)_0$ solutions case.

In conclusion, our new results in Einstein-Weyl gravity show a solution space mostly filled by attractive wormholes, characterized by the prohibited region $r < r_0$ in favor of the new spacial region $r > r_0, \rho < 0$, which has a finite proper volume and both vanishing temporal and radial metric components for $r \rightarrow \infty$. Future works will deeply investigate the characteristics of these interesting solutions.

References

- [1] D. Anselmi. “Fakeons and Lee-Wick models”. In: *Journal of High Energy Physics* 2018.2 (2018), pp. 1–49. arXiv: [1801.00915](#).
- [2] A. Bonanno and S. Silveravalle. “Characterizing black hole metrics in quadratic gravity”. In: *Physical Review D* 99.10 (2019). DOI: [10.1103/PhysRevD.99.101501](#). arXiv: [1903.08759](#).
- [3] M. Goroff and A. Sagnotti. “Quantum gravity at two loops”. In: *Physics Letters B* 160.1-3 (1985), pp. 81–86. DOI: [10.1016/0370-2693\(85\)91470-4](#).
- [4] S. Hawking and T. Hertog. “Living with ghosts”. In: *Physical Review D* 65.10 (2002). DOI: [10.1103/PhysRevD.65.103515](#). arXiv: [hep-th/0107088](#).
- [5] B. Holdom and J. Ren. “Not quite a black hole”. In: *Physical Review D* 95 (2017). DOI: [10.1103/PhysRevD.95.084034](#). arXiv: [1612.04889](#).
- [6] G. ’t Hooft and M. Veltman. “One-loop divergencies in the theory of gravitation”. In: *Euclidean quantum gravity*. World Scientific, 1993, pp. 3–28.
- [7] H. Lu et al. “Spherically Symmetric Solutions in Higher-Derivative Gravity”. In: *Physical Review D* 92 (2015). DOI: [10.1103/PhysRevD.92.124019](#). arXiv: [1508.00010v2](#).
- [8] W. Nelson. “Static solutions for fourth order gravity”. In: *Physical Review D* 82.10 (2010). DOI: [10.1103/PhysRevD.82.104026](#). arXiv: [1010.3986v2](#).
- [9] A. Perkins. “Static spherically symmetric solutions in higher derivative gravity”. Doctoral Thesis. Imperial College London.
- [10] A. Salvio and A. Strumia. “Quantum mechanics of 4-derivative theories”. In: *The European Physical Journal C* 76.4 (2016), pp. 1–15. arXiv: [1512.01237](#).
- [11] S. Silveravalle. “Black holes in Einstein-Weyl gravity”. Master Thesis. Università degli Studi di Milano-Bicocca.
- [12] K. S. Stelle. “Classical gravity with higher derivatives”. In: *General Relativity and Gravitation* 9 (1978), pp. 353–371. DOI: [10.1007/BF00760427](#).
- [13] S. Weinberg. “Ultraviolet divergences in quantum theories of gravitation”. In: *General relativity: an Einstein centenary survey*. 1979.

8 Ringraziamenti

Finalmente posso scrivere in italiano!

Grazie a chiunque ci sia stato, vicino o lontano, in questo periodo finale del mio percorso.

Al professor Alfio Bonanno, che mi ha dato la possibilità di scrivere questo lavoro e di poterlo continuare in futuro.

A Samuele che c'è sempre stato durante lo svolgimento della tesi, con grande disponibilità e gentilezza e con i suoi utili consigli.

A Nicolò con cui ho condiviso l'intero percorso universitario e che mi ha sostenuto anche in questo momento finale.

A tutti i BRC e agli amici del breaking di Pisa, con cui ho passato un'inifinità di esperienze positive, e anche nel vederci più raramente in quest'ultimo anno sono sempre stati fondamentali.

Ad Ema che mi da' sempre motivazione (gasi), con cui condivido pensieri, viaggi, ed esperienze.

A Nicola che anche se conosco da poco si è dimostrato un vero amico, una persona positiva e il miglior vicino di casa che si possa avere.

Agli Amici, Davide, Roberto, Giuseppe, Marco e Pietro, quelli che ci sono da tutta la vita e che sempre ci saranno, che trasformano ogni situazione in divertimento, che anche senza dirmelo so che mi sostengono. Senza di voi non sarei quello che sono oggi.

Alla famiglia Freni e alla famiglia Fiumara, che mi hanno sempre accolto come uno di loro.

Ai miei zii, ai miei nonni, e anche a loro che non ci sono più, che mi hanno sempre dato l'affetto che si dà a un figlio, vi ringrazio per essere sempre stati fieri di me.

A Diletta, con cui ho stretto il miglior rapporto che potessi avere in questi ultimi anni. Che c'è sempre stata, mi ha sopportato, e mi ha aiutato infinitamente, che

condivide con me questa vittoria come fosse sua. Grazie per impegnarti con me a rendere felici i nostri giorni insieme.

A mia sorella e ai miei genitori. Mi avete sempre dato fiducia e sostegno e so che sempre lo farete, e anche se non lo dimostro spesso, io vi penso ogni giorno e ogni giorno vi sono grato.